IOSUD –„DUNĂREA DE JOS” UNIVERSITY OF GALAȚI

Doctoral School of Mechanical Engineering

PH.D. THESIS

STUDIES ON FREE SURFACE FLOW AROUND JUNCTIONS

ABSTRACT

Ph.D. student,

eng. Costel UNGUREANU

Scientific Coordinator,

Prof. Ph.D. Eng. Costel Iulian MOCANU

Seria I 6: Inginerie mecanica nr. 54

GALAȚI

2020

IOSUD –„DUNĂREA DE JOS” UNIVERSITY OF GALAȚI

Doctoral School of Mechanical Engineering

PH.D. THESIS

STUDIES ON FREE SURFACE FLOW AROUND JUNCTIONS

ABSTRACT

Ph.D. student,

eng. Costel UNGUREANU

President:	**Prof. Ph.D. Eng. Elena MEREUȚĂ** „Dunărea de Jos” University of Galați
Scientific Coordinator,	**Prof.univ.dr.ing. Costel Iulian MOCANU** „Dunărea de Jos” University of Galați
Scientific Reviewers:	**Prof. Ph.D. Eng. Anton HADĂR** University POLITEHNICA of Bucharest **Prof. Ph.D. Eng. Ilare BORDEAȘU** Politehnica University of Timișoara **Prof. Ph.D. Eng. Leonard DOMNIȘORU** „Dunărea de Jos” University of Galați

Seria I 6: Inginerie mecanica nr. 54

GALAȚI

2020

Seriile tezelor de doctorat susținute public în UDJG începând cu 1 octombrie 2013 sunt:

Domeniul fundamental ȘTIINȚE INGINEREȘTI

Seria I 1: **Biotehnologii**
Seria I 2: **Calculatoare și tehnologia informației**
Seria I 3: **Inginerie electrică**
Seria I 4: **Inginerie industrială**
Seria I 5: **Ingineria materialelor**
Seria I 6: **Inginerie mecanică**
Seria I 7: **Ingineria produselor alimentare**
Seria I 8: **Ingineria sistemelor**
Seria I 9: **Inginerie și management în agicultură și dezvoltare rurală**

Domeniul fundamental ȘTIINȚE SOCIALE

Seria E 1: **Economie**
Seria E 2: **Management**
Seria SSEF: **Știința sportului și educației fizice**

Domeniul fundamental ȘTIINȚE UMANISTE ȘI ARTE

Seria U 1: **Filologie- Engleză**
Seria U 2: **Filologie- Română**
Seria U 3: **Istorie**
Seria U 4: **Filologie - Franceză**

Domeniul fundamental MATEMATICĂ ȘI ȘTIINȚE ALE NATURII

Seria C: **Chimie**

Domeniul fundamental ȘTIINȚE BIOLOGICE ȘI BIOMEDICALE

Seria M: **Medicină**

Content

Key words: junctions, juncture flow, hydrofoil, free surface, turbulent flow, drag, NACA 0012

Introduction

Free surface flow is a hydrodynamic problem with a seemingly simple geometric conFiguretion but with a flow topology complicated by the pressure gradient due to the presence of the obstacle, the interaction between the boundary layer and the free surface, turbulence, breaking waves, surface tension effects between water and air. As the appendages become more and more used and larger in size, the general understanding of the flow field around the appendages and the junction between them and the hull is a topical issue for naval hydrodynamics.

When flowing with a boundary layer, when the current lines meet a body mounted on a solid flat or curved surface, detachments appear in front of it due to the blocking effect. As a result, vortex structures develop in the fluid, also called horseshoe vortices, the current being one with a completely three-dimensional character, complicated by the interactions between the boundary layer and the vortex structures thus generated.

Despite the importance of the topic, the literature records the lack of coherent methods for investigating free surface flow around junctions, the lack of consistent studies on the influence of the inclination of the profile on the body and the influence of the radius of curvature of the support plate on the flow field. the main one being the insufficient understanding of the complex mechanisms that govern such flow processes. As a result of this paper, ***"Studies on free surface flow around junctions",*** aims to systematically study the influence of profile inclination to the support plate, the influence of plate curvature, the influence of free surface, but also the influence of Reynolds and Froude numbers on junctions

In this context, the numerical and experimental research carried out during the doctoral studies aimed at the following scientific objectives:

- Deepening and implementing a methodology for determining experimental and numerical errors and experimental and numerical uncertainties.
- Establishing the calculation methodology and numerical schemes used in the study of viscous flow without free surface around the junctions;
- Establishing the calculation methodology and numerical schemes used in the study of viscous flow with free surface around the junctions;
- Study of the flow around the profile mounted on a flat, concave and convex plate, without free surface;
- Study of the flow around the profile mounted on a flat, concave and convex plate with free surface;

Chapter 1, ***Introduction***, motivates the choice of this research topic, presents the importance and timeliness of the topic and the state of the art on the flow around the junctions. It also describes the scientific objectives that underlie the development of the research topic.

Chapter 2, ***Mathematical models, algorithms and discretization schemes***, presents the mathematical model used in the numerical simulation of the flow around the junctions, methods and method of discretization of numerical problems, as well as the numerical schemes and algorithms used.

Chapter 3, ***Verification and Validation***, presents the numerical and experimental verification and validation methodology as well as the methodology for determining the errors and uncertainties of the experimental and numerical determinations. It also describes the own experiment performed in the towing tank of the Faculty of Naval Architecture as a support for validating the numerical methodology of free surface flow, and validates the flow

methodology around the junction completely immersed using benchmark experiments in the literature.
Chapter 4, ***Flow around the junction without free surface***, presents the results of numerical investigations on the free surface flow around the junctions, more precisely the study of the influence of the angle between profile and plate, the study of the influence of plate curvature, the study of the influence of current velocity on the junction. .
Chapter 5, ***Free surface flow around junctions***, presents the studies on the influence of the free surface height, the study of the influence of current speed and the study of the profile inclination to the plate on the free surface junction.
Chapter 6, ***General Conclusions***, presents the main conclusions resulting from systematic studies on free surface flow around junctions with an impact on naval hydrodynamics.
In Chapter 7, final, ***Personal contributions and perspectives***, are presented the original contributions of the doctoral thesis, with impact on the development of knowledge in the field and perspectives for further research and dissemination of research results.
The research activities within the doctoral thesis were carried out with the help of the modern research infrastructure of the "Naval Architecture" Research Center (CCAN).

During the phd studies, the phd student was involved as a member in the teams of two research grants (Grant PNII-IDEI, CNCSIS ID_790 and Grant PNII, TOYROV, 2003401/12116 / 1.10), of a SOPHRD project (PiiF, 86 / 1.2 / S / 61830), but also in research-design contracts with the private companies.
The results of the research carried out within the doctoral thesis were presented for dissemination in 18 scientific articles published in journals listed ISI proceedings and indexed in international databases, a book "Ship board systems", EDP Bucharest, 2017, 8 papers at scientific events representative for the naval field.

Chapter 1. State of the art

1.1.The importance and the topicality of the research

In recent years, interest in global warming has grown significantly, and topics such as energy efficiency, environmental pollution, and reducing greenhouse gas emissions are very current. International efforts to reduce the impact of climate change began in 1992 in Rio, where more than 150 governments signed a framework agreement for sustainable development. In 1997, the Kyoto Protocol was adopted, by which the signatory states, 37 industrialized states and the European Community, committed themselves to reducing the level of greenhouse gases by an average of 5.2% by 1990 compared to 1990. internationally, shipping could not be explicitly addressed in the Kyoto Protocol (Annex 1). Instead, public and political pressure on greenhouse gas emissions from shipping has shifted to the International Maritime Organization (IMO). According to the "Second IMO GHG Study 2009", "the most comprehensive and authoritative estimate of greenhouse gases in the naval field", in 2007, the naval transport of goods produced approximately 1046 million tons of gas emissions, representing approx. 3.3% of global emissions, of which 870 million tons of carbon dioxide (CO2), 2.7% globally. Carrying out calculations on various gas emission scenarios, the IMO found that in the absence of concrete environmental policies, by 2050, the level of CO2 emissions will increase by 150-200% compared to the level of 2007. Thus, from 1 January 2013, the design energy efficiency index (EEDI-Energy Efficiency Design Index) and the operating efficiency index (EEOI-Energy Efficiency Operational Index) become mandatory for all ships over 400 tons (MPEC 62, 2011). According to the IMO resolution, these indices are specific to each type of vessel and should be reduced by 2025, by up to 30% from a reference value. In fact, these indices represent the ratio between the total CO2 emissions on board the ship and the transport capacity, speed and parameters related to the ship's operating conditions.

Ships in operation are less suitable for major design changes, and are rather based on upgrading the engine compartment or using energy-saving devices. For new ship projects, the task of naval architects to increase energy efficiency is increasingly difficult, as any new ship already incorporates the latest developments and innovations in the field existing on the market at that time. According to Ungureanu et al., (2013) the measures that a naval architect can take to reduce the design energy efficiency index fall into four distinct categories:

- Structural measures;
- Technological measures;
- Operational measures;
- Hydrodynamic measures.

The structural measures contribute to the decrease of EEDI by increasing the ship's transport capacity. This is possible either by optimizing the ship's strength structure or by using high-alloy steels that lead to a decrease in the thickness of the sheets used and thus the weight of the hull. Thus, at the same displacement of the ship and at a lower mass of the empty ship, the transport capacity increases.

The technological measures aim to reduce the power placed on board by improving the energy efficiency of engines, main and auxiliary, by using alternative fuels or by implementing alternative energy production systems. In general, these measures require substantial financial investment to achieve substantial reductions in greenhouse gas emissions. The main pollutant on board the ship is the main engine (or engines). The required power as well as its (their) gauge depend on the forward resistance and the efficiency of the propulsion system. The classic main propulsion engine is the fuel oil

powered two-stroke engine. Two-stroke engines are slow, economical but oversized and highly polluting. The efficiency of the propulsion systems is greater the larger the diameter of the propeller. This often causes the ship to be designed "around" the propulsion system and not the other way around. Also, tree lines can have considerable dimensions influencing the efficient use of spaces in the stern area. One way to increase efficiency on board is to replace the classic propulsion system with diesel-electric systems. They replace the classic engine-shaft-propeller propulsion system with diesel batteries-generators and electric propellers. So the remaining space in the area of engine compartment can be used for freight. Even if these diesel generators are optimized to operate at certain speeds and loads, they do not solve the problem of environmental pollution. According to AEA Energy & Environment (2008), the engine consumes only approx. 43% of the energy of hydrocarbons used, the rest being lost through exhaust gases, 27%, and heat, 30%. Knowing this, an important step in reducing engine emissions on board is the use of dual-fuel engines, diesel / LNG, or LNG-only engines. According to a study by the Norwegian classification register, Det Norske Veritas (2010), the use of natural gas leads to a 20% reduction in CO2 emissions. It also eliminates emissions of sulfur oxides (SOx) and particles into the atmosphere and reduces emissions of nitrogen oxides (NOx). Instead, there are two drawbacks to adopting these systems. One is the cost of investment, currently being 10-20% more expensive than the classic ones, and the other is the recharging infrastructure, which limits the autonomy of the ship.

Another direction of efficiency improvement is the use of alternative energy production systems such as:

- heat recovery systems evacuated through the chimney (MAN, 2012);
- solid sailing systems with photovoltaic panels, which use wind energy and solar energy at the same time (Sommer, 2013);
- the use of parachutes for the exploitation of air currents (Ockels et al., 2006; Naaijen et al., 2007; Erhard et al., 2012);
- the use of wind turbines on board the ship for electricity production (Sommer, 2013);

Operational measures refers to the way the ship is operated. This category includes measures such as reducing service speed, optimizing ballast and trim, cleaning the hull and engine, maintaining the propulsion machine and optimizing the navigation route and scheduling in ports. These measures involve modest investments in hardware and software. The most important measure in this category is speed reduction. Even if the speed is found in the calculation formula of the EEDI at the denominator, it has an extraordinary effect on the index by the dependence of the power placed on the speed board on the third power. For example, the German classification register, Germanisher Lloyd (2011) proposed to reduce the speed from 19 to 16 knots for a container ship type of 1200 TEU. The result was a reduction in the power of the main propulsion machine from 11, 2 MW to 9 MW. However, speed reduction as the main measure cannot be applied to perishable goods and remains unpopular among shipowners, as it influences the delivery time of goods and operating costs and thus the shipowner's profit. So any reduction in cruising speed must somehow balance the costs of operating the cargo with the profit of the shipowner.

Hydrodynamic measures are the most important measures that can be taken in the design phase. These measures are materialized by optimizing the size and shape of the ship or by designing propellers adapted to the ship's wake. The main purpose is to reduce the ship resistance and increase the efficiency of the propulsion system which ultimately lead to a reduction in the power placed on board the ship. Given that the shapes of a ship are far from hydrodynamically perfect, they are the result of a compromise between the main dimensions imposed by the size of the locks, the depth of the waterway, the depth of the aquarium in the

port, the price of taxes, transport capacity (deadweight, volume), ship equipment (machinery, deck installations, hull installations), hydrostatic performances and last but not least the hydrodynamic performance of the ship, are increasingly uingthe so-called flow control devices or devices Energy Saving Devices (ESD) to improve flow around the ship. Without taking into account corrections of possible design errors, these devices are appendages mounted on the hull of the ship, in the stern area of the ship, in the vicinity of the engine. Their role is to even out the flow field in the propeller disc, by mounting it in front of the propeller, or to recover from the propeller energy lost by the tangential component of the speed, in which case it is mounted in the aft of the propeller. Carlton (2007) makes a complex description of all control devices. Among the best known flow control devices are the networks of upstream and downstream propeller profiles, Schneekluth nozzle, Mewis nozzle, Grim device; the network of profiles on the propeller shaft (figure 1.1).

a) Schneekluth duct, (www.schneekluth.com)

b) Mewis system, (Svardal si Mewis, 2011);

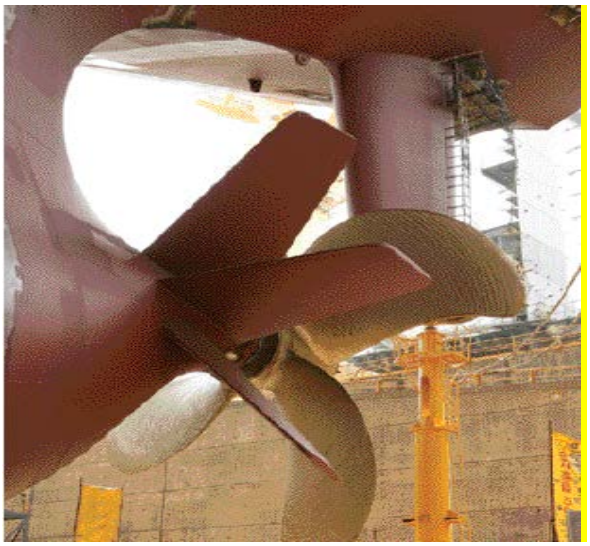

c) DSME prestator, (Daewoo Shipbuilding & Marine Engineering, 2008)

d) Grim device, (de Jong, 2011)

e) Hydrofoil network on propeller boss, (de Jong, 2011)

Figure 1.1. Energy saving devices

1.2.Motivation of the research

The idea of using devices in the stern of the ship is not new at all. Although the first reference in the literature belongs to Van Lammeren in 1949, the first commercial device appeared only in 1980 and belongs to the Mitsui shipyard, the Mitsui integrated nozzle. Although it was not well known how the Mitsui system helped reduce onboard fuel consumption, the global oil crisis led to the success of these types of devices. Neglected after the stabilization of crude oil prices, these energy-saving devices return to the forefront amid the volatile oil market, due to the conflicts in the Middle East, on the one hand, and due to the introduction of energy efficiency indices, on the other. Thus, a possible reduction of even 5% of the installed power on board makes these devices very attractive for shipowners.

Free surface flow is a hydrodynamic problem with a seemingly simple geometric conFiguretion but with a flow topology complicated by the pressure gradient due to the presence of the obstacle, the interaction between the boundary layer and the free surface, turbulence, breaking waves, cavitation, surface tension effects water and air. As the appendages become more and more used and larger in size, the general understanding of the flow field around the appendages and the junction between them and the hull is a topical issue for naval hydrodynamics.

When flowing with a boundary layer, when the current lines meet a body mounted on a solid flat or curved surface, detachments appear in front of it due to the blocking effect. As a result, vortex structures develop in the fluid, also called vortex horseshoes, the current being one with a completely three-dimensional character, complicated by the interactions between the boundary layer and the vortex structures thus generated. The whirlwind is generated by the combination of two effects: compression and elongation of the transverse component of the vortex present in the turbulent boundary layer of the current, bypassing the obstacle, on the one hand and the development of vortex structures near the leading edge, vertically due to gradient high pressure generated by the geometry of the appendix, on the other hand.

In the physical world around us we find the flow around the junction between trees and buildings with the ground, at the foot of bridges built in rivers, turbomachines or the wing-fuselage connection to an airplane. In naval hydrodynamics, in addition to ESD, the junctions are also found in drifts, rudders, easels, roll keels or stabilizing wings (Fig. 1.5).

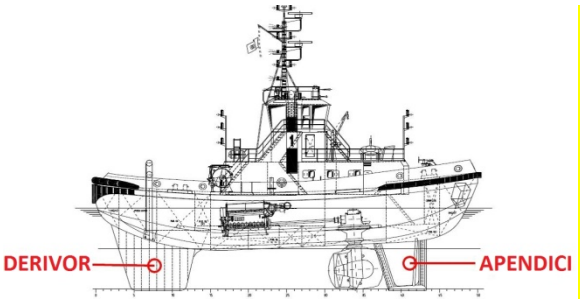

a) Tug with skek and appendiges, (Ionaș, 2012)

b) Sailing yacht (http://trends.nauticexpo.com)

c) Shaft line brackets (personal collection)

d) Passanger ship with stabilising wings

Figure 1.2. Ships with appendices

1.3.Research methodology

Despite the importance of the topic, the literature records the lack of coherent methods for investigating free surface flow around junctions, the lack of consistent studies on the influence of the inclination of the profile on the body and the influence of the radius of curvature of the support plate on the flow field. the main one being the insufficient understanding of the complex mechanisms that govern such flow processes. As a result, this paper, ***"Studies on free surface flow around junctions",*** aims to systematically study the influence of the inclination of the profile to the support plate, the influence of plate curvature, and the influence of free surface on junctions. The influence of Reynolds and Froude numbers will also be studied. First, the profile mounted vertically on the flat plate will be studied. It will tilt in three steps, by 15^{o}, first in the plane perpendicular to the plane of symmetry of the profile, and then in the plane of symmetry upstream and downstream, while maintaining the leading edge parallel to the trailing edge. Because in practice, it is rare when the plate is flat, and the hull of the ship is generally a three-dimensional surface with double curvature, the plate is curved with various radii, concave and convex. For each radius of curvature, the inclination of the profile on the flat plate is maintained. The curvature of the plate is a simple one symmetrical with respect to the angle of attack of 0 degrees. In the case of free surface flow, the undisturbed free surface parallel to the base plate is considered, the profile being a penetrating type.

The chosen aero-hydrodynamic profile is a symmetrical one, intensively studied and used in aerodynamics, NACA 0012, for which there is information in the literature on the dependence

of the forward resistance on the Reynolds number as well as the distribution of pressure and friction coefficients on the profile string. from this research in order to increase the certainty of numerical investigations.

Taking into account the multitude of geometric conFiguretions of the junctions, the existence of the free surface, the variation of Reynolds and Froude numbers as well as the need to study flow parameters, this paper will use numerical simulation in parametric calculations, plate radius of curvature and angle. between the profile and the plate, and by the experimental investigations in the towing tank in order to validate the calculation methodology with free surface, for a surface piercing vertical profile, with zero angle of attack.

Chapter 2. Mathematical models, algoritms and discretization shemes

The present paper has a pronounced interdisciplinary character, consisting in the mathematical modeling of the viscous flow with the free surface around the junctions, the numerical solution of the flow and the establishment of the induced hydrodynamic and energetic performances. According to Hirsch (2007), the numerical simulation of a flow problem involves five steps. First, a mathematical model is adopted consisting of a set of differential or integro-differential equations with partial derivatives that define the level of approximation of the physical phenomena to be simulated. Equations in their differential form cannot be solved directly on computing machines because at the computational level computing machines work only with numbers. As a result, the equations that govern flow are transformed into algebraic equations, which are easy to solve numerically. Also, the area of fluid of interest, also called computational domain, undergoes a process of division into a network of discrete points, connected in various ways, in which the variables of the algebraic equations will be calculated. This process of transforming the equations as well as the one of dividing the computational domain is called discretization, and represents the second step in performing a numerical simulation. Then the numerical schemes used in solving the flow equations are analyzed and established. Step four consists in choosing an algorithm with which to solve the system of algebraic equations. The final stage consists in processing and processing the results of the numerical simulation. In this stage, the order of accuracy as well as the degree of uncertainty of the simulation are estimated, integral global physical quantities (eg load-bearing force, resistance to advance) or derivatives (vorticity, tangential stresses) are calculated, or the physical quantities are represented graphically.Teza este structurată pe două etape:

- In the first stage, the junction completely immersed in steady flow is studied. In this case the pressure equation (pressure correction) is discretized with the standard scheme. The equation of the pulse, the turbulent kinetic energy and the specific dissipation rate are discretized with second-order upwind schemes. The pressure and speed are coupled with a SIMPLEC scheme. Relaxation factors retain the standard values in the Ansys Fluent program.
- In the second stage, the flow with free surface around the junctions is calculated, using a technique of capturing the VOF interface, in non-stationary regime. In this case, the pressure with the PRESTO scheme and the equation of the volume fraction with the geometric reconstruction are discretized in order to avoid the numerical diffusion. First, the impulse equation and the turbulence model equations are discretized using the QUICK scheme. The pressure was coupled to the speed via the PISO scheme.

In both stages the flow gradients are evaluated using the Green-Gauss cells based method, and the equations are solved with the pressure-based solver in a segregated manner.

Chapter 3. Verification and Validation

3.1.Introduction

3.1.1. Objectives

The objectives that define the structure of this chapter are:

➢Implementing a methodology for determining experimental and numerical errors and experimental and numerical uncertainties.

➢ Establishing the calculation methodology and numerical schemes used in the study of viscous flow with free surface around the junctions:

- Carrying out an experiment in the towing tank to study the hydrodynamic performance of a vertical profile NACA0012 that penetrates the free surface.
- Verification and validation of numerical results of free surface flow in relation to experimental results.

➢ Establishing the calculation methodology and numerical schemes used in the study of viscous flow without free surface around the junctions:

- Verification of the numerical results of the incompressible flow on the flat plate and validation with experimental results from the specialized literature
- Verification of numerical results of incompressible flow around the hydrodynamic profile NACA 0012 and validation with experimental results from the literature

3.2. Verification and Validation Methodology

In the general sense, the error of a simulation or an experiment, is a measurable deficiency that is not due to lack of knowledge. At the same time, the error is the difference between the calculated or measured value and the "exact" or "true" value. For this reason, errors are estimated rather than accurately known and lead to the need to determine the uncertainties of computational or experimental errors,.

ASME V&V 20, (2009), (figure 3.2), defines the validation comparison error, E, as the difference between the numerical solution result,S, and the experimental result,D.

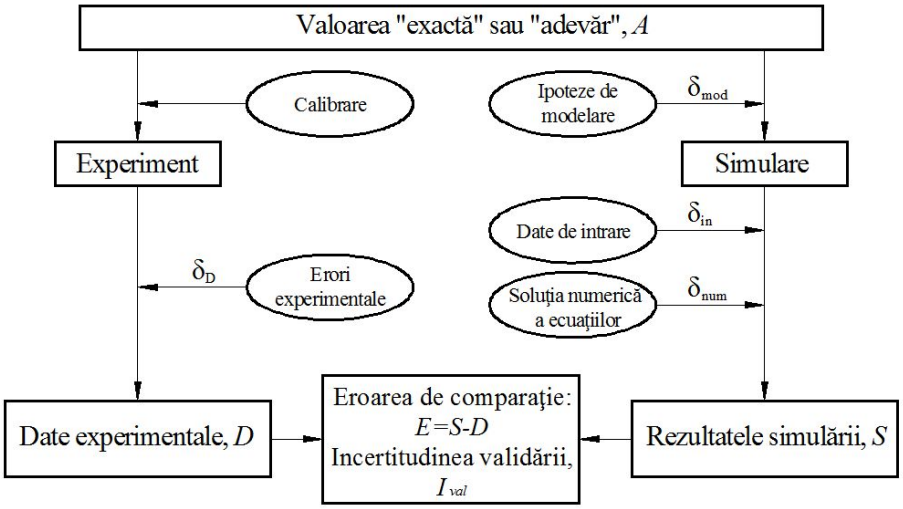

Figure 3.1. Verifiation and Validation error sources (ASME V&V 20, 2009)

$$E = S - D \tag{3.1}$$

Numerical simulation errors can be grouped into three categories:

➢Errors due to modeling hypotheses; δ_{SM}

➢Errors due to the numerical solution of the equations governing the flow, δ_{SN}

➢Errors introduced in the numerical solution of erroneous values of the input parameters, δ_{SIn}.

As a result, the error of a numerical simulation can be described as:

$$\delta_S = \delta_{SM} + \delta_{SN} + \delta_{SIn} \tag{3.5}$$

The relation of the uncertainty of the numerical simulation is:

$$I_S^2 = I_{SM}^2 + I_{SN}^2 + I_{SIn}^2 \tag{3.6}$$

Errors and uncertainties associated with input data usually result from the use of previously obtained experimental data or a numerical simulation; results that present uncertainties and that tend to amplify numerical simulation errors.

3.3. Free surface flow around a surface piercing hydrofoil NACA 0012

3.3.1. Towing tank experiment

This phd thesis aims to study the viscous flow with free surface around the junctions. In the previous chapter, Mathematical models, algorithms and discretization schemes, the advantages of systematic numerical studies over the experimental ones were presented. In the literature there are experimental tests for aerodynamic profile NACA0012, while hydrodynamic tests with free surface, no. In order to establish and validate the methodology but also the numerical results of the free surface flow, the need for the experiment in the hull basin appeared, an experiment that will be described below. Numerical studies with or without free surface in this research will be done at the unit length of the profile strings. Due to the speed of the trolley and the influence of the basin walls on the experimental tests, the length of the rope was reduced to 0.5 m.

3.3.1.1. Towing tank

The experiments were performed in the Towing tank of the Faculty of Naval Architecture, "Dunărea de Jos" University of Galați. The main dimensions are $L \times B \times H = 45 \times 4 \times 3$ m, and it is equipped with a self-propelled carriage, CUSSONS Technology brand, equipped with speed control systems, acceleration / deceleration and experimental data acquisition system. The maximum speed of the carriage is 4 m/s for a model with a length of 4m and a mass of 200 kg.

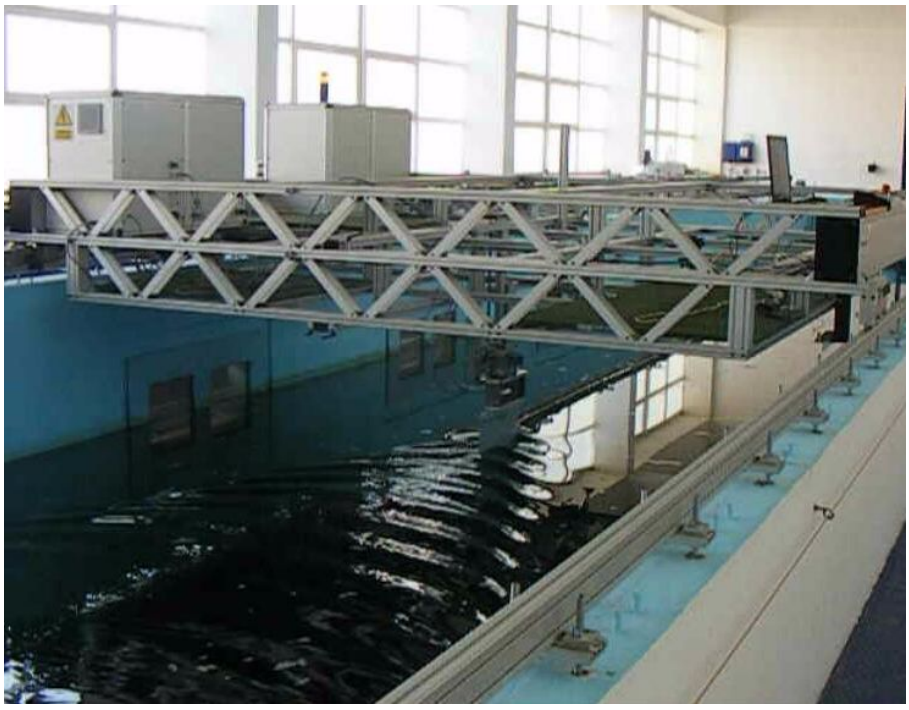

Figure 3.2. Towing tank carriage during tests

The acquisition system records the instantaneous values with an imposed frequency of 0.1Hz. Tests of resistance to advance, self-propulsion, propeller in open water, measurements of sediment and elevation of the free surface can be performed. The equipment used in the endurance tests consists of the R35E dynamometer.

3.3.1.2. Experimental model NACA 0012

The experimental model is made of water-resistant plywood, used in naval interiors, with a thickness of 20 mm. To avoid alteration of the model in prolonged contact with water, it was insulated with epoxy resin. The main dimensions are $c \times t \times h = 0.5 \times 0.06 \times 1.2$ m with a maximum tolerance of ± 1mm for each dimension according to ITTC (7.5-01-01-01) on the manufacture of experimental models. To measure the profile of the free surface on the model, a sticker printed with a fine grid, 5×5mm , was glued to its surface (figure 3.7).

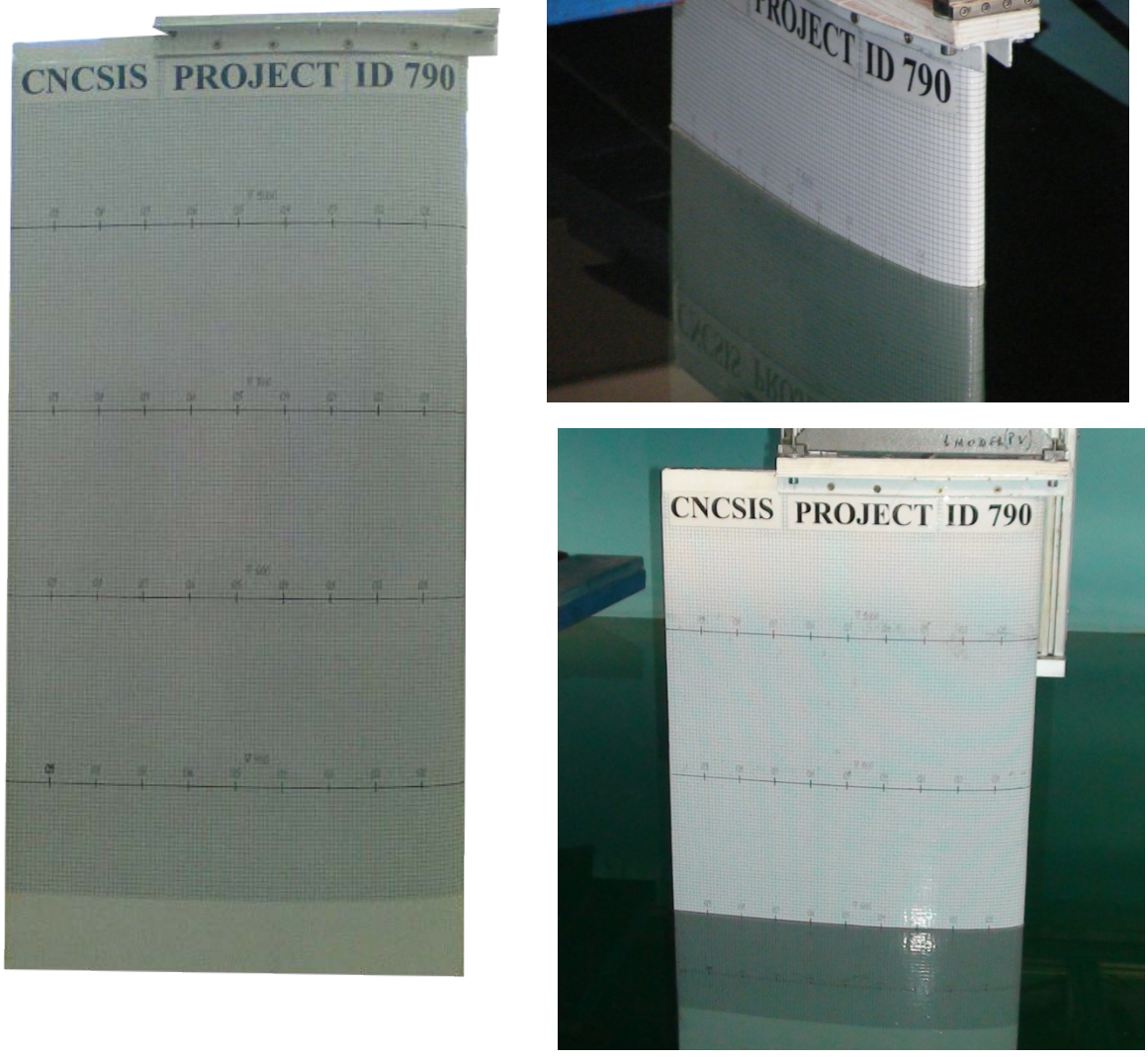

(a) NACA 0012, vedere laterală (b) Model imersat

Figure 3.3. NACA 0012 experimental model

3.3.1.3. Experimental conditions

In an attempt to cover as much of the areas of use as possible, the flow regimes around a vertical profile with free surface, as well as to study the evolution of the resistance to forward as a function of speed, 12 Froude numbers were chosen, from 0.16 at 1.04, with a step of 0.08. Also, in order to study the influence of profile dives on the forward resistance, 4 drafts

were chosen, 1, 0.8, 0.6, 0.4 m. The value of the minimum draft (0.4 m) is influenced by the constructive limits of elevation of dynamometer coupling system on the model. Throughout the experimental samples, the water temperature was monitored, recording the value of 12oC. Measurements on calm water in the hull basin presuppose a calm state of the water. This leads to a test program with breaks of 45-60 minutes, necessary to calm the water.
Table 3.1 shows the velocities, Fn numbers, as well as Rn numbers related to the experimental tests.

Table 3.1. Experimental conditions

Test	1	2	3	4	5	6
U_c [m/s]	0,35	0,53	0,71	0,88	1,06	1,24
Fn	0,16	0,24	0,32	0,40	0,48	0,56
Rn [$\times 10^5$]	1,435	2,152	2,869	3,587	4,304	5,021

Test	7	8	9	10	11	12
U_c [m/s]	1,42	1,60	1,77	1,94	2,12	2,30
Fn	0,64	0,72	0,80	0,88	0,96	1,04
Rn [$\times 10^5$]	5,739	6,456	7,173	7,891	8,608	9,325

Table 3.2 presents the ITTC criteria (7.5-02-02-01) regarding the avoidance of the negative effects of the side walls or the bottom of the basin on the experimental measurements. Values of similar tests from the literature are also presented.

Table 3.2. Experimental resitrictions

Study \ **Criteria**		$Fn_H \leq 0.7$	$\frac{H}{d} \geq 4$	$\frac{B}{c} \geq 0.35$	$\frac{B}{t} \geq 4$	$\frac{A_b}{A_m} = \frac{BH}{td} \geq 15$
Chow (1967)		0,13-0,31	1	2,33	8,97	7,58
Zhang (1996)		0,12-0,35	2	2,5	10	20,8
Pogozelski (1997)		0,04-0,4	1,1	3,33	10	11,1
Kandasamy (2006)		0,12-0,35	2	2,5	10	20,8
			4	2,5	10	41,7
Current research	d=0,4m	0,424-0,065	7,5	8	66,66	500
	d=0,6m		5	8	66,66	333
	d=0,8m		**3,75**	8	66,66	250
	d=1m		**3**	8	66,66	200

It is observed that all conditions are met, except the ratio H/d for the two largest drafts, 1 m and 0.8 m, respectively. Comparing the values with those in the literature and taking into account that the other criteria are met well above the recommended values , non-compliance with the criterion is neglected H/d .

3.3.1.4. Experimental results

The results of the experimental tests carried out in the hull basin for all 12 speeds and for the 4 drafts, expressed in N are shown in Figure 3.8.

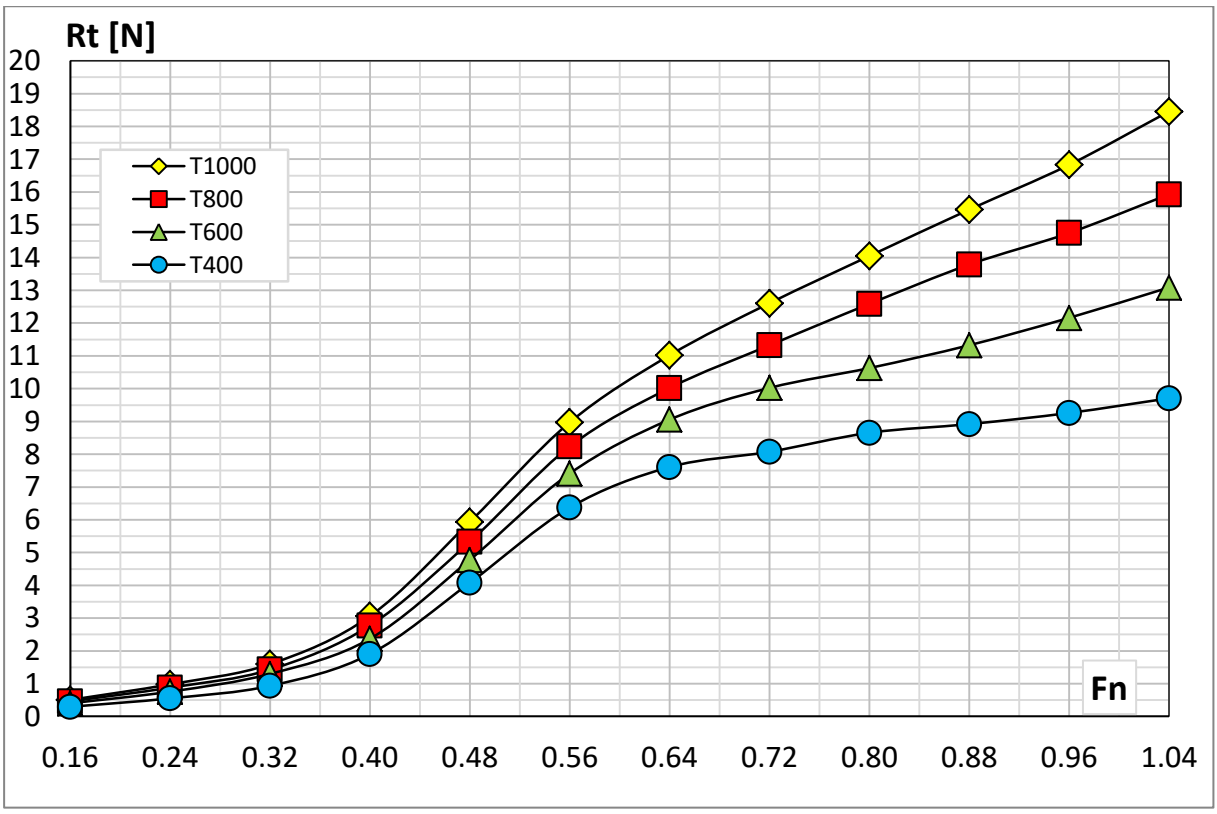

Figure 3.4. Hydrofoil drag

It is observed that as the draft decreases, the value of the tensile strength decreases constantly, on average by 10% from 1000 mm to 800 and 600 mm, the decrease being more consistent than 20% for the reduction of the draft from 600 mm to 400 mm.

Figure 3.10 shows the development of the free surface on the experimental profile for Froude numbers from 0.32 to 0.64. At low speed, the wave on the surface of the model has 2 or 3 wave crests. As the speed increases, the wave in the area of the leading edge thins and rises until it breaks, and the second wave ridge migrates to the flight board as a result of the increase in wavelength. It is also observed that as the speed increases the angle made by its own system of divergent waves increases, as a result of the detachment of power lines, as a result of the interaction between the turbulent boundary layer and the free surface. It is also observed that the detachment of the current lines from the profile in the area of the flight board generates a wave with a height comparable to the first wave ridge, and with a similar shape of a "whale tail".

0,32

0,40

Figure 3.5. Free surface deformation

Figure 3.11 shows the free surface elevation on the profile surface dimensioned with the profile rope, Z / C, for the 1m draft and the Froude numbers from 0.32 to 0.72, less the Froude numbers 0.16 and 0.24, where the free surface has deformations comparable to the reading error. Also, the large Froude numbers (0.8 ÷1.04) were excluded from the analysis because the free surface did not stabilize during the experimental test, the flow being strongly turbulent manifested by the violent breaking of the wave in the area of the attack board.

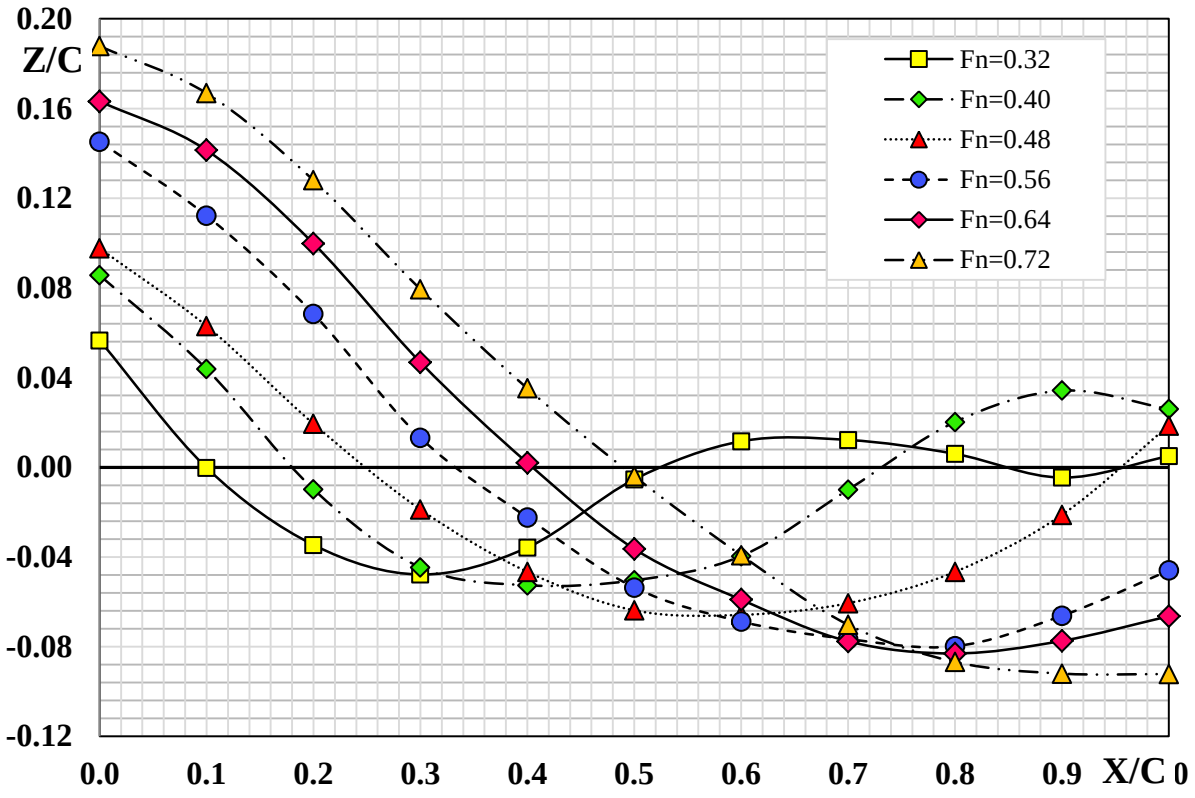

Figure 3.6. Non dimensioned free surface elevation on hydrofoil surface, draft 1m

3.3.1.5.Experimental uncertainty

Tables 3.6 and 3.7 summarize the bias and accuracy limits of possible sources of error, as well as the experimental uncertainty. The results are expressed as a percentage of the respective source of error. At low speeds the values measured by the dynamometer are close in size to the bias limits, as a result the uncertainty also has a high value, around 70% for the lowest speed. As the forward resistance values ncrease and deviate in size from the sources of permanent error (bias), the uncertainty values decrease, reaching up to 3% at the highest speed.

Table 3.3. Experimental uncertainty, draft 1000 mm, Fn 0,16 - 0,56

	Froude					
Surse erori	**0,16**	**0,24**	**0,32**	**0,40**	**0,48**	**0,56**
Geometria modelului						
$B_S\,[\%S]$	1.02E+00	1.02E+00	1.02E+00	1.02E+00	1.02E+00	1.02E+00
$B_S^2\theta_S^2\,[\%C_T]$	2.460E-04	3.467E-04	5.383E-04	1.328E-03	3.034E-03	4.888E-03
Viteza căruciorului						
$B_{Uc}\,[\%I_C]$	3.500E-05	5.300E-05	7.100E-05	8.800E-05	1.060E-04	1.240E-04
$B_{Uc}^2\theta_{Uc}^2\,[\%C_T]$	9.301E-08	1.336E-07	2.094E-07	5.078E-07	1.169E-06	1.893E-06
Proprietățile apei din bazin						
$B_T\,[\%\rho_t]$	8.33E-01	8.33E-01	8.33E-01	8.33E-01	8.33E-01	8.33E-01
$B_{\rho 1}\,[\%\rho_t]$	1.124E-03	1.124E-03	1.124E-03	1.124E-03	1.124E-03	1.124E-03
$B_{\rho 2}\,[\%\rho_t]$	7.128E-03	7.128E-03	7.128E-03	7.128E-03	7.128E-03	7.128E-03
$B_\rho\,[\%\rho_t]$	7.214E-02	7.214E-02	7.214E-02	7.214E-02	7.214E-02	7.214E-02
$B_\rho^2\theta_\rho^2\,[\%C_T]$	1.241E-08	1.749E-08	2.716E-08	6.699E-08	1.531E-07	2.466E-07
Rezistența la înaintare a modelului						

B_{R1} [%R]	5.000E-03	5.000E-03	5.000E-03	5.000E-03	5.000E-03	5.000E-03
B_{R2} [%R]	3.511E+01	1.971E+01	1.185E+01	6.003E+00	3.257E+00	2.139E+00
B_R [%R]	3.511E+01	1.971E+01	1.185E+01	6.003E+00	3.257E+00	2.139E+00
$B_R^2\theta_R^2$ [%C_T]	2.938E-01	1.305E-01	7.321E-02	4.637E-02	3.118E-02	2.167E-02
Coeficientul rezistenței la înaintare						
B_{C_T} [%C_T]	**35.12**	**19.73**	**11.89**	**6.09**	**3.41**	**2.37**
P_{C_T} [%C_T]	**69.15**	**64.35**	**28.54**	**19.53**	**10.27**	**7.60**
I_{C_T} [%C_T]	**77.56**	**67.31**	**30.92**	**20.46**	**10.82**	**7.96**

Table 3.4. Experimental uncertainty, draft 1000 1000 mm, Fn 0.64 -1,04

	Froude					
Surse erori	**0,64**	**0,72**	**0,80**	**0,88**	**0,96**	**1,04**
Geometria modelului						
B_S [%S]	1.02E+00	1.02E+00	1.02E+00	1.02E+00	1.02E+00	1.02E+00
$B_S^2\theta_S^2$ [%C_T]	5.482E-03	5.452E-03	5.180E-03	4.999E-03	4.831E-03	4.753E-03
Viteza căruciorului						
B_{Uc} [%I_C]	1.420E-04	1.600E-04	1.770E-04	1.940E-04	2.120E-04	2.300E-04
$B_{Uc}^2\theta_{Uc}^2$ [%C_T]	2.132E-06	2.127E-06	2.003E-06	1.919E-06	1.861E-06	1.836E-06
Proprietățile apei din bazin						
B_T [%ρ_t]	8.33E-01	8.33E-01	8.33E-01	8.33E-01	8.33E-01	8.33E-01
$B_{\rho 1}$ [%ρ_t]	1.124E-03	1.124E-03	1.124E-03	1.124E-03	1.124E-03	1.124E-03
$B_{\rho 2}$ [%ρ_t]	7.128E-03	7.128E-03	7.128E-03	7.128E-03	7.128E-03	7.128E-03
B_ρ [%ρ_t]	7.214E-02	7.214E-02	7.214E-02	7.214E-02	7.214E-02	7.214E-02
$B_\rho^2\theta_\rho^2$ [%C_T]	2.765E-07	2.750E-07	2.613E-07	2.522E-07	2.437E-07	2.397E-07
Rezistența la înaintare a modelului						
B_{R1} [%R]	5.000E-03	5.000E-03	5.000E-03	5.000E-03	5.000E-03	5.000E-03
B_{R2} [%R]	1.727E+00	1.510E+00	1.372E+00	1.247E+00	1.141E+00	1.039E+00
B_R [%R]	1.727E+00	1.510E+00	1.372E+00	1.247E+00	1.141E+00	1.039E+00
$B_R^2\theta_R^2$ [%C_T]	1.583E-02	1.204E-02	9.448E-03	7.533E-03	6.098E-03	4.975E-03
Coeficientul rezistenței la înaintare						
B_{C_T} [%C_T]	**2.37**	**2.00**	**1.82**	**1.71**	**1.61**	**1.53**
P_{C_T} [%C_T]	**7.53**	**6.96**	**6.12**	**6.10**	**5.45**	**2.77**
I_{C_T} [%C_T]	**7.79**	**7.20**	**6.36**	**6.31**	**5.66**	**3.13**

3.3.1.6. Wave profile on hydrofoil

The wave profie on the surface of the experimental model is obtained based on the fine grid of 5x5 mm glued on the profile and the filming perpendicular to the diametrical plane of the profile. The wave height is dimensioned by dividing the profile string by the data reduction relationship.

Table 3.8 shows the uncertainties calculated for Fn = 0.32 for each reading point on the free surface. The wave height, z, is presented in values relative to the calm water level.

Table 3.5. Wave profile on hydrofoil uncertainty, pescaj 1000 mm, Fn 0,32

C [m]	x/C	Z [m]	B_z [m]	θ_z [%C]	B_c [m]	θ_c [%C]	B_ς [m]	P_ς [m]	I_ς [m]	I_ς [%C]
0	0	0.0283	2.000E-03	2.000E+00	2.000E-03	1.132E-01	4.006E-03	5.000E-03	6.407E-03	1.281E
0.05	0.1	-0.0001	2.000E-03	2.000E+00	2.000E-03	-4.000E-04	4.000E-03	5.000E-03	6.403E-03	1.281E
0.1	0.2	-0.0173	2.000E-03	2.000E+00	2.000E-03	-6.920E-02	4.002E-03	5.000E-03	6.405E-03	1.281E
0.15	0.3	-0.0239	2.000E-03	2.000E+00	2.000E-03	-9.560E-02	4.005E-03	5.000E-03	6.406E-03	1.281E
0.2	0.4	-0.0179	2.000E-03	2.000E+00	2.000E-03	-7.160E-02	4.003E-03	5.000E-03	6.405E-03	1.281E
0.25	0.5	-0.0027	2.000E-03	2.000E+00	2.000E-03	-1.080E-02	4.000E-03	5.000E-03	6.403E-03	1.281E
0.3	0.6	0.0058	2.000E-03	2.000E+00	2.000E-03	2.320E-02	4.000E-03	5.000E-03	6.403E-03	1.281E
0.35	0.7	0.0061	2.000E-03	2.000E+00	2.000E-03	2.440E-02	4.000E-03	5.000E-03	6.403E-03	1.281E
0.4	0.8	0.003	2.000E-03	2.000E+00	2.000E-03	1.200E-02	4.000E-03	5.000E-03	6.403E-03	1.281E
0.45	0.9	-0.0023	2.000E-03	2.000E+00	2.000E-03	-9.200E-03	4.000E-03	5.000E-03	6.403E-03	1.281E
0.5	1	0.0025	2.000E-03	2.000E+00	2.000E-03	1.000E-02	4.000E-03	5.000E-03	6.403E-03	1.281E

It is observed that the components with the geometry of the model and the reading accuracy limit have the highest weight. The uncertainty of reading the free surface by the method used is 1.28% of the length of the rope and is maintained in the other waves presented above.

3.3.2.Numerical calculation of the free surface flow around hydrofoil

3.3.2.1.Introduction

Next, the numerical study of the flow around the vertical profile NACA 0012 that penetrates the free surface is presented. Using the Ansys 12.1 program, the RANS equations were solved in a segregated manner, supplemented by the equations of the turbulence model suitable for free surface calculations. In this case, two turbulence models with two equations were tested, $k-\omega$ SST and $k-\varepsilon$ Realizable ($k-\varepsilon$ R). For the calculation of the free surface the VOF technique was used, considering the free surface as an iso-surface of 0.5 water / air. The coupling of pressure and speed was solved with the PISO algorithm. The pressure was discretized with the PRESTO numerical scheme, for the free surface the geometric reconstruction was used, and for the impulse and turbulent sizes the QUICK scheme was used.

The numerical model has the same dimensions as the experimental model, namely 0.5 m rope and 1.2 m wingspan. The computational domain (figure 3.14, a, b) is of parallelepiped shape, having a length equal to the width of the upstream profile to meet the radiation condition upstream, two lengths downstream and laterally, to allow the body wave system produced to leave the computing range only across the downstream border. Also, the range extends one span below the profile and half a span above the profile thus avoiding the influence of possible end eddies and limited bottom effect.

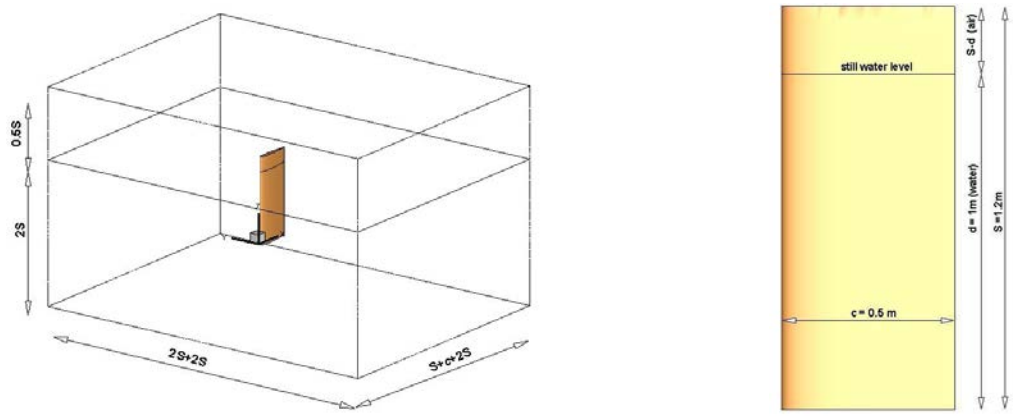

. (a) Computational domain (b) Numerical NACA 0012 model

Figure 3.7 Computational domain dimensions

The solution of the system of equations was done in non-stationary regime, with the passage of time correlated with the volume of the smallest finite volume. It took around 4000 time steps to stabilize the forward resistance and the free surface, with the convergence obtained in a maximum of 20 iterations per time step. The calculations were performed for all 12 experimental speeds and for all 4 drafts.

3.3.2.2.Numerical uncertainties

For the numerical calculations required for validation, three sources of possible errors were identified: truncation errors, iterative errors and discretization errors. The double precision solver was used and in this way the truncation errors were neglected. The iterative errors were neglected, decreasing the residual value from 10^{-3}, recommended by Fluent, to 10^{-4}, obtaining at the same time the convergence on each time step. As a result, the analysis of errors and uncertainties focused on discretization errors, the errors with the largest share in the numerical calculation.

Three discretization grids (Table 3.9) were generated with $\sqrt{2}$ as ratio and the same dimensioned wall distance, $y^+ = 1$, so that in the boundary layer the turbulence models to calculate in a similar way.

Table 3.6. Generated grids

Grila	Fina (1)	Medie (2)	Rară (3)
N_i	2425174	1212587	606294
$\sum V_i$ [m^3]	59,04	59,04	59,04
h_i [m^3]	0,00493	0.00698	0,00987
r21		1,414	
r32			1,414

Hydrofoil resistance is considered as a reference value, and based on the 3 grids, the discretization uncertainty or the convergence index of the grid is calculated, as it is also known in the literature. The following is a tabular calculation for Froude numbers 0.32, 0.48, 0.64. The study variable was considered resistant to advancement.

Table 3.7. Grid uncertainty

Model turbulență	Fn	Grila 1 Rt [N]	Grila 2 Rt [N]	Grila 3 Rt [N]	δG[%]	IG[%]
KWSST	0.16	0.92	0.95	0.97	3.62	4.52
	0.24	1.77	1.85	1.88	3.58	4.48
	0.32	3.47	3.65	3.72	3.42	4.27
	0.40	5.81	6.13	6.26	3.65	4.56
	0.48	8.95	9.85	10.21	6.67	8.33
	0.56	13.60	15.10	15.70	7.21	9.01

	0.64	17.37	19.35	20.24	9.36	11.70
	0.72	20.05	22.47	23.81	14.76	18.46
	0.80	22.74	26.45	28.61	22.77	28.47
	0.88	25.21	29.83	32.42	23.56	29.45
	0.96	27.89	33.86	36.88	21.80	27.25
	1.04	30.80	38.66	42.51	24.52	30.65
KER	0.16	1.21	1.25	1.27	2.52	7.57
	0.24	2.63	2.74	2.80	6.18	7.72
	0.32	4.43	4.66	4.78	6.72	8.40
	0.40	6.76	7.16	7.37	7.04	8.80
	0.48	10.97	12.30	12.78	6.91	8.64
	0.56	15.36	17.12	17.80	7.13	8.91
	0.64	19.86	22.33	23.62	13.66	17.08
	0.72	23.17	26.04	27.75	18.35	22.94
	0.80	26.26	30.60	33.22	25.38	31.73
	0.88	29.14	35.34	38.92	29.11	36.39
	0.96	32.69	39.98	44.00	27.43	34.29
	1.04	36.26	45.87	50.84	28.36	35.45

It is observed that in the area of large froude numbers, where the phenomenon of breaking the wave is consistent, the level of uncertainties is higher than in the area of froude numbers where the free surface is not affected by the broken wave. The basic principle of VOF theory says that the two fluids considered in the calculation are immiscible, and how the phenomenon of breaking the wave manifests itself with a mixture of air bubbles in the water, and this can lead to a high degree of uncertainty. Another possible source of errors and uncertainties at high speeds is the grid itself. As the wave grew, the grid area for the free surface had to be increased to include the entire elevation of the wave on the body. For reasons of hardware resources, the calculation went on a single fine grid for all speeds, hence and probably the high level of uncertainty at high speeds.

3.3.3. CFD-EFD comparison

The forward resistance was calculated (CFD) for both turbulence models tested and compared with the experimental results (EFD), and shown for the 1m draft in Figure 3.17. It is observed that both turbulence models qualitatively describe the evolution of the forward resistance in relation to the Froude number, but quantitatively the $k-\omega$ SST turbulence model produces results by 60%, on average, compared to the experimental ones compared to 85% obtained with the $k-\varepsilon$ R model.

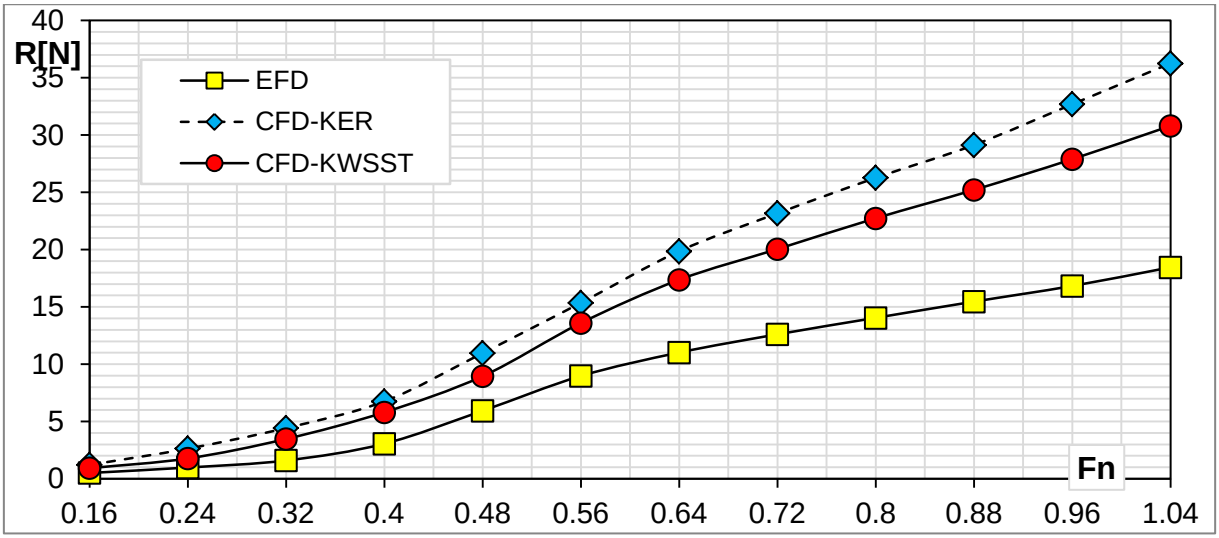

Figure 3.8. Hydrofoil drag, comparison experiment (EFD) – numerical calculation (CFD), draft 1m

Table 3.11 presents in value the experimental and numerical results obtained with the fine grid, together with the comparison error, E, the numerical uncertainty, D, as well as the validation uncertainty, I_{val}. It is pointed out that the comparison error is less than the uncertainty of validation, as a result the modeling errors are insignificant.

Table 3.8. Drag coefficient based on the fine, medium and coarse grid

Fn	**EFD**	**CFD-KWSST**	**E=S-D**	**D**	**I_{val}**	**CFD-KER**	**E=S-D**	**D**	**I_{val}**
	Rt[N]	Rt[N]	[%]	[%]	[%]	Rt[N]	[%]	[%]	[%]
0.16	0.506	0.925	82.77	4.52	82.9	1.211	139.27	7.57	139.5
0.24	0.982	1.775	80.75	4.48	80.9	2.628	167.66	7.72	97.1
0.32	1.597	3.475	117.59	4.27	117.7	4.430	177.38	8.40	96.6
0.4	3.062	5.805	89.59	4.56	89.7	6.757	120.69	8.80	92.9
0.48	5.936	8.953	50.82	8.33	51.5	10.969	84.79	8.64	79.2
0.56	8.972	13.595	51.53	9.01	52.3	15.356	71.16	8.91	71.2
0.64	11.019	17.368	57.62	11.70	58.8	19.862	80.25	17.08	68.4
0.72	12.607	20.047	59.01	18.46	61.8	23.166	83.75	22.94	66.6
0.80	14.047	22.739	61.88	28.47	68.1	26.264	86.97	31.73	69.1
0.88	15.463	25.214	63.06	29.45	69.6	29.135	88.42	36.39	68.6
0.96	16.829	27.895	65.75	27.25	71.2	32.691	94.25	34.29	64.0
1.04	18.458	30.804	66.89	30.65	73.6	36.262	96.46	35.45	61.9

Figure 3.18 shows the waves on the hydrodynamic profile. The numerically calculated waves are compared with the experimental waves and presented graphically in Figure 3.18, for the Froude numbers 0.32, 0.48 and 0.64. The abscissa of the diagrams represents the level of calm water, and the values presented were dimensioned with the length of the profile string.

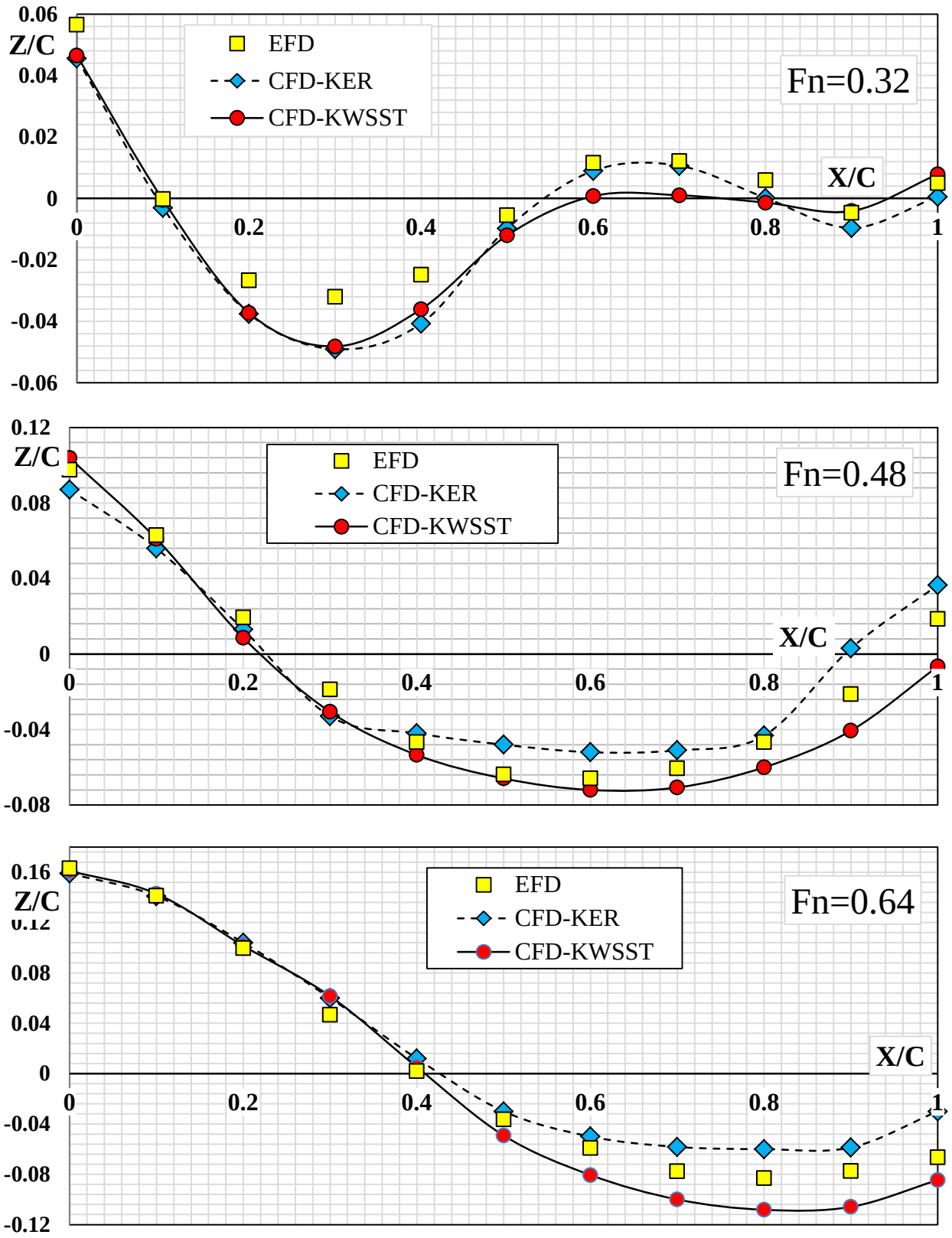

Figure 3.9. Wave profile on hydrofoil, comparison EFD vs CFD

Qualitatively, both models of turbulence capture the shape of the free surface on the profile, and quantitatively it is observed that in the area of the leading edge, both models of turbulence manage to capture the development of the experimental wave at close values. The $k-\omega$ SST model underestimates the wave gap, which is visible in all three Froude numbers, but also the second wave ridge at Fn = 0.32, while the $k-\varepsilon$ R model

overestimates the wave gap, and at Fn = 0.32 it manages to approach of the second wave ridge.
The numerical studies validated by the experimental ones led to the establishment of the methodology for numerical calculation of the free surface flow around a hydrodynamic profile. In future systematic studies, the $k-\omega$ SST turbulence model will be used. By Froude similarity, the height of the wave in the area of the attack board can be approximated so that the discretization grid accurately captures the deformed free surface.

3.4.Junction flow

The flow around the junctions between a profile and a plate is manifested by the generation of vortex structures as a result of the interaction between the boundary layer on the plate and the boundary layer on the profile. Two benchmark tests have been identified in the literature: one for the flat plate, and the other for the NACA 0012 profile. As a result, the study for the validation of the immersion junction calculation methodology will have two components: on the one hand, the flow on the plate will be studied. flat in relation to the results obtained by Yang and Voke (1993), and centralized in case 73 of the ERCOFTAC database, and on the other hand will study the flow around the aerodynamic profile NACA0012 in relation to the results obtained by NASA Langley Research Center- Turbulence Modeling Resource.

3.4.1.Flow over flat plate
3.4.1.1.Benchmark

The study considered for the validation of the viscous flow on the flat plate is the numerical experiment performed by Yang and Voke in 1993 and made public with the number C.73 from the ERCOFTAC database, Classic collection. The numerical study consists in the calculation using LES (Large Eddies Simulation) at parallel flow with a flat plate measuring 300mmx20mm, without pressure gradient, with 5% turbulence imposed and a speed of 9.6 m/s.

3.4.1.2.Verification and Validation

Taking into account the peculiarity of the flow, three two-dimensional grids, 300mm x 30mm, with grid thinning ratios, $r_{ij} = 2$, were generated, according to ASME V&V 20 (2009). To keep the same solving conditions in the boundary layer, the grids were generated starting from the same distance to the dimensionless wall, y+ = 1.

Table 3.9. Generated grids

Grila	Fina (1)	Medie (2)	Rara (3)
N_i	8000	2000	500
$\sum A_i$ [m^2]	0,009	0,009	0,009
h_i [m^2]	1,125E-06	4,500E-06	1,800E-05
r21		2	
r32			2

The numerical simulations were performed with Ansys Fluent v12, with the pressure-based solver, related to the incompressible flow. The input border was defined as “velocity inlet, the output border was defined as presure outlet. The wall condition was applied to the plate, and the symmetry condition was applied to the upper border. All calculations were performed with the double precision solver, and for convergence the value 10^{-6} was imposed for residues. As a result, rounding and iterative errors were neglected, being considered only discretization errors in determining numerical errors.

Simulările numerice au fost realizate cu Ansys Fluent v12, cu solverul bazat de presiune, aferent curgerii incompresibile. Frontiera de intrare a fost definită ca „ velocity inlet, frontiera de ieșire a fost definită ca presure outlet. Pe placă s-a aplicat condiția de perete, „wall", iar pe frontiera superioară s-a aplicat condiția de simetrie, „symmetry". Toate calculele au fost realizate cu solverul cu dublă precizie, iar pentru convergență a fost impusă valoarea 10^{-6} pentru reziduuri. Drept urmare, erorile de rotunjire și iterative au fost neglijate, fiind considerate numai erorile de discretizare în determinarea erorilor numerice.

Au fost testate toate modelele de turbulență pentru curgerea în regim staționar disponibile în Ansys v12, iar rezultatele coeficientului de rezistență la înaintare împreună cu eroarea și incertitudinea de discretizare sunt prezentate în Table 3.13. Deși nu este un model de turbulență, a fost considerat totusi și cazul curgerii laminare, deoarece se studiază și tranziția de la curgerea laminară la curgerea turbulentă. Modelele de turbulență din familia $k-\varepsilon$ se pretează mai bine pe grilele cu y^+>30. Drept urmare, pentru a putea fi utilizate pe grila de studiu, la y^+=1, au fost activate funcțiile la perete prin opțiunea „ Enhanced wall treatment".

Table 3.10. Drag coefficient based on the fine, medium and coarse grid

Model turbulenta	**Fina (1)**	**Medie (2)**	**Rara (3)**	**δ_G [%]**	**I_G [%]**
		Cd [x10^3]			
Laminar*	3.224	3.206	3.118	0.1370	0.1713
SA	6.905	6.964	6.970	0.0902	0.1127
$k-\varepsilon$ Standard	7.016	7.036	7.074	0.2931	0.3663
$k-\varepsilon$ RNG	7.007	7.025	7.055	0.3517	0.4397
$k-\varepsilon$ Realizable	7.021	7.043	7.088	0.2932	0.3665
$k-\omega$ Standard	6.614	6.548	6.004	0.1388	0.1735
$k-\omega$ SST	6.348	6.594	6.124	4.2711	5.3389
$k-\omega$ SST-TF	6.713	6.594	6.124	0.5959	0.7448
RSM-LPS-EWT	6.630	6.716	6.990	0.6042	0.7553
RSM-LR	6.180	5.805	5.390	6.0764	7.5955
RSM-LR-TF	5.243	4.874	4.435	7.0378	8.7972

Rezultatele obținute cu grila fină se compara cu cele obținute de Yang și Voke, și împreună cu eroarea de validare și incertitudinea de validare, sunt prezentate în Table 3.14.

Table 3.11. Drag coefficient validation error and uncertainty

Model turbulenta	**Fina (1)**	**Experiment.**	**E**	**D**	**I_{val}**
	Cd [x10^3]		**[%]**	**[%]**	**[%]**
Laminar*	3.224	2.970	8.570	0.1713	8.569
SA	6.905	6.883	0.318	0.1127	0.297
$k-\varepsilon$ Standard	7.016	6.883	1.940	0.3663	1.905
$k-\varepsilon$ RNG	7.007	6.883	1.804	0.4397	1.750
$k-\varepsilon$ Realizable	7.021	6.883	2.001	0.3665	1.967
$k-\omega$ Standard	6.614	6.883	-3.908	0.1735	3.904
$k-\omega$ SST	6.348	6.883	-7.767	5.3389	5.642
$k-\omega$ SST-TF	6.713	6.883	-2.467	0.7448	2.351
RSM-LPS-EWT	6.630	6.883	-3.680	0.7553	3.601
RSM-LR	6.180	6.883	-10.206	7.5955	6.816
RSM-LR-TF	5.243	6.883	-23.818	8.7972	22.134

It is observed that the turbulence model with an equation, Spalart Allmaras produces the result closest to the experimental value, and the highest values of the validation error are obtained with the Reynolds Stress Model with the option Low Reynolds transitional flow.

3.4.2.Flow around NACA 0012 hydrofoil

3.4.2.1.Benchmark

For the validation of the viscous flow around the aero-hydrodynamic profile NACA 0012 was chosen the study presented by NASA Langley Research Center and presented on Turbulence Modeling resources, in case of flow without angle of attack at Reynolds number $3x10^6$.

The NACA 0012 profile is generated with the polynomial:

$$y = \pm 0.6 \cdot \left[0.2969\sqrt{x} - 0.1260x - 0.3516x^2 + 0.2843x^3 - 0.1015x^4 \right] \quad (3.69)$$

3.4.2.2.Verification and Validation

Three 3D O-H grids, with grid coarsening ratios, $r_{ij} = \sqrt{2}$, were generated, according to ASME V&V 20 (2009), on a circular calculation range with a minimum radius of three rope lengths. The generation of the fine grid is performed by hyperbolic extrusion, starting from the profile rope, discretized with 150 nodes, with the cell growth ratio in the boundary layer, r = 1.1, obtaining the two-dimensional shape of type O having 301x94 cells. On the height of the calculation range, or on the width of the profile, the basic grid is extruded on a unit length with 80 equidistant nodes, finally obtaining the grid with 301x94x80 knots. To keep the same solving conditions in the boundary layer, the grids were generated starting from the same distance to the dimensionless wall, y+ = 1.

Table 3.15 presents the grids generated in the study, fine, medium and rare.

Table 3.12. Generated grids

Grila	Fina (1)	Medie (2)	Rara (3)
N_i	2204100	771680	269100
$\sum V_i$ [m^3]	34.3	34.3	34.3
h_i [m^3]	1.555E-05	4.441E-05	1.274E-04
r21		1,414	
r32			1,414

All RANS turbulence models for steady flow available in Ansys v12 were tested, and the results of the forward resistance coefficient together with the discretization error and uncertainty are presented in Table 3.16. The lowest values of the discretization uncertainty are obtained with the $k-\omega$ Standard and Reynolds stress model-Linear pressure strain models, around 3%, and the highest values are obtained with the Reynolds stress model with the Low Reynolds option.

Table 3.13. Drag coefficient based on the fine, medium and coarse grid

Model turbulenta	Fina (1)	Medie (2)	Rara (3)	δ_G [%]	U_G [%]
	Cd [x10^3]				
SA-VB	7.426E-03	8.117E-03	9.026E-03	29.40	36.75
SA-S/VB	7.363E-03	8.055E-03	8.964E-03	29.78	37.22
$k-\varepsilon$ Standard	1.086E-02	1.998E-02	1.658E-02	49.94	62.42
$k-\varepsilon$ RNG	6.497E-03	9.475E-03	1.466E-02	61.87	77.33
$k-\varepsilon$ Realizable	4.986E-03	5.823E-03	6.948E-03	48.89	61.11
$k-\omega$ Standard	1.724E-02	2.061E-02	4.558E-02	3.06	3.82

$k-\omega$ SST	7.102E-03	6.121E-03	7.423E-03	42.30	52.87
$k-\omega$ SST-TF	6.263E-03	4.372E-03	5.365E-03	33.40	41.75
RSM-LPS-EWT	4.886E-03	5.738E-03	1.254E-02	2.50	3.12
RSM-LR	4.520E-03	5.315E-03	6.302E-03	72.65	90.82

The results obtained with the fine grid are compared with those obtained by Ladson, 1988, Gregory and O'Reilly, 1970, Abbott and von Doenhoff, 1959, and Jespersen et al. 2016, and together with the validation error and the validation uncertainty, are presented in table 3.17.

Table 3.14. Drag coefficient validation error and uncertainty

Model turbulenta	Fina (1)	Experiment	E	D	I_{val}
	Cd [x10^3]		[%]	[%]	[%]
SA-VB	7.426	8.255	-10.042	36.750	38.097
SA-S/VB	7.363	8.255	-10.803	37.219	38.755
$k-\varepsilon$ Standard	10.857	8.255	31.530	62.421	69.932
$k-\varepsilon$ RNG	6.497	8.255	-21.293	77.334	80.212
$k-\varepsilon$ Realizable	4.986	8.255	-39.601	61.107	72.817
$k-\omega$ Standard	17.236	8.255	108.804	3.824	108.871
$k-\omega$ SST	7.102	8.255	-13.960	52.869	54.681
$k-\omega$ SST-TF	6.263	8.255	-24.127	41.751	48.220
RSM-LPS-EWT	4.886	8.255	-40.808	3.120	40.928
RSM-LR	4.520	8.255	-45.242	90.817	101.462

If the $k-\omega$ standard model is excluded from the error analysis, it is observed that the turbulence model with an equation, Spalart Allmaras, with both options, Voticity based and Strain / Vorticity-based, produces the result closest to the experimental value, within 10%, and the biggest differences are obtained with the Reynolds stress model with the Low Reynolds option. Regarding the validation uncertainty, the models that obtain the values minimum, 38%, and maximum, 101%, are kept.

Chapter 4. Flow around the junction without free surface

4.1.Introduction

This chapter presents the results of numerical investigations on the free surface flow around the junctions, more precisely the study of the influence of the angle between the profile and the plate, the study of the influence of plate curvature, the study of the influence of current velocity on the junction. The influence of the angle between the profile and the plate is studied by tilting the profile in three directions: lateral, upstream and downstream, with three steps, 15, 30 and 45 degrees in relation to the normal vertical direction to the plate, and joins the vertical profile as a sum ten geometric positions of the profile relative to the motherboard. For the study of the influence of the curvature of the base plate, the flat plate is curved with four radii of curvature in each side of the flat plate, obtaining concave and convex plates. The curvature of the plate is achieved by changing the coordinates of the grid nodes, so that the area of the plate as well as the distribution of the grid lines in relation to the profile are identical to the case of the flat plate. To study the influence of speed, consider the flow at three Reynolds numbers: 10^6, $5x10^6$ and 10^7, so as to cover the flow area of a profile mounted on a vessel shell that acts as a flow correction device (ESD). As a result, the results presented below centralize 9x10x3 (plate curvature x profile angle x velocities) = 270 calculation cases, respecting, of course, the calculation methodology together with the numerical model established in the previous chapter.

4.2. Objectives

Starting from the factors that influence the flow around the junctions described in Chapter 1, the objectives that define the structure of this chapter are:

- Study of the influence of the profile inclination in relation to the motherboard;
- Study of the influence of flat, concave and convex plate;
- Study of the influence of the velocity

4.3.Numerical model

4.3.1. Boundary conditions

Being circular in shape, the calculation range has five boundaries: profile, base plate, fluid inlet, fluid outlet, and upper boundary, (figure 4.1). The no slip condition (wall) is imposed on the profile surface as well as on the base plate. If in reality the objects move through the fluid, in numerical simulations the object is held in a fixed position and the fluid moves. Thus, on the input border, the speed is declared at infinity upstream through the condition "velocity inlet". As the flow is aligned with the horizontal plane, only the horizontal longitudinal component for zero angle of attack is declared. The pressure outlet is used on the fluid outlet boundary of the field. As the flow is turbulent, turbulent boundary conditions are declared on the entry and exit borders. In the case of the Spalart-Allmaras turbulence model, Fluent recommends for the ratio between turbulent viscosity and molecular viscosity, μ_t/μ ,the value 5. On the upper boundary the sliding wall condition is required, namely symmetry. The symmetry condition was chosen due to its simplicity and robustness. The initial tests led to the minimum radius of the range of three rope lengths, a dimension at which the influence of the boundaries on the flow in the vicinity of the profile is not felt.

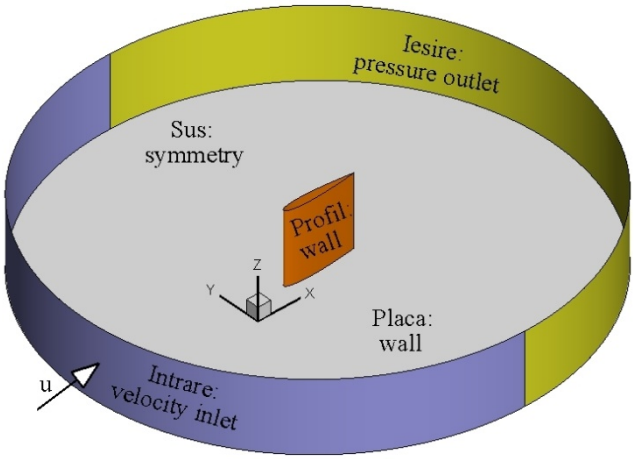

Figure 4.1. Boundary conditions

4.3.2. Numerical schemes

The RANS equations together with the equation related to the Spalart-Allmaras turbulence model are solved with Ansys v12, by the finite volume method. Pressure and speed are coupled by the SIMPLEC algorithm. The pressure is interpolated using the standard scheme, and the turbulent impulse and viscosity with first and second order schemes in countercurrent. For the stability of the solution, first the convergence is obtained based on the first order schemes and then the calculation is continued until the convergence with the second order schemes is obtained in countercurrent.

All calculations were performed with the double precision solver, and for convergence the value 10^{-6} was imposed for residues.

4.3.3.Grid generation

The generation of the grid is performed by hyperbolic extrusion, starting from the profile rope, discretized with 150 knots, in the $O\eta$ direction, with the growth rate of the cells in the boundary layer, obtaining the two -dimensional O shape (figure 4.2) having 301x94 cells . At the threshold of 94 cells, the minimum radius of three rope lengths required by the pilot tests is obtained. The first grid line corresponds to the dimensionless distance, $y^+ = 1$. The discretization grid in the basic plan is the same grid considered fine in previous verification and validation calculations (Chapter 3.8).

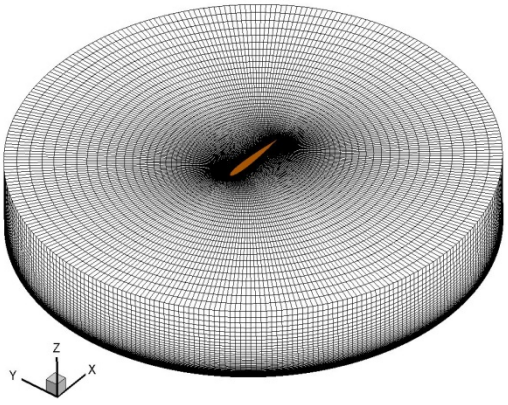

Figure 4.2. O-H grid

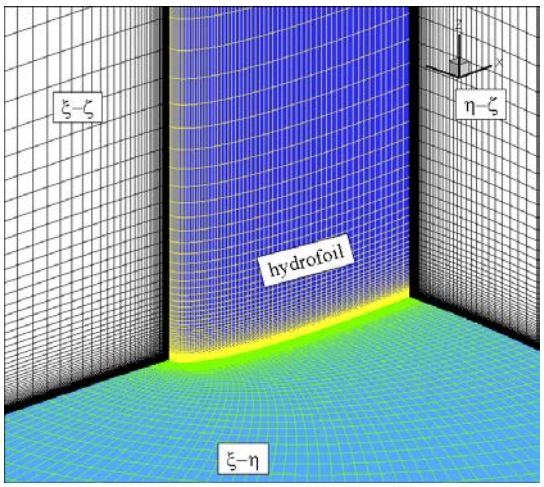

Figure 4.3. O-H grid on hydrofoil an base plate

In order to study the influence of the inclination angle of the profile on the junction, the basic plane $O\xi\eta$ is extruded in the direction of each inclination angle, obtaining a grid of 301x94x80 nodes that respect the quality criteria, orthogonality and spacing of the grid lines (figure 4.3). In all ten hypostases of the profile, the horizontal section NACA 0012 parallel to the flow is kept.

4.4.Results and discussions

The flow is assumed to be completely turbulent and numerical simulations were first performed for the Reynolds number 10^6 to clarify the flow mechanisms, but also to provide a detailed description of the forces acting around the junction. When the fluid moves along the base plate and encounters an obstacle, the profile, the blocking phenomenon appears which, due to the high adverse pressure gradients, lead to the separation of the boundary layer, but also to the development of vortex structures. Depending on the flow conditions, these vortex structures may consist of one or more vortices, counter-rotating, Figure 4.4. A main vortex is observed, whose core is approximately 2% of the rope length upstream of the profile and 0.2% of the rope length in the vicinity of the plate, but also a secondary vortex of rotation opposite to the primary one.

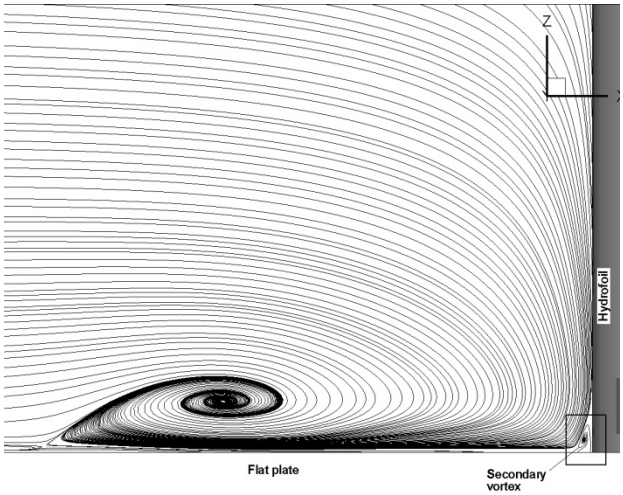

(a)

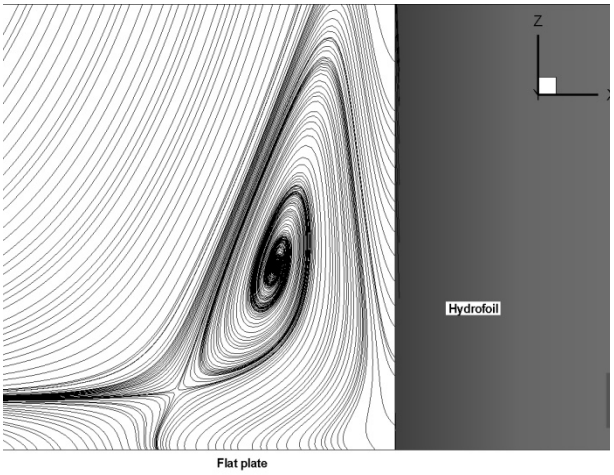

(b)

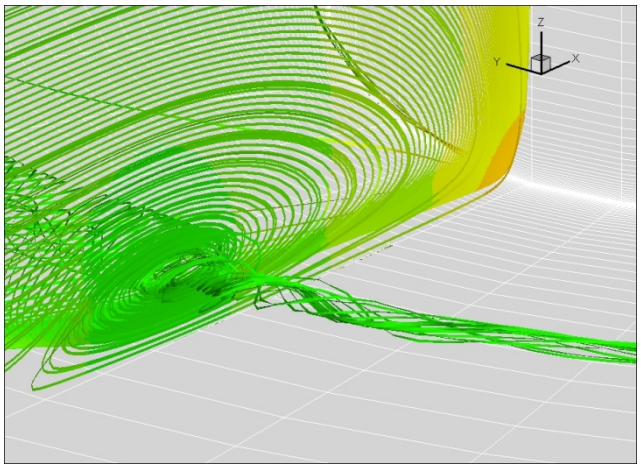

(c)

(a) Main vortice- streamlines in symmetry plane
(b) Secondary vortice- streamlines in symmetry plane
(c) Main vortice- 3D streamlines

Figure 4.4. Vortices

The filaments in the vortices that form upstream move downstream, along the profile, forming the so-called whirlpool system. The intensity of the vortices decreases with the distance of the plate and the leading edge of the profile.

4.4.1.The influence of the hydrofoil inclination angle

The influence of the angle between the profile and the plate is studied by tilting the profile in three directions: lateral, upstream and downstream, with three steps, 15, 30 and 45 degrees from the vertical plane, constantly keeping the profile cord parallel to the flow direction. Together with the case of the right vertical profile, it sums up ten geometric positions of the profile in relation to the motherboard.

First, the influence of the inclination angle on the junction for the diametrically inclined profile, upstream and downstream, mounted on the flat plate, was studied. In the case of the upstream inclined profile, see Figure 4.6, it is observed that the area exposed to high pressure gradients decreases and approaches the junction area as the angle of inclination increases. In the case of the downward-sloping profile, Figure 4.7, the high pressure gradients move downstream and towards the top of the profile away from the area of the leading edge of the junction, as a result of viscous dissipation.

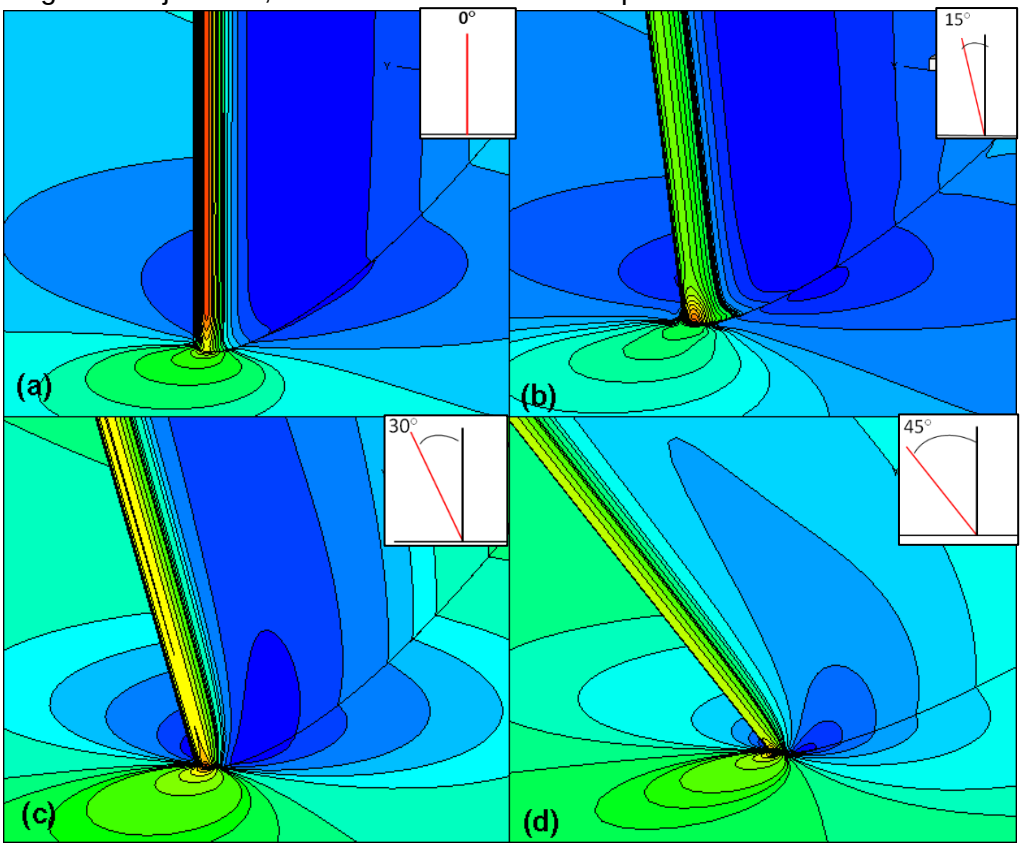

Figure 4.5. Pressure distribution around junction –comparison between vertical and upstream inclined hydrofoil

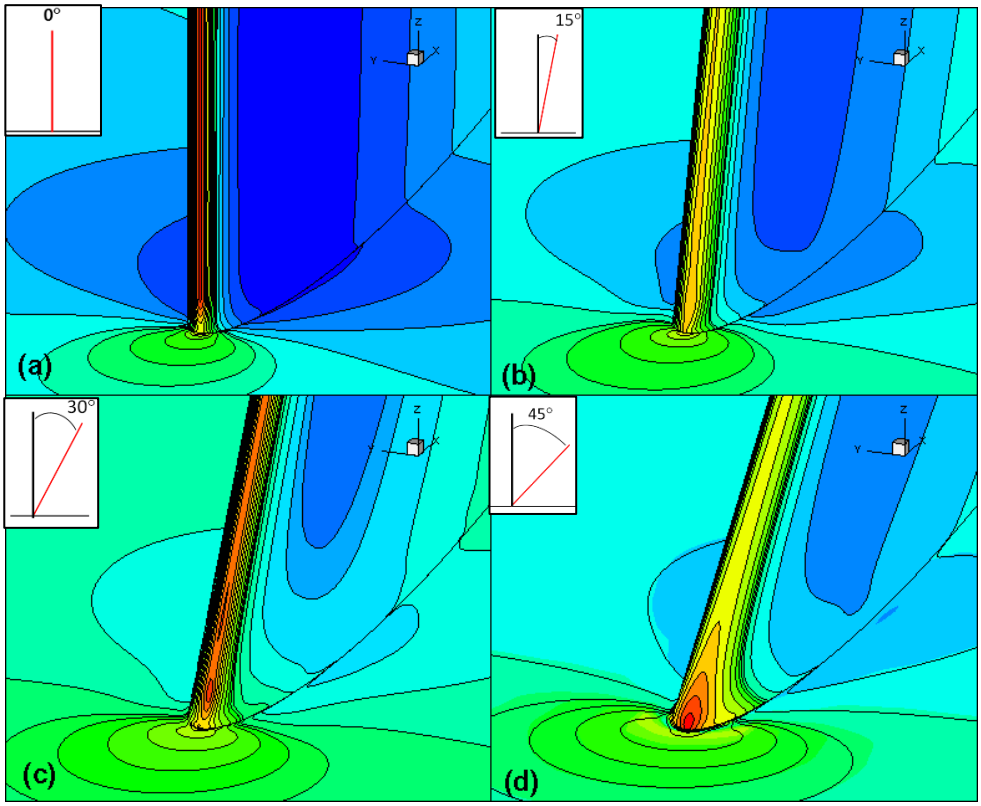

Figure 4.6. Pressure distribution around junction –comparison between vertical and downtream inclined hydrofoil

It is also observed the decrease of the turbulent intensity of the turbulent structures from the inclined profile upstream to the inclined profile downstream through the two-dimensional current lines, figures 4.8 and 4.9, and three-dimensional ones drawn in figure 4.10. At an upstream inclination of 15o, a concentration of the core of the main vortex is observed together with an approximation of the secondary one. Also, the development of a new pair of counter-rotating vortices is observed, upstream of the main vortex. As can be seen from the images, as the angle of inclination increases, the vortex system is pressed between the solid surfaces, until its effects diminish.

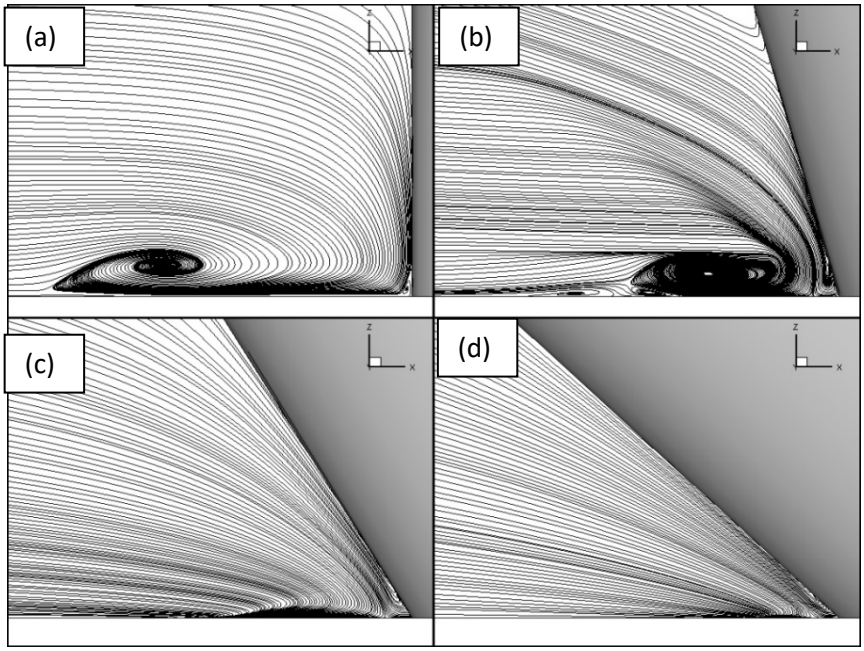

Figure 4.7. Streamlines –comparison between vertical and upstream inclined hydrofoil

La profilul înclinat spre aval liniile de curent se apropie de muchia de atac a profilului conducând la o rocadă a poziției vârtejului principal cu cel secundar, împreună cu creșterea în intensitate și a nucleului vârtejului principal. Dacă la profilul vertical drept, vârtejul secundar este în proximitatea bordului de atac, la 30 și 45 de grade acesta se depărtează de profilul de atac.

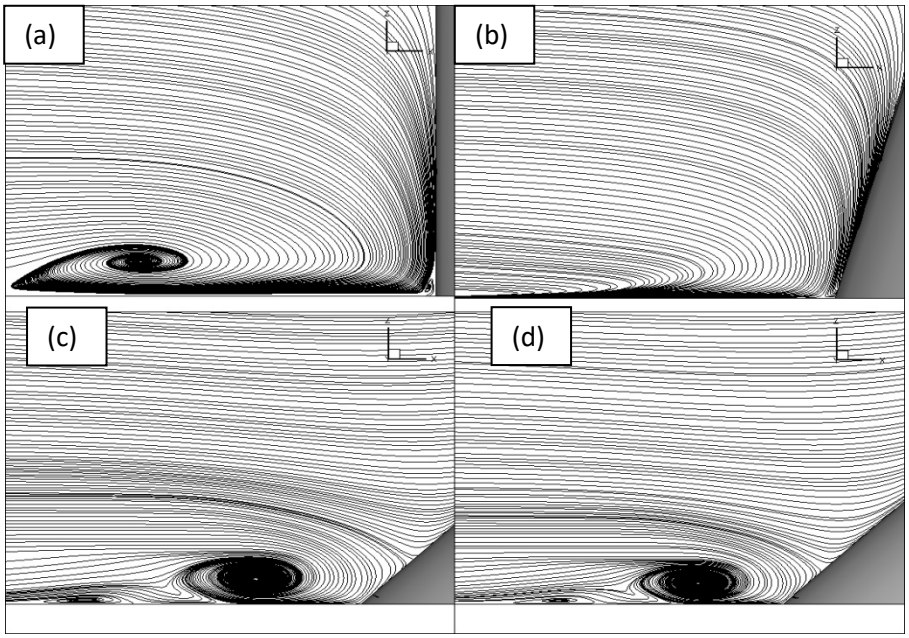

Figure 4.8. Streamlines –comparison between vertical and downstream inclined hydrofoil

If the profile is tilted to the side, the flow field is no longer symmetrical, neither on the plate nor on the profile. Tilt to the side induces a translation of the stagnation point to the side with the smaller angle. The effect of the lateral inclination is observed in figure 4.11, through the current lines drawn in the vicinity of the plate but also through the distribution of the pressure contours on the profile. The same phenomenon is observed as in the case of flow with angle of attack (Kuwahara, 2000).

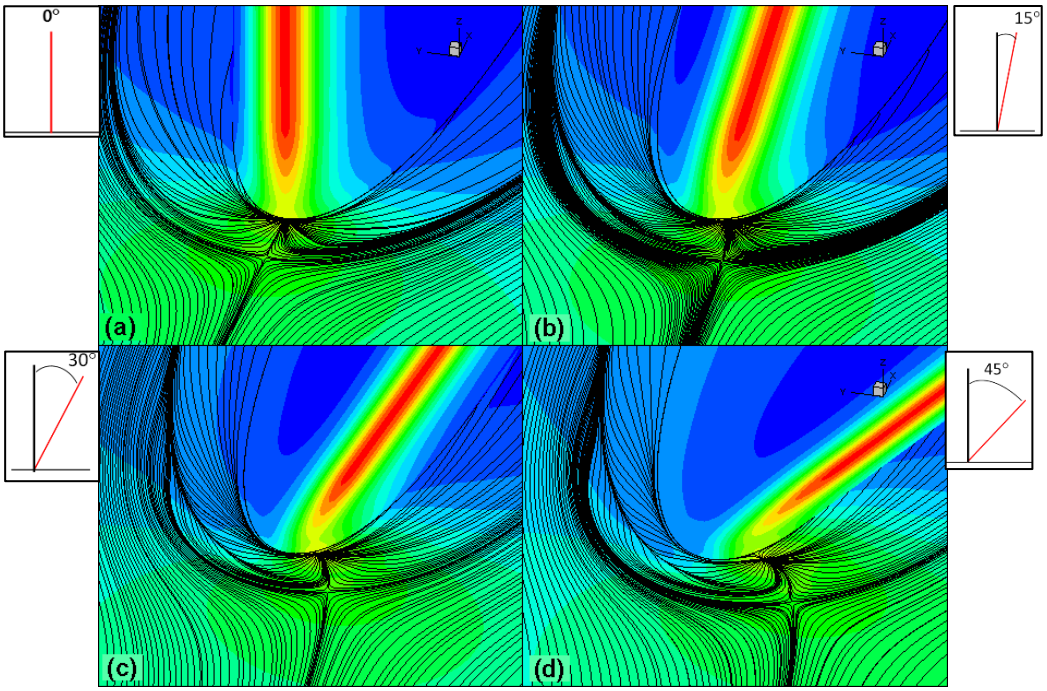

Figure 4.9. Streamlines –comparison between vertical and laterally inclined hydrofoil

Regarding the evolution of the coefficients of resistance to advance on the support plate, numerical studies showed a decrease of 0.5% on average, but not more than 1%, in the case of flat plate regardless of the direction of inclination of the profile, concave and convex plate for the upstream and downstream inclined profile. Also, a decrease of 9% of the total coefficient of forward resistance for the concave and convex plate at the inclination of the hydrodynamic profile to the side was observed. As a result, the evolution of the forward resistance coefficients for the hydrodynamic profile is presented below.
Figure 4.12 shows the forward resistance coefficients for the profile mounted on the flat plate. The curves are plotted for the total coefficients of resistance, Cd, of viscous pressure, Cdp, and for the coefficients of viscous resistance, Cdv, for each of the four angles of inclination. It is observed that as the angle of inclination increases, the total coefficients increase for the lateral inclined profile and decrease for the upstream and downstream inclined profile. The viscosity coefficients increase the same for the lateral inclined profile, but decrease with very small differences for the inclined profile in the diametrical plane. There is also a downward trend in pressure coefficients as the angle of inclination increases.

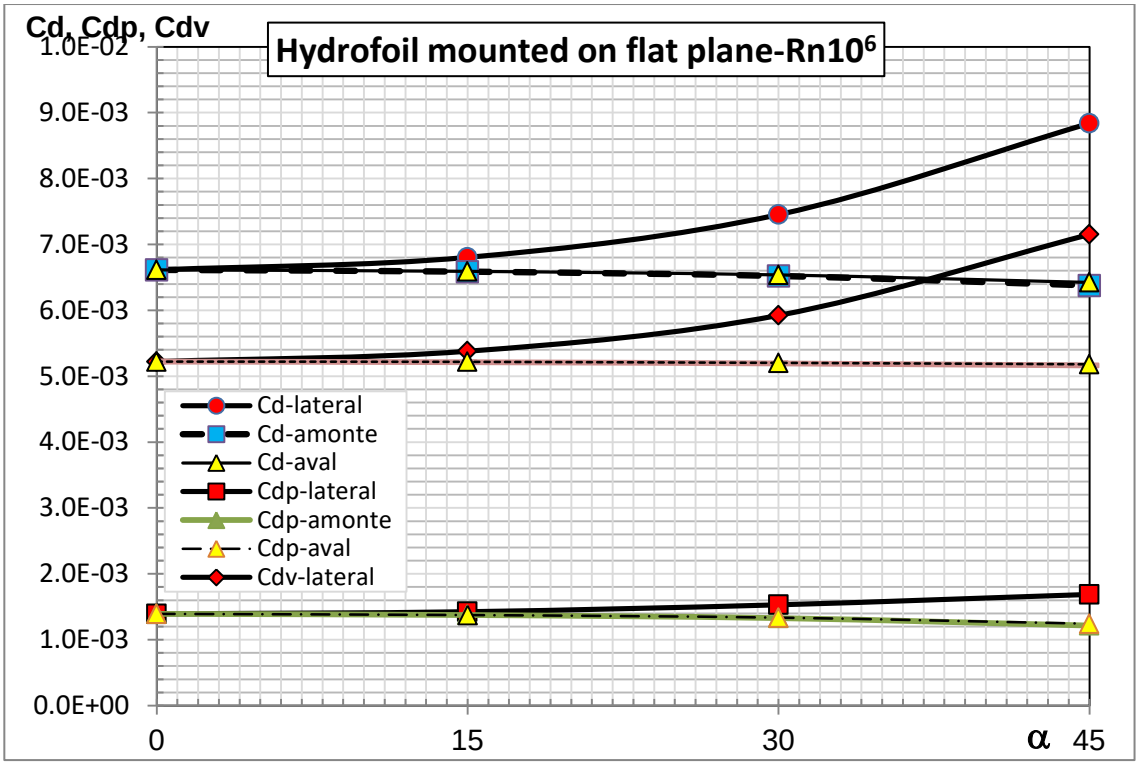

Figure 4.10. Drag coefficients for the hydrofoil mounted on flat plane, Rn 10^6

There is an increase of up to 33% of the total coefficient in the case of lateral inclination and a decrease of about 3% in the case of inclination in the upstream and downstream diametrical plane.

4.4.2. Base plate curvature influence: concave / convexe

In naval practice there are few cases when a hydrodynamic profile is mounted on a flat plate. As a result, the profile was mounted on the curved, concave and convex plate, and the influence of the plate curvature on the flow around the junctions was studied. Four radii of curvature were considered, 1.5C (R1), 2C (R2), 3C (R3) and 6C (R4) where C represents the length of the profile string. Figure 4.15 shows a sketch with the profile mounted on the curved plate at various radii of curvature, but also a cross section, the YOZ plane, in the vicinity of the hydrodynamic profile, near the maximum thickness, t = 0.12m. For each radius of

curvature, convex or concave, the inclination of the profile is kept as in the case of the flat plate, namely three angles (15°, 30°, 45°) of lateral inclination, three angles (15°, 30°, 45°) in the plane of symmetry upstream and three angles (15°, 30°, 45°) in the plane of symmetry downstream.

In order to be able to compare the radii of curvature, it is necessary for the nodes to have the same distribution on the board. This can be done by altering the Cartesian coordinates of the nodes on the initial two-dimensional grid by applying the relations:

$$y_1 = y_0 + R\sin\left(\frac{y_0}{R}\right)$$

$$z_1 = z_0 + R\left[1-\cos\left(\frac{y_0}{R}\right)\right] \quad z_1 = z_0 + R\left(1-\cos\left(\frac{y_0}{R}\right)\right)\text{-pentru placa convexă} \qquad (4.1)$$

$$z_1 = z_0 - R\left[1-\cos\left(\frac{y_0}{R}\right)\right] \quad z_1 = z_0 - R\left(1-\cos\left(\frac{y_0}{R}\right)\right)\text{- placa concavă}$$

where: y_1 and z_1 and y_0 and z_0 represents the final coordinates and also the initial coordinates of the points in the grid, R represents the radius of curvature of the plate and is obtained by dividing the y_{max} of the plane grid by 0.5, 1, 1.5, and 2.

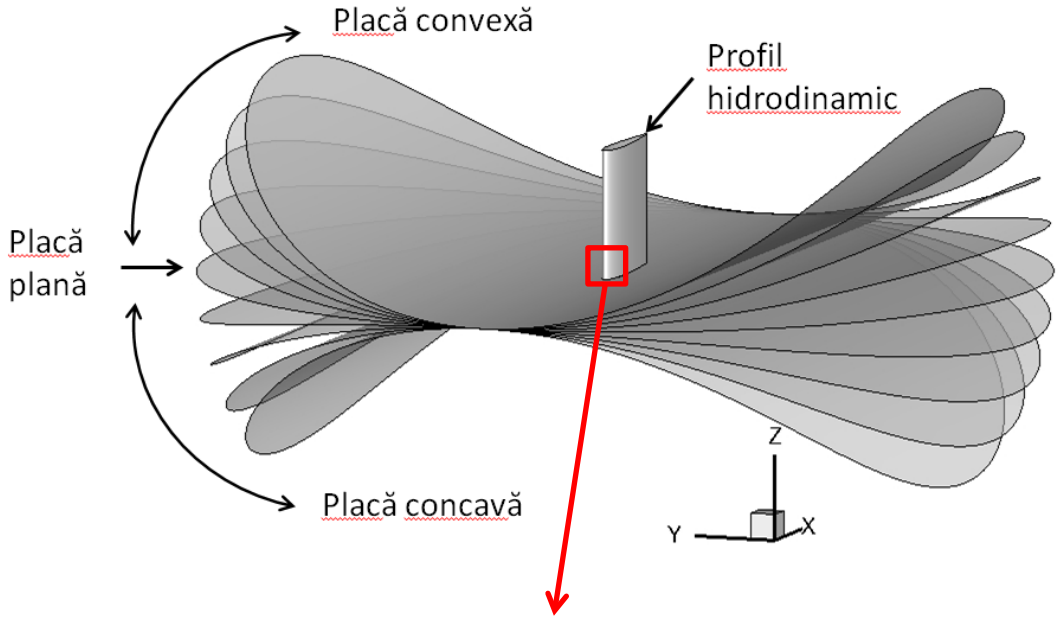

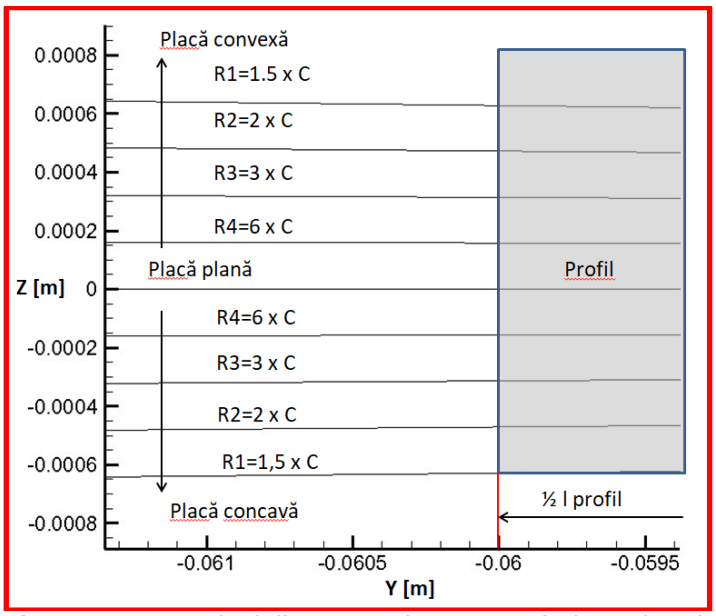

Figure 4.11. Hydrofoil mounted on curved plate sketch

4.4.2.1.Concave plate

As in the case of the profile mounted on the flat plate, the viscosity coefficients increase for the lateral inclination and with a very small slope for the upstream / downstream inclination. The viscous and total pressure coefficients decrease with increasing angle of inclination, less the total coefficients for the lateral case 45 degrees.

Figure 4.20 shows the influence of the plate curvature on the forces acting on the inclined hydrodynamic profile in all directions, for Reynolds number 10^6.

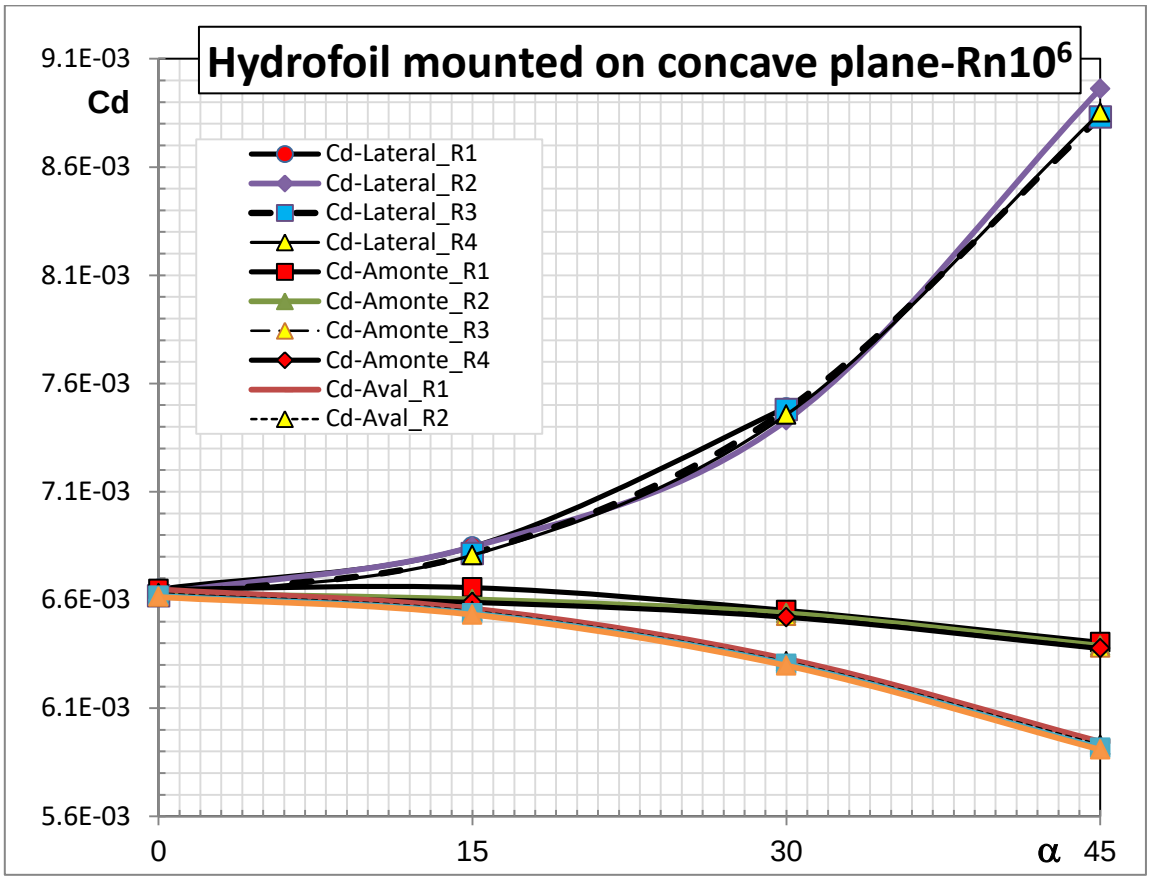

Figure 4.12. Drag coefficients for hydrofoil mounted on concave plate, Rn 10^6

4.4.2.2.Convexe plate

Figure 4.27 shows the influence of the curvature of the convex plate on the forces acting on the hydrodynamic profile inclined in all directions, for each Reynolds number considered. The decrease of the radius of curvature determines high pressure gradients, materialized by high coefficients of resistance to advance.

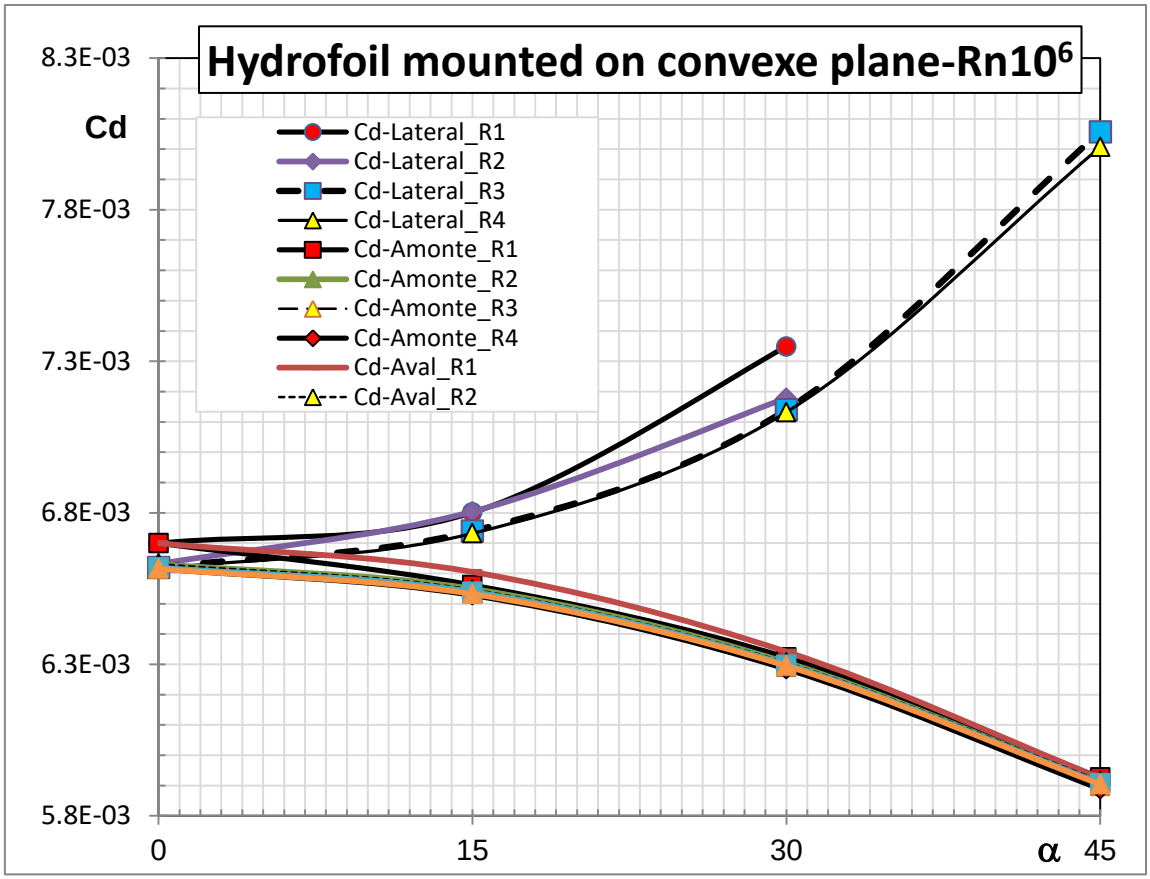

Figure 4.13. Drag coefficients for hydrofoil mounted on convexe plate, Rn 10^6

4.4.3.Reynolds number influence

For the study of the influence of velocity on the flow around the junction, three Reynolds numbers 10^6, $5x10^6$ and 10^7 were considered. The dependence on the inclination and curvature angle of the plate has already been presented previously, independent for each Reynolds number. The following are the centralized results for all three speeds considered.

As the Reynolds number increases, so does the dynamic pressure. This can be seen in Figure 4.30, which shows the evolution of the secondary vortex. Due to the increase of the dynamic pressure, the core of the secondary vortex moves towards the leading edge of the profile, and the vortex loses its turbulent intensity. Not only the vortex structures change but also the pressure distribution around the junction. An advantage of increasing the Reynolds number is that the maximum pressure area, where the speed is canceled, decreases on the profile, this can be seen in Figure 4.31 on the pressure iso-contours drawn both on the plate and on the side-sloping profile.

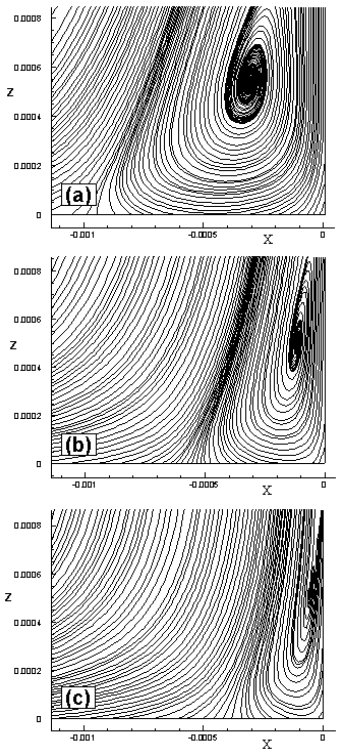

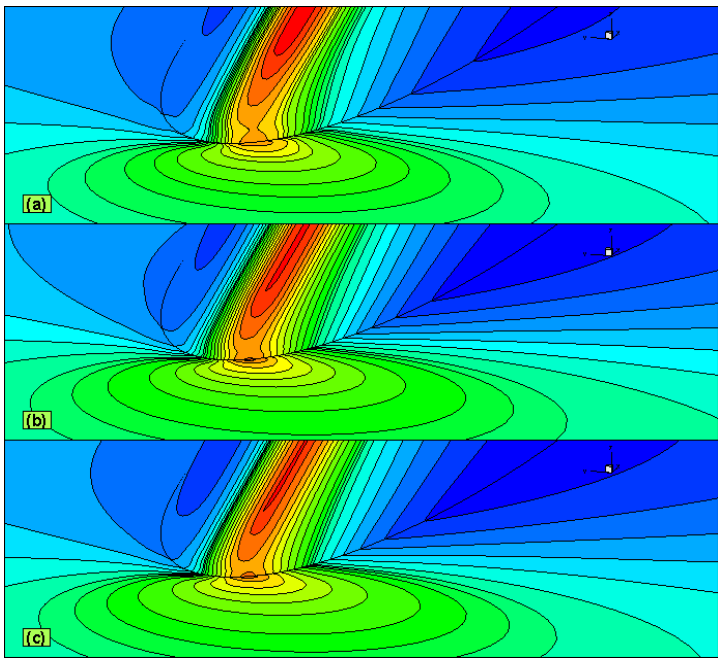

Figure 4.14. Secondary vortex

Figure 4.15. Pressure distribution around junction

The variation of the coefficients of the total resistance in relation to the Reynolds number for the profile mounted on the flat plate is shown in figure 4.32. There is a decrease in the values of the coefficients in relation to the Reynolds number, less at the lateral inclinations by 30 and 45 degrees, where the coefficients have the highest value at Reynolds $5x10^6$.

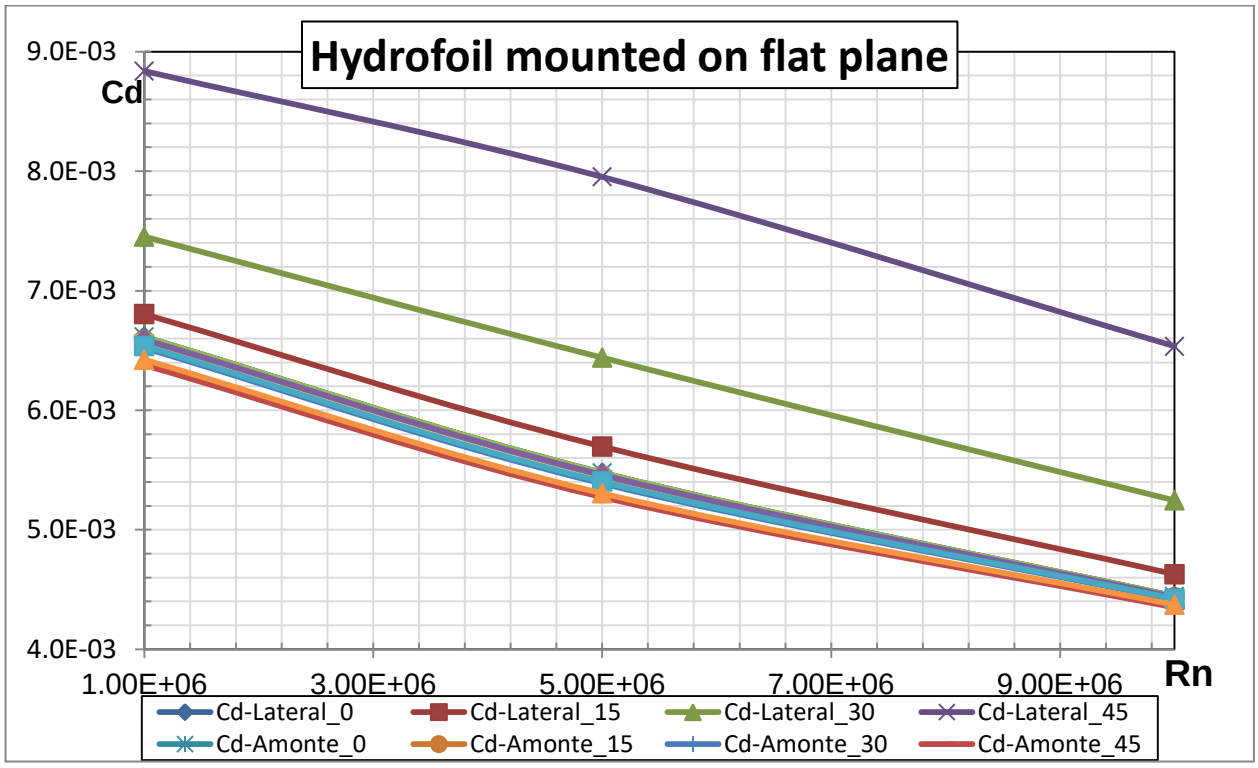

Figure 4.16. Drag coefficients on hydrofoil mounted on flat plate

The following is the variation of the coefficients of the total resistance in relation to the Reynolds number for the lateral, upstream and downstream inclined profile mounted on the concave or convex plate.

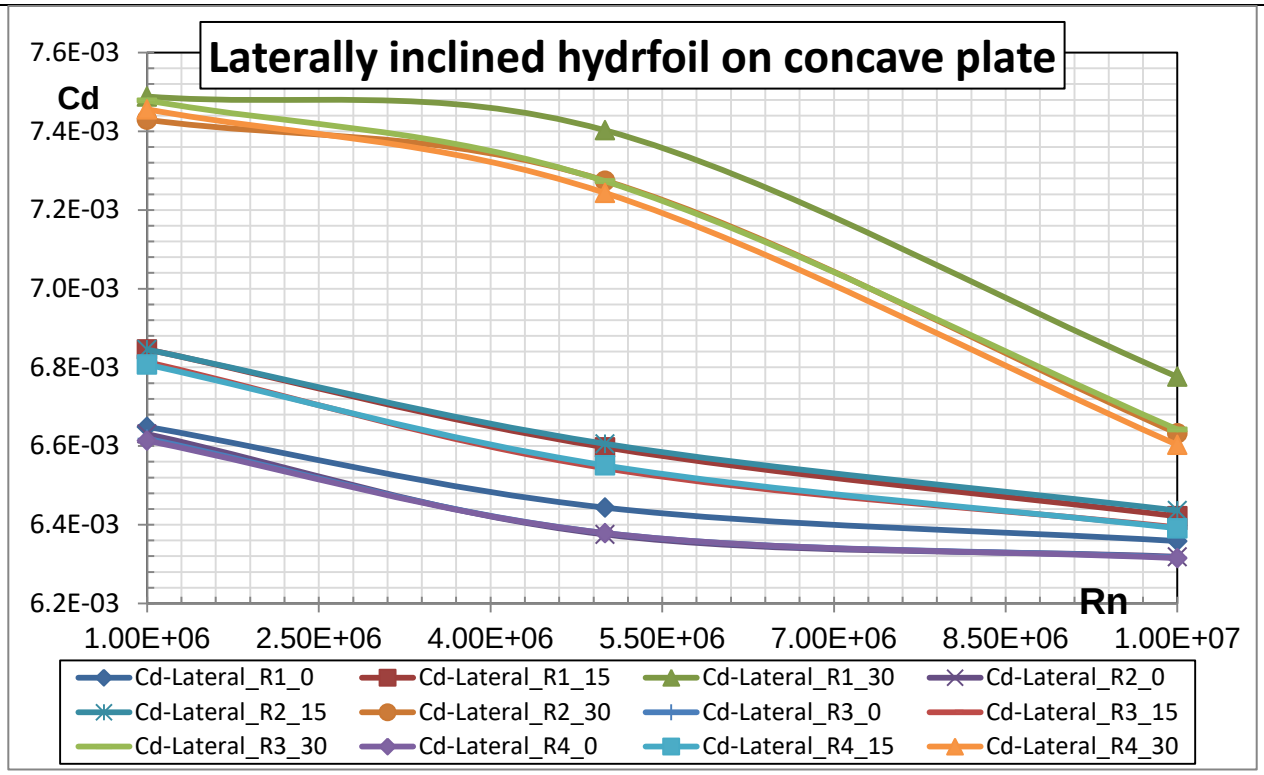

Figure 4.17. Drag coefficients on laterally inclined hydrofoil mounted on concave plate

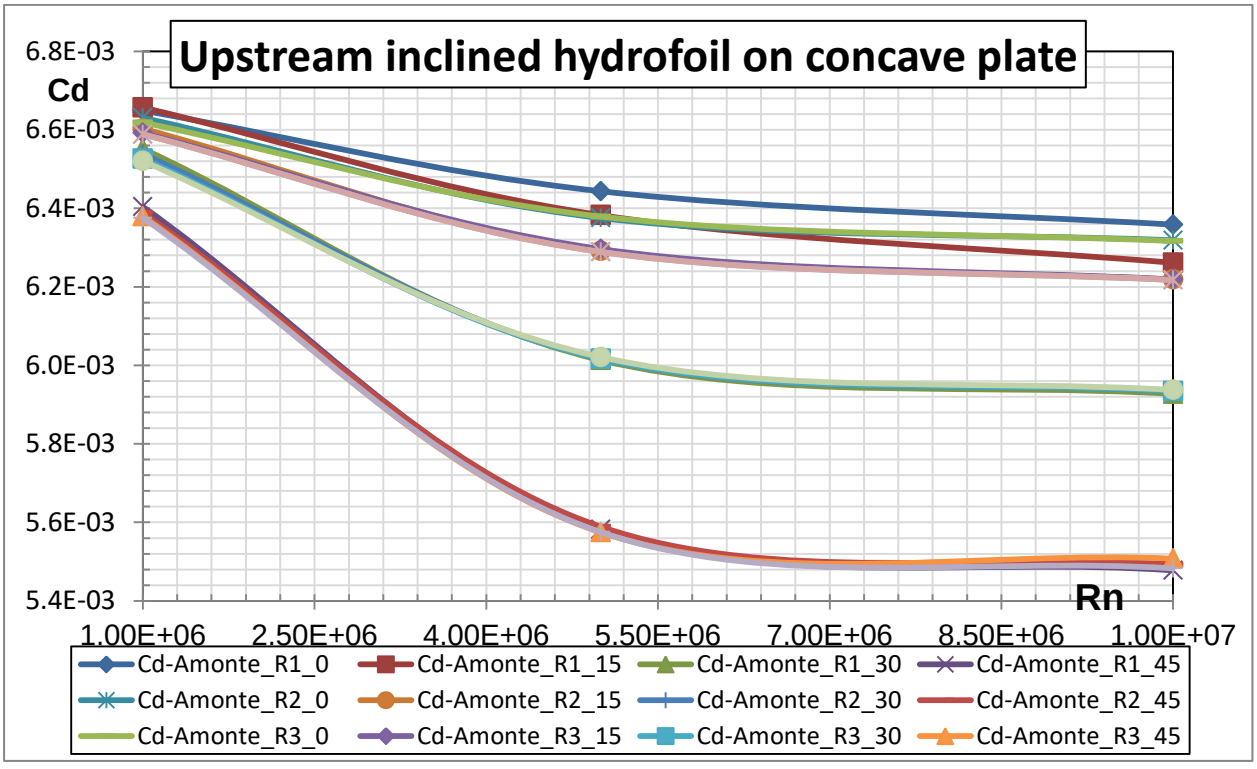

Figure 4.18. Drag coefficients on upstream inclined hydrofoil mounted on concave plate

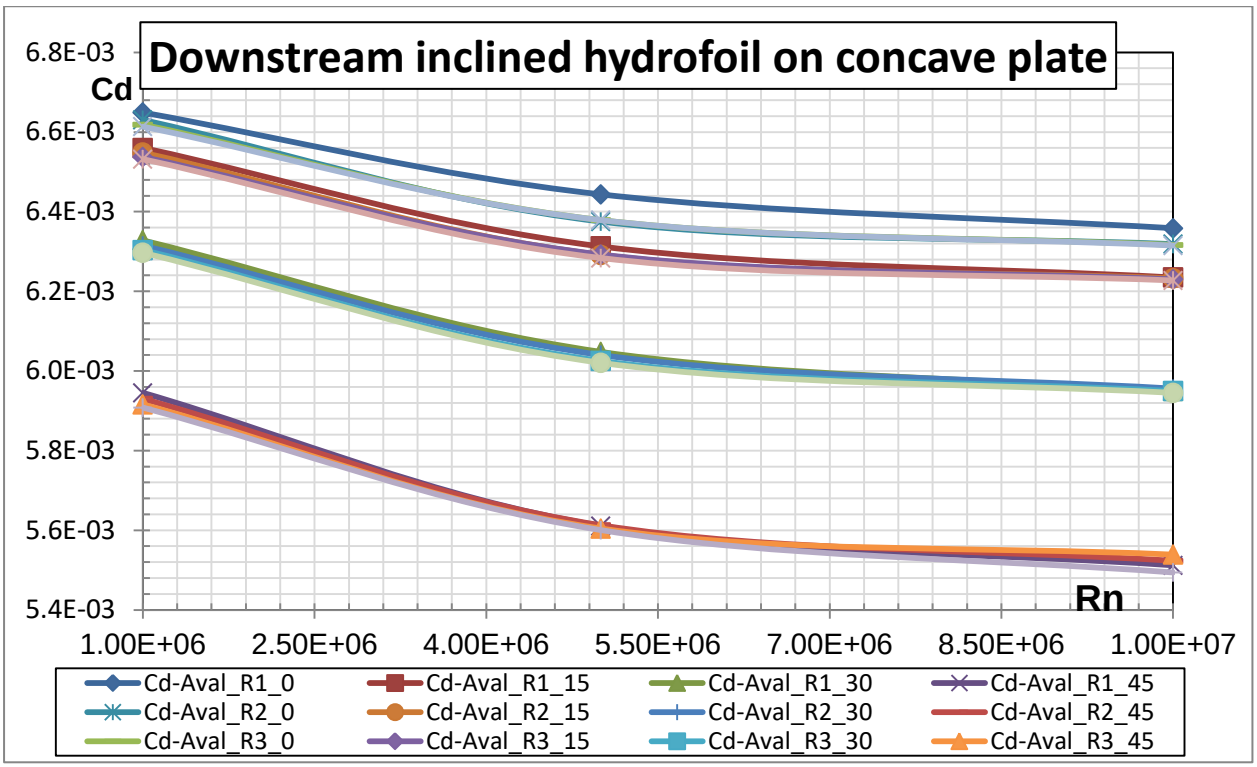

Figure 4.19. Drag coefficients on downstream inclined hydrofoil mounted on concave plate

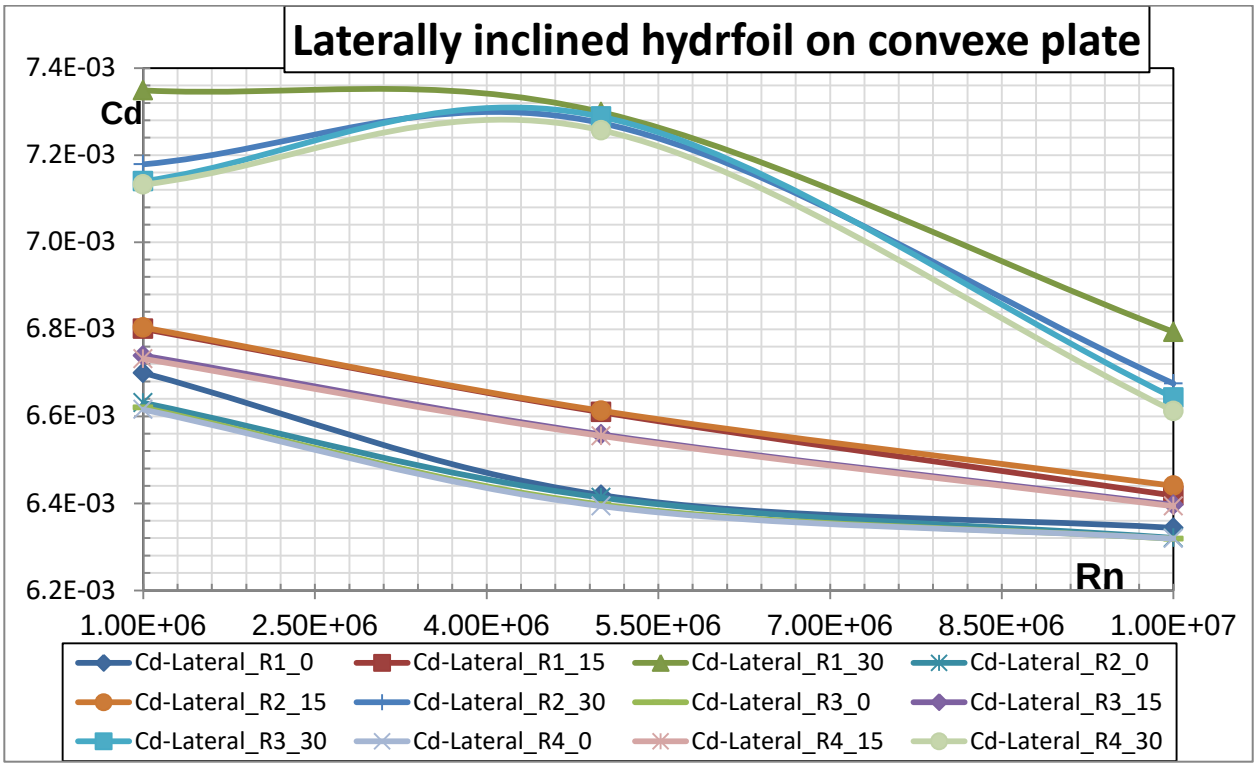

Figure 4.20. Drag coefficients on laterally inclined hydrofoil mounted on concvexe plate

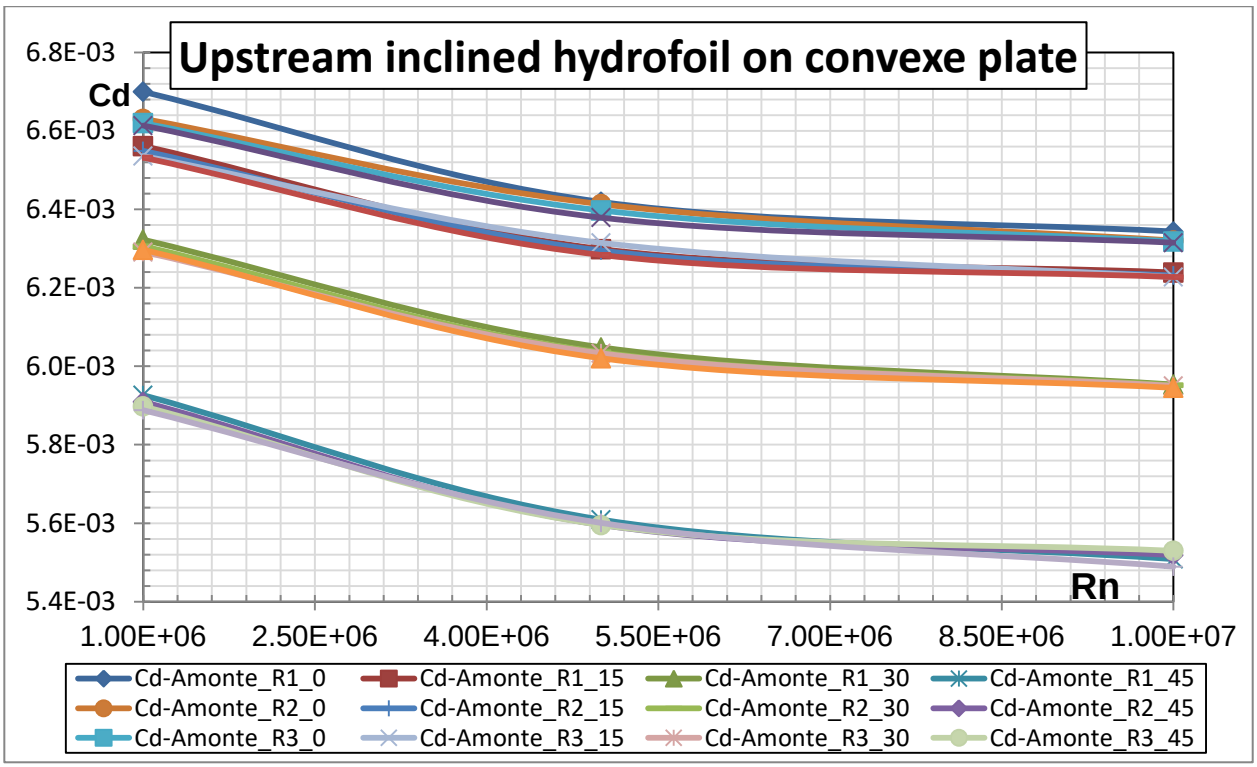

Figure 4.21. Drag coefficients on upstream inclined hydrofoil mounted on concvexe plate

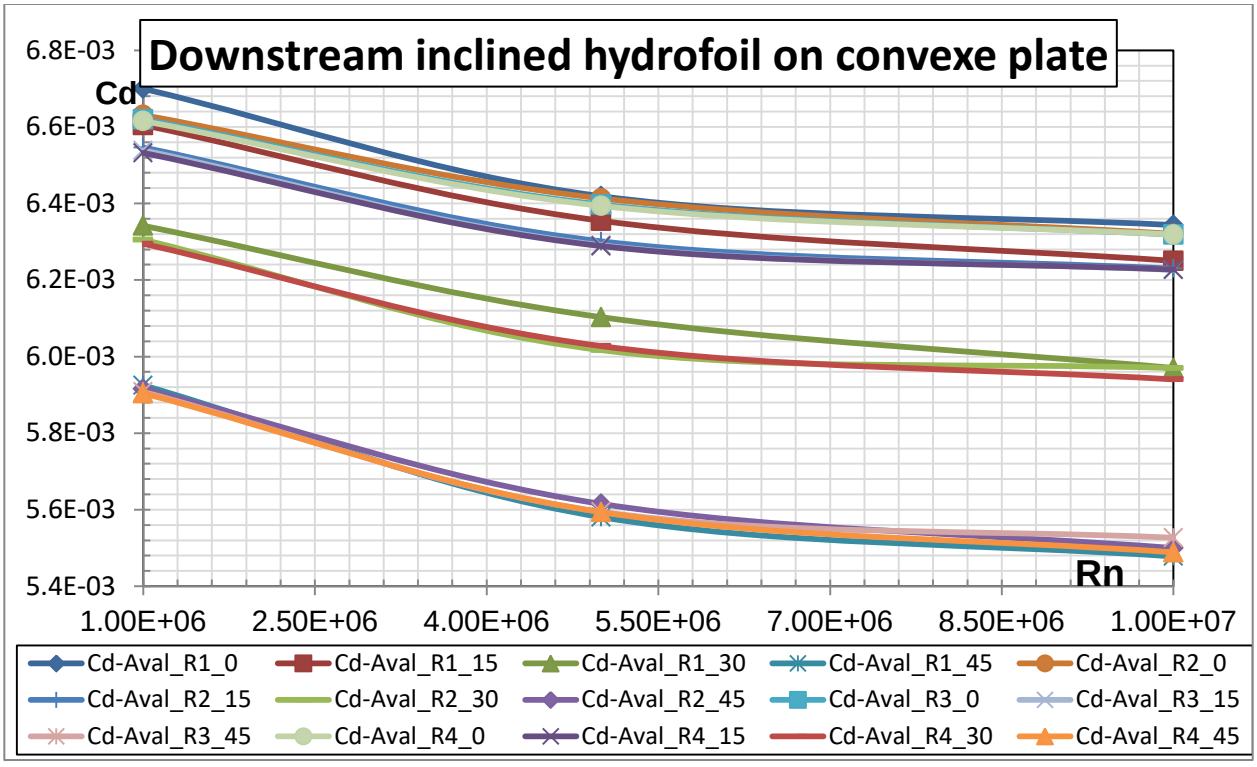

Figure 4.22. Drag coefficients on downstream inclined hydrofoil mounted on concvexe plate

The same pattern is observed, of the decrease of the resistance coefficients to advance even in the cases of lateral inclination both on the concave plate and on the convex plate where the maximum is at the Reynolds number $5x10^6$.

Chapter 5. Free surface flow around junctions

5.1.Introducere

Free surface flow around a hydrodynamic profile mounted on a plate near the free surface is a complicated one that combines nonlinear, three-dimensional and turbulent phenomena such as the boundary layer on solid surfaces, the whirlpool system developed around junctions and the effects of the free surface. as if turbulent, breaking the wave. As a result, this chapter presents the results of the numerical study on free surface flow around junctions, more precisely the study of the influence of the angle between profile and plate, the study of the influence of current speed, the study of free surface influence on the junction. As in the studies without free surface in the previous chapter, the influence of the angle between the profile and the plate is studied by tilting the profile in three directions: lateral, upstream and downstream, with three steps, 15, 30 and 45 degrees. For the study of the influence of speed, the flow is considered to have five Froude numbers, from 0.16 to 0.48, so as to cover the flow area of a profile mounted on a vessel shell that acts as a flow correction device (ESD). , but also the speed range covered by the own experiment in the hull basin around the right penetrating profile, presented in chapter 3. In order to study the influence of the free surface, the height of the immersed area is systematically modified. Due to the complexity of the discretization grid generated on a computational domain with constraints imposed by numerical resolution of the free surface in the Ansys Fluent program, numerical simulations were performed only for the junction between the hydrodynamic profile and the flat plate, following in perspective with the development of channel flow from Fluent or other hydrodynamic calculation programs to address the problem of generating curved border grids for free surface calculation. Of course, it should be noted that all numerical simulations are based on the calculation methodology set out in Chapter 3 by experimental validation.

5.2. Objectives

Starting from the factors that influence the flow around the junctions described in Chapter 1, the objectives that define the structure of this chapter are:

- Study of the influence of the profile inclination in relation to the base plate;
- Study of the influence of depth;
- Study of the influence of speed.

5.3. Numerical model

5.3.1.Boundary conditions

When flowing with a free surface, the penetrating profile generates a system of divergent waves whose windings propagate at an angle of approximately 20 °. In order to avoid the radiation of the waves upstream, the entrance border is arranged at 1.5 rope lengths upstream of the profile. In order to avoid the reflection of the wave system from the lateral borders, producing numerical instabilities, the width of the calculation domain as well as the length of the downstream area are established so that the wave system leaves the integral domain through the downstream border. As a result, the downstream border is arranged at five rope lengths from the profile flight edge, and the side borders at two 2.5 rope lengths from the profile plane of symmetry. The position of the upper border is chosen so as to allow the natural elevation of the free surface (figure 5.1). Initial tests established that 0.5 of the profile string length is sufficient.

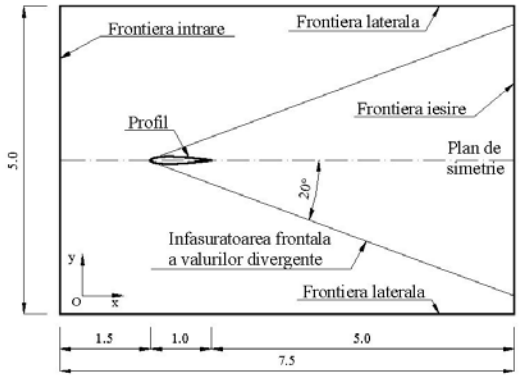

Figure 5.1. Calculation model

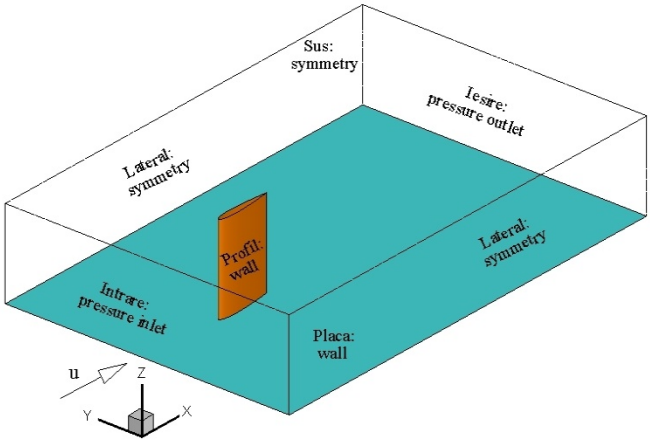

Figure 5.2. Boundary conditions

Free surface flow is governed by gravitational force and inertial forces, represented by the dimensionless parameter Froude. As a result, the boundary conditions imposed must take into account the effects of gravity. In this sense, the calculation field is modeled for open channel flow. Figure 5.2 shows the computational domain together with the boundary conditions imposed. The inlet and outlet boundaries of the fluid in the field are defined as pressure inlets and outlets.

5.3.2.Numerical schemes

The system of RANS equations together with the equations of the $k-\omega$ SST turbulence model are solved in a non-stationary regime, in a quasi-explicit manner, using the finite volume method from Ansys Fluent. The gradients of the solution are obtained by applying the cell-based Green-Gauss theorem. Solving problems with the free surface in the Fluent program is done by the VOF method and is solved using the geometric reconstruction scheme. The coupling of speed and pressure is solved by the PISO algorithm, imposed by the non-stationary calculation. The pressure is described by the PRESTO scheme, and the convective and diffusive terms are solved by the QUICK scheme.

5.3.3.Grid generation

If in the case of the fully immersed junction, the grid is generated by extrusion in the direction of the profile span resulting calculation areas with inclined boundaries at the same angle as the profile, in free surface calculations, the boundary conditions implemented in Fluent impose vertical boundaries for both input and for the exit of fluids from the field. Figure 5.3 shows the calculation range for the case of the profile inclined by 30 degrees in the downward symmetry plane where the delimitation lines of the component grids can be observed.

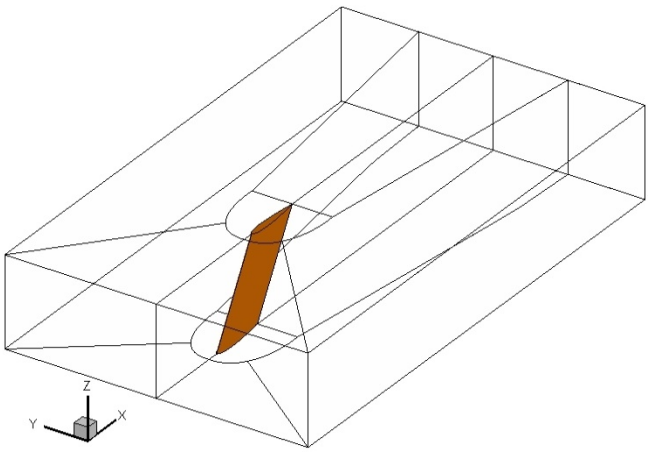

Figure 5.3. Multiblock calculation model

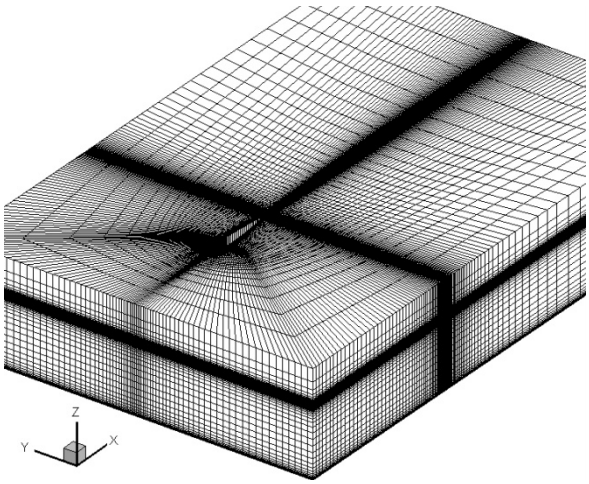

Figure 5.4. C-H tridimensional grid

The flow around the junction is described by phenomena such as the interaction of two boundary layers, one on the plate and the other on the profile. At the same time the grid must meet quality conditions such as spacing and orthogonality on solid boundaries. In addition, if the free surface is added, the discretization for solving by the VOF method must describe a band of condensed nodes in the area where the formation of the wave system is expected. Taking into account all the conditions imposed for solving the imposed physical problems, a structured multiblock grid is generated that perfectly overlaps the rectangular computing range, ensuring orthogonal and condensed grid lines on the motherboard and on the hydrodynamic profile but which in the same time to ensure the minimum space necessary to capture the elevation of the free surface. This results in a discretization grid with approximately two million hexahedral cells. Figure 5.4 shows the discretized computing domain in structured multiblock style of type C-H.

5.4. Results and discussions

5.4.1.Influence of the hydrofoil inclination angle

The influence of the angle between the profile and the plate is studied by tilting the profile in three directions: lateral, upstream and downstream, with three steps, 15, 30 and 45 degrees, starting from the position of the right vertical profile, constantly keeping the profile cord parallel to the direction. flow. Together with the case of the right vertical profile it forms the set of geometric hypostases of the profile in relation to the base plate.

The following are the vortex structures that develop at the meeting of power lines with the attack board of the hydrodynamic profile due to the blocking phenomenon. Figure 5.5 shows the system of two counter-rotating vortices, one main of higher intensity and one secondary of intensity. smaller located in the vicinity of the leading edge of the profile as well as the evolution in relation to the inclination of the profile in the normal direction to the vertical plane of symmetry. The influence of the motherboard is observed as the profile tilts, causing the main vortex to move towards the hydrodynamic profile.

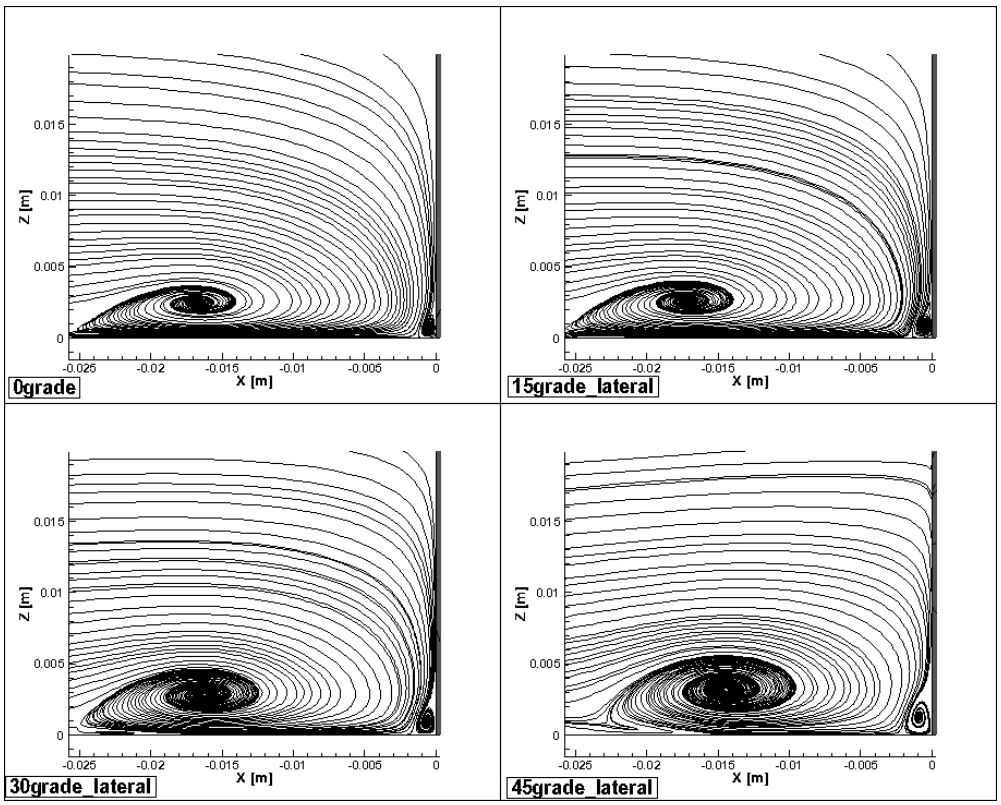

Figure 5.5. Streamlines –comparison between vertical and laterally inclined hydrofoil

In the upward inclined profile (figure 5.7) it is observed that the main vortex moves towards the base plate and due to the high pressure gradients generated by the presence of the two solid surfaces, at 30° and 45° the vortex structures are no longer formed, a sustained phenomenon and by graphically presenting the velocity vectors in the plane of symmetry upstream of the profile (figure 5.8).

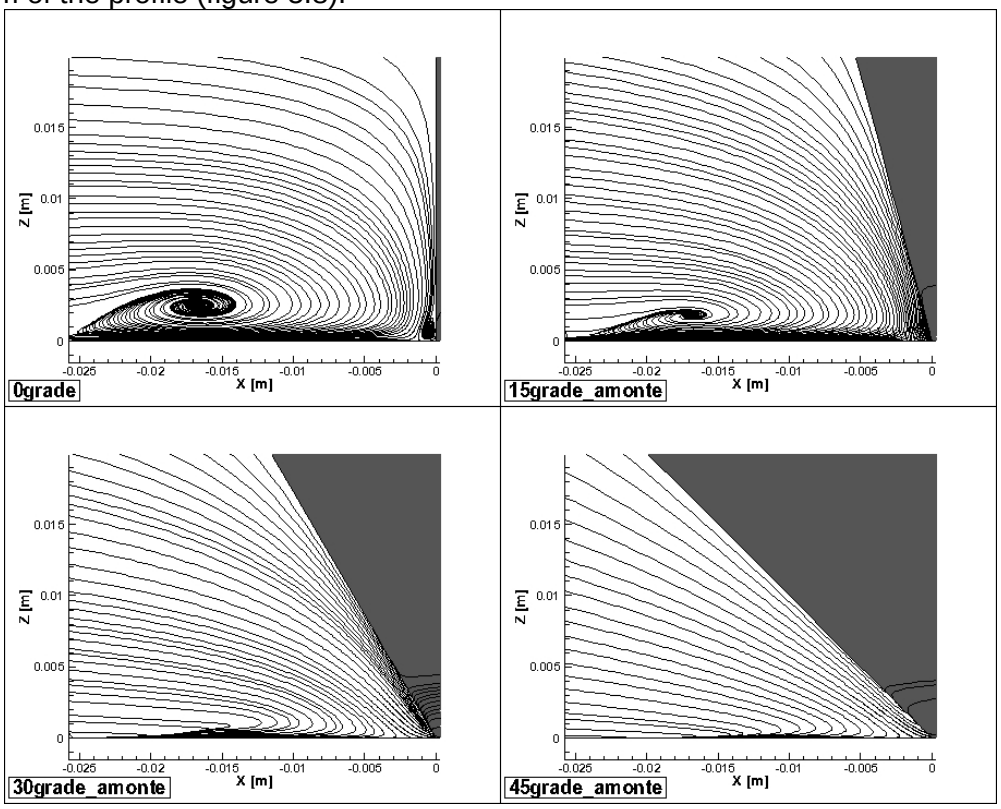

Figure 5.6. Streamlines –comparison between vertical and upstream inclined hydrofoil

When the profile is inclined downstream, the current lines approach the leading edge of the profile leading to a ring of the position of the main vortex with the secondary one, together with the increase in intensity and diameter of the core of the main vortex. If at the right vertical profile, the secondary vortex is in the vicinity of the leading edge, at 30 and 45 degrees it moves away from the leading profile.

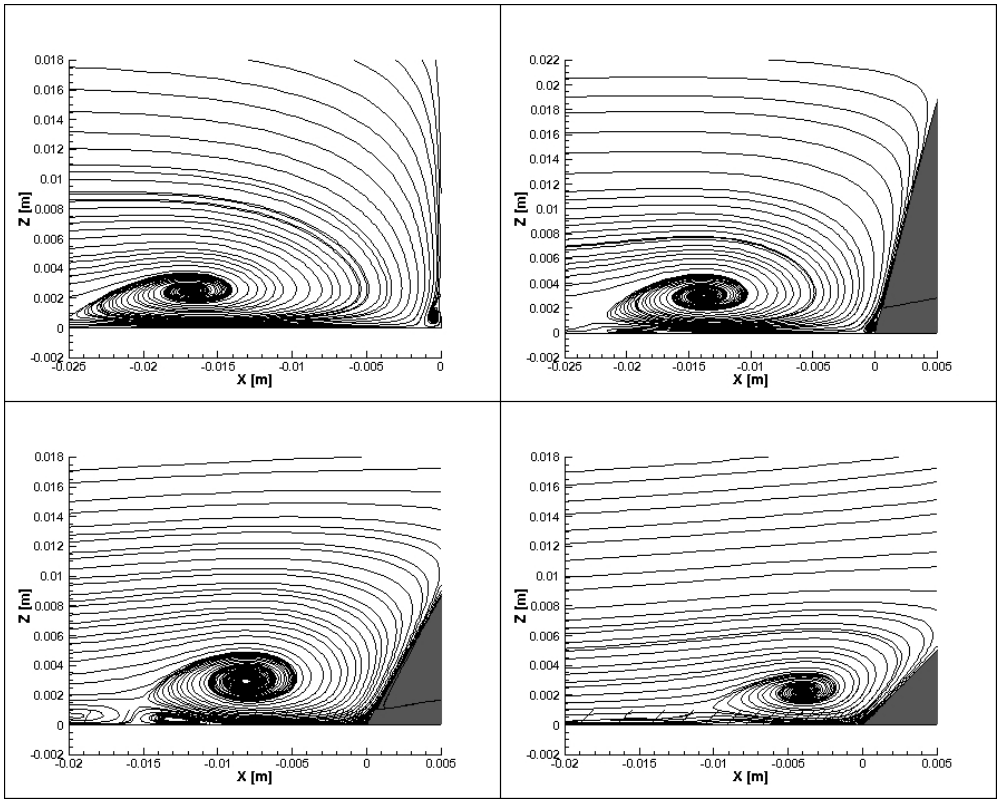

Figure 5.7. Streamlines –comparison between vertical and downstream inclined hydrofoil

It can also be seen that if at the vertical profile the presence of the profile leads the current lines in the downward direction, the large angle of inclination allows the current lines to slide in the horizontal and upward direction. This allows a reduction of the pressure gradient and thus facilitates the translation of the main vortex to the hydrodynamic profile.

Figures 5.11 and 5.12 show the evolution of the free surface in relation to the angle of inclination of the profile to the side. It is observed that the geometric asymmetry induces differences between the two edges of the profile and of the generated wave system, asymmetry in the flow field, but also a phase shift of the ridge / wave gap alternation. The yellow and red colors show the wave crests and the shades of blue show the wave gap. There is also an increase in the size of the wave crest as well as a deepening of the wave gap as the angle of inclination increases. The numerical free surface was generated as iso-surface of the water-air volume fraction equal to 0.5.

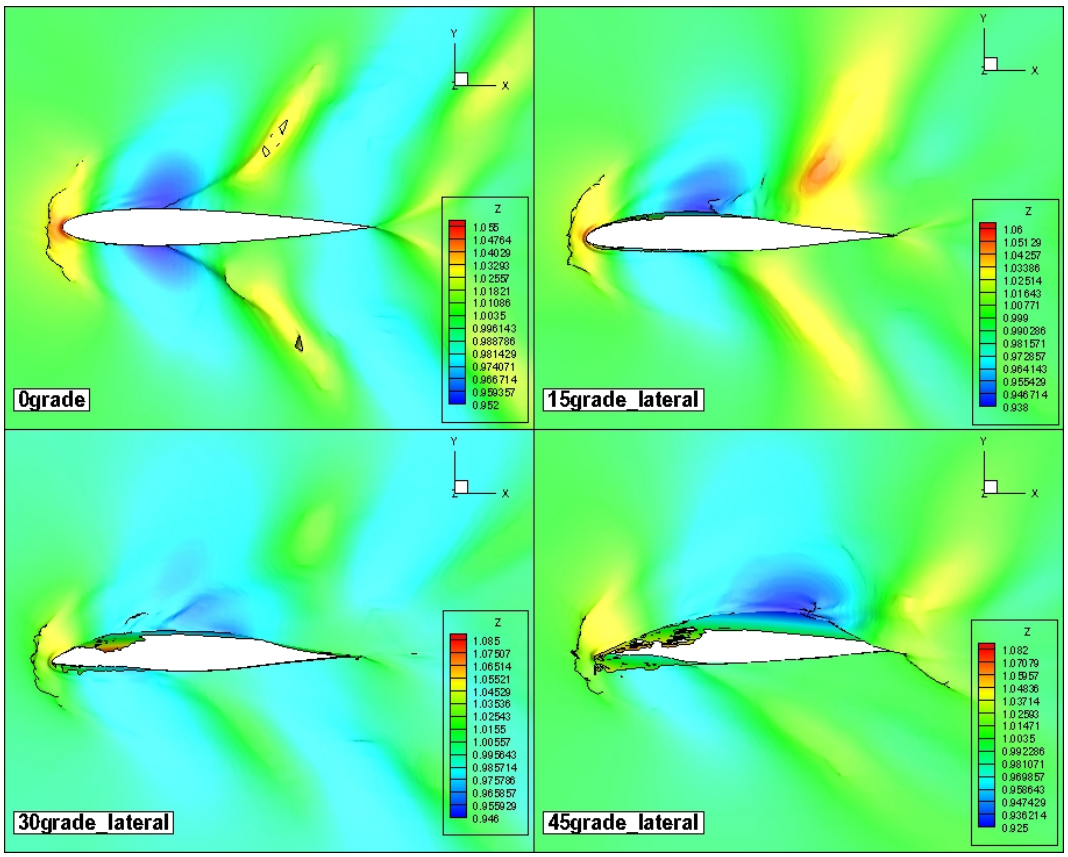

Figure 5.8. Free surface –comparison between vertical and laterally inclined hydrofoil, top view

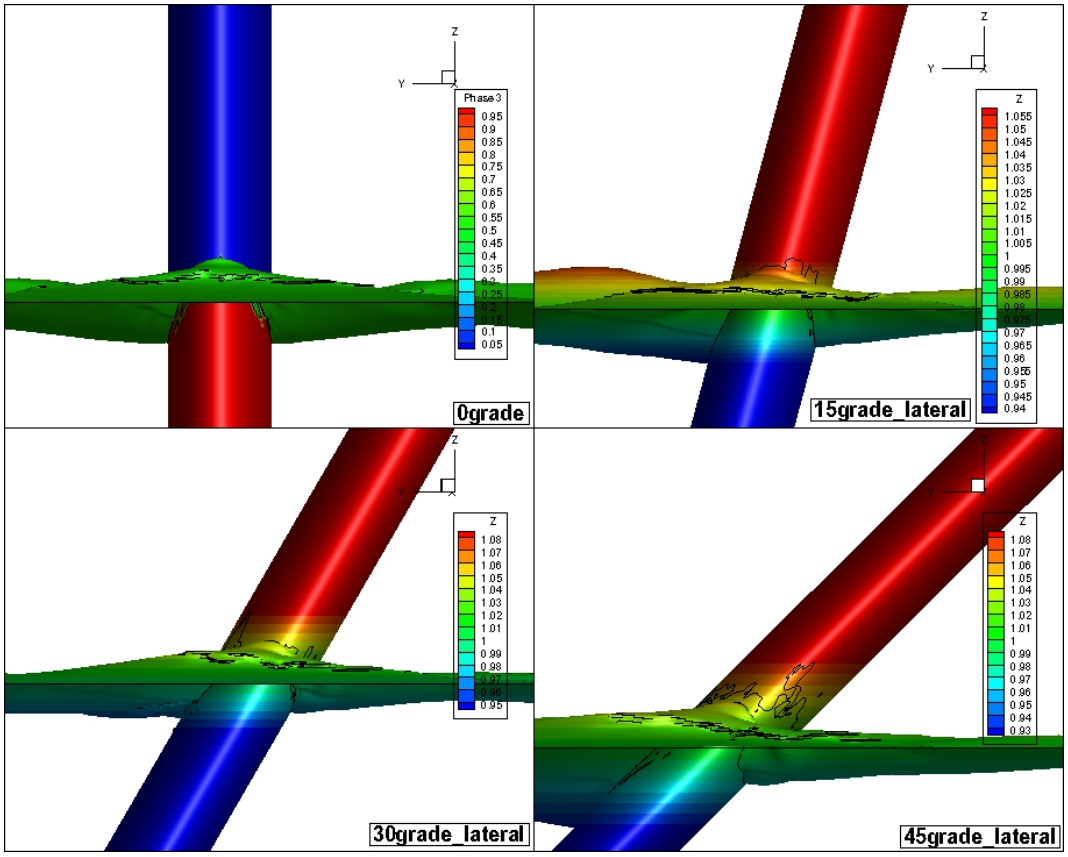

Figure 5.9. Free surface –comparison between vertical and laterally inclined hydrofoil, front view

Figure 5.13 shows the evolution of the free surface in relation to the angle of inclination of the downstream profile. It is observed that as the angle of inclination increases, the amplitude of the first wave generated by the profile increases.

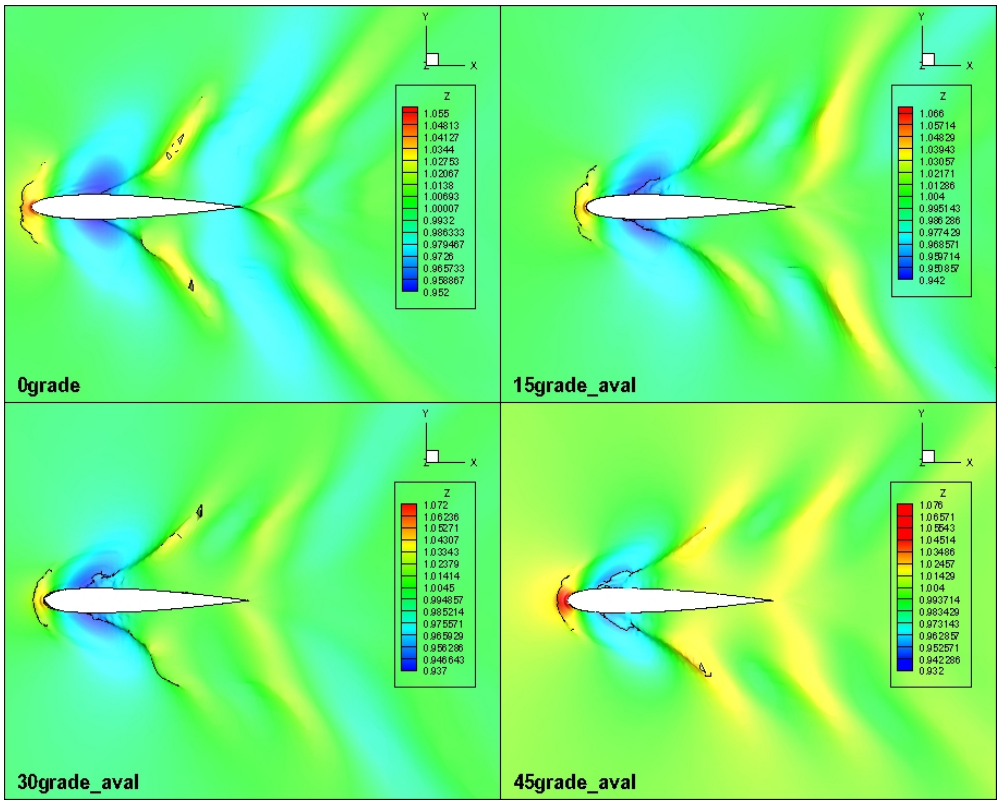

Figure 5.10. Free surface –comparison between vertical and downstream inclined hydrofoil, top view

Figure 5.14 shows the evolution of the free surface in relation to the angle of inclination of the profile upstream. It is observed that the amplitude of the first wave generated by the profile decreases with increasing angle of inclination, because the current lines are driven downwards, similar to the junction at the base of the profile. If in the case of the straight vertical profile the second wave ridge is prominent, it decreases in amplitude as the angle between the plate and the profile increases.

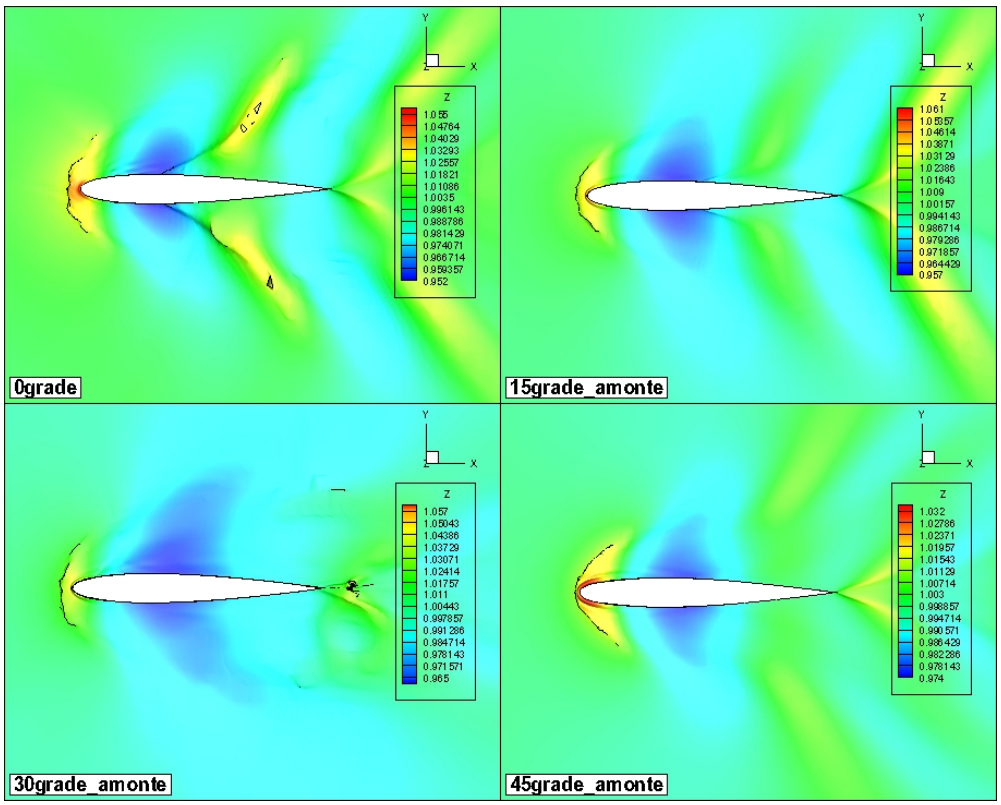

Figure 5.11. Free surface –comparison between vertical and upstream inclined hydrofoil, top view

Calculate the coefficients of resistance to advance and are shown in Figure 5.15 as well as in Table 5.1 together with the relative error in relation to the straight vertical profile. There is a decrease of up to 10% of the total coefficient in the case of lateral inclination and a decrease of up to 55% in the case of inclination in the upstream and downstream diametrical plane.

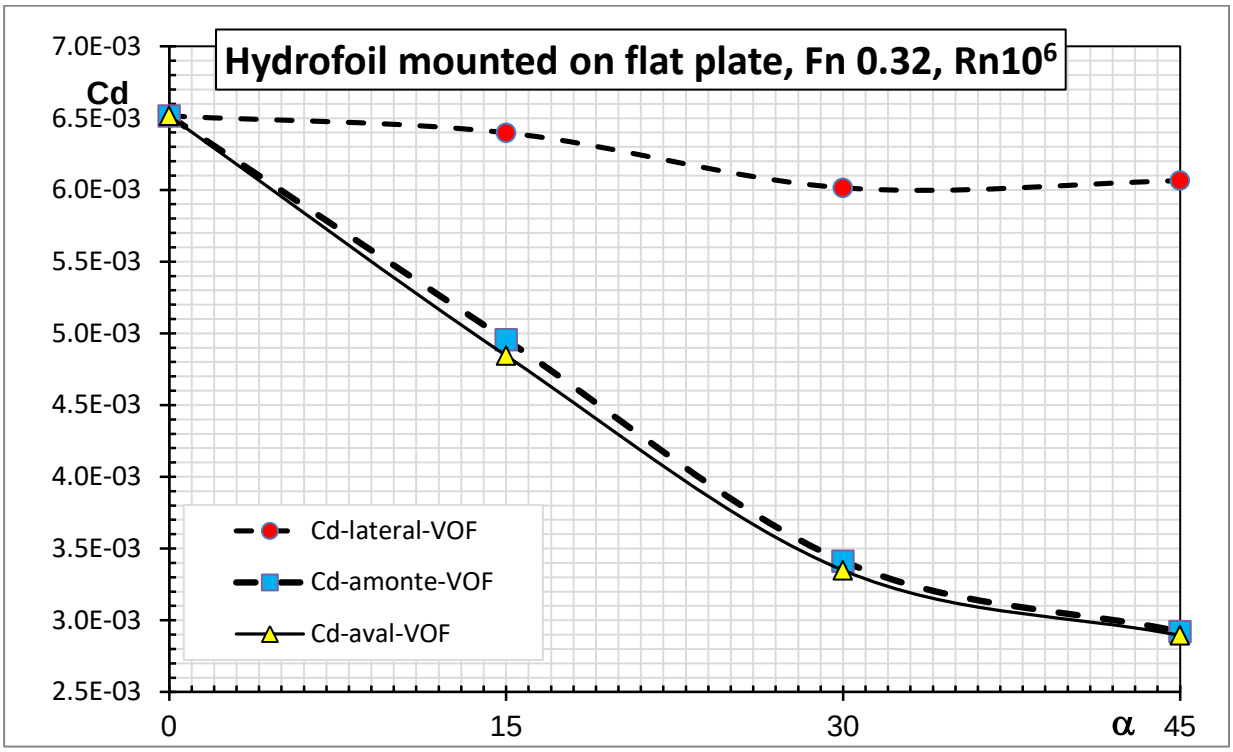

Figure 5.12. Drag coefficients in respect to inclination angle

5.4.2. Influence of the water depth

If the lower boundary is very close to the level of the free surface, it is considered to be flowing in shallow aquariums. In this situation the main parameter that characterizes the flow is the froude number calculated based on the water depth, Fnh. Four ratios between water depth and profile rope were considered: 1, 0.75, 0.50 and 0.25. It is expected that when the level of the free surface changes, that the presence of the plate will significantly influence the development of the flow. The lower the water depth, the higher the crest of the waves, possibly to the point of rupture. On the numerically simulated free surface, figure 5.16, broken lines of the contours are observed, which means that the turbulence condition has been met.

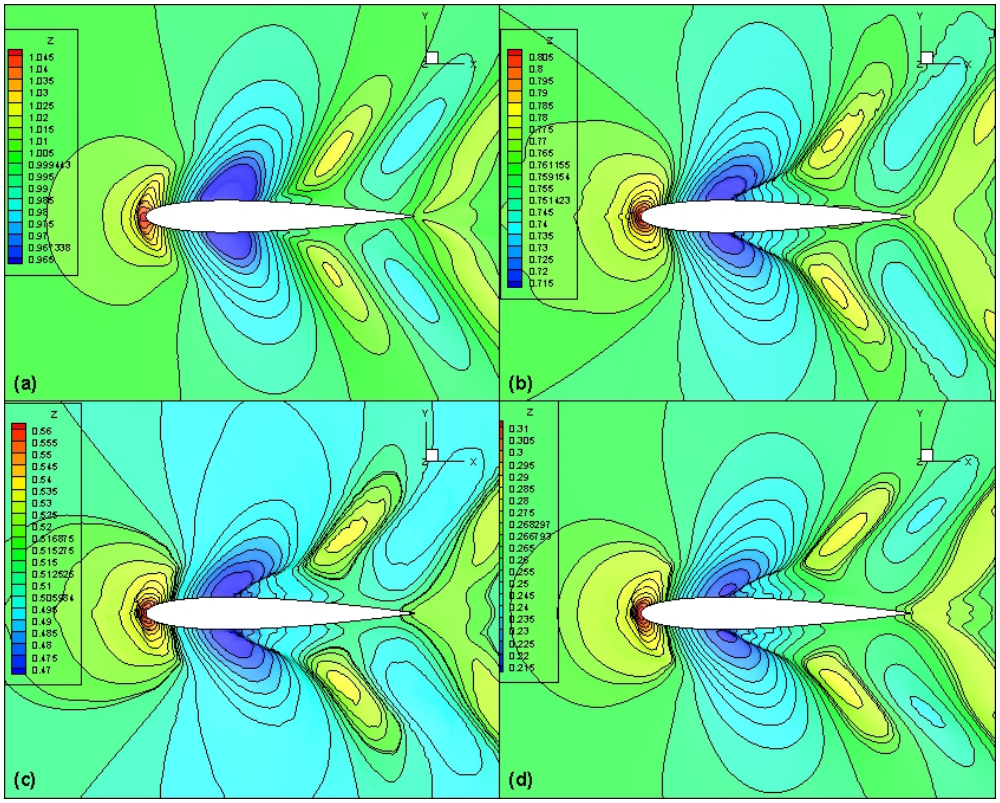

Figure 5.13. Free surface –comparison between different drafts, top view

a) h=1m, b) h=0,75m, c) h=0,5m, d) h=0,25m.

At small Frh numbers (Frh = 0.16), the amplitudes of the developed waves are relatively small and the influence of the shaft on the junction is not obvious. On the other hand, major interactions are observed at Frh = 0.369 (corresponding to the smallest depth), where the formed waves have very thin and high ridges. The results of the numerical simulations show recirculation areas starting with the sudden variations of the free surface.

5.4.3.Influence of the velocity

Five Froude numbers were considered for the study of the influence of speed, from 0.16 to 0.48, where the Froude number was calculated based on the length of the profile string. At small Froude numbers (0.16), the free surface shows waves of small amplitudes, almost imperceptible. At Fr = 0.32 the wave system generated by the presence of the profile is similar to the Kelvin wave system. At Fr = 0.48, due to the blocking phenomenon and the fluid separations, the second wave ridge breaks and is carried by the profile upstream. (Figure 5.18)

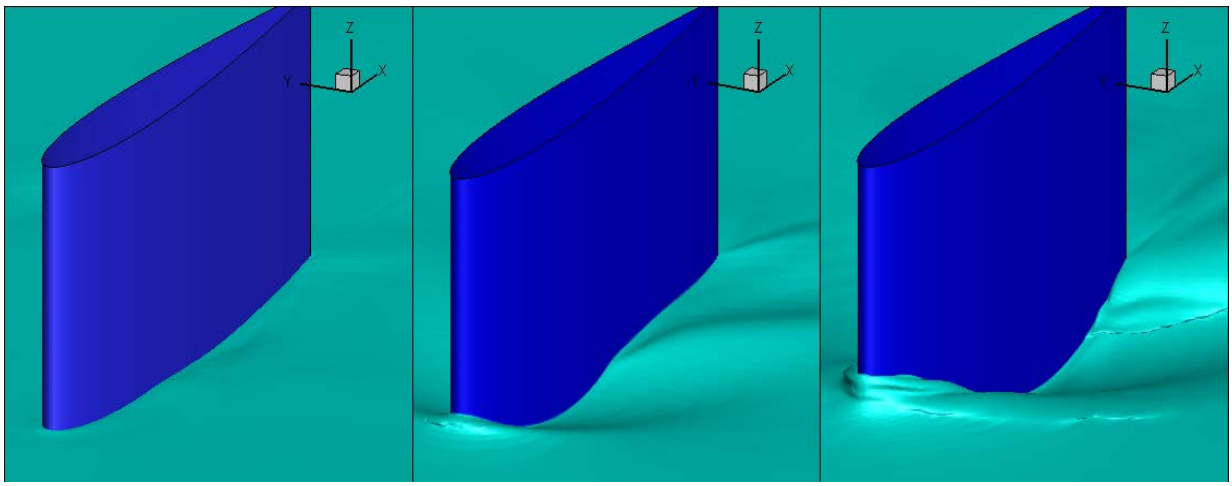

Figure 5.14. Free surface deformation: left-Fn=0,16, middle- Fn=0,32, and right- Fn=0,48.

Figure 5.19 shows the forward resistance coefficients. On the abscissa is the Froude number, and on the ordinate are the values of the coefficients. It is observed that up to Fr = 0.32, the total and viscosity coefficients decrease slightly, and then show a slight increase. At low speeds the profile has the largest immersed surface, with increasing speed the wet surface of the profile decreases. This explains the decrease in coefficients. But as the speed increases, the detachments and turbulent movements increase, so does the pressure component, leading to an increase in the coefficients of resistance to advance. It is also observed that in small Froude numbers the viscosity component predominates, while in large Froude numbers, the pressure component becomes significant.

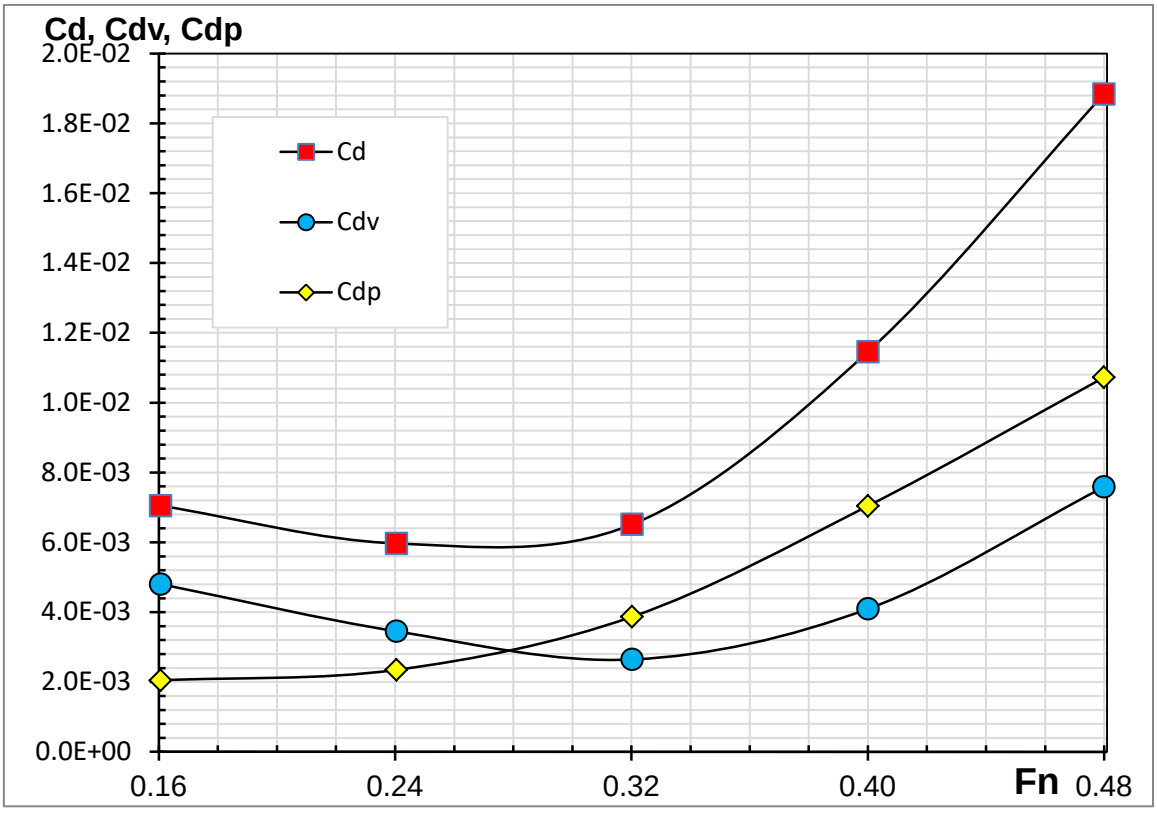

Figure 5.15. Hydrofoil drag coefficients in respect to Froude number

Chapter 6. Conclusions

The studies carried out in accordance with the scientific objectives of the doctoral thesis aimed at analyzing the flow around the junction formed by a plate and a hydrodynamic profile with practical applications in naval hydrodynamics. Based on the partial conclusions presented at the end of each chapter, a number of general conclusions are summarized, as follows:

- A complete procedure for determining numerical and experimental errors based on the ASME V&V 20 (2009) methodology, for verification and validation of numerical calculations, and ITTC (2008) for determining experimental errors and uncertainties was theoretically described and implemented;
- A calculation methodology and numerical schemes used in the study of viscous flow without free surface around the junctions were established:

- Calculations were performed for flat plate flow and flow around a hydrodynamic profile, NACA0012, and the results were verified and validated with results from the literature. The Spalart Allmaras turbulence model was identified and used as having good results in the systematic study of the flow around the immersed junctions without the influence of the free surface.
- A systematic numerical study of the flow around the junctions was presented and the influence of factors such as the inclination of the profile, the curvature of the base plate or the speed of the current on the flow around the junction between a hydrodynamic profile and a plate were studied. The results were presented for tilting the profile in 3 directions with three angle steps, 15, 30 and 45 degrees, mounted on a flat, concave or convex base plate (at 4 radii of curvature), at three Reynolds numbers, 10^6, $5x10^6$ and 10^7.
- A study was also carried out to identify the grid convergence index, or as it is also called a study of discretization errors and uncertainties. It was observed that both qualitatively and quantitatively, the grids used, but especially the fine grid used leads to realistic results. As a result, it can be considered that the numerical results of the systematic study have a high degree of confidence. A fost stabilită o metodologie de calcul a curgeri vâscoase cu suprafață liberă în jurul profilelor hidrodinamice;

- The experiment was performed and presented in the hull basin on a NACA 0012 model, at 4 drafts and 12 speeds for which the evolution of the resistance to advance and the elevation of the free surface on the experimental model were studied;
- Numerical calculations were performed and the results were verified and validated with the experimental results. The turbulence model with which the free surface calculations were performed was SST.
- A systematic numerical study of the flow around the junctions was presented and the influence of factors such as the inclination of the profile, the speed of the current and the influence of the depth on the flow around the junction between a hydrodynamic profile and a flat plate were studied. The results were presented for tilting the profile in 3 directions with three angle steps, 15, 30 and 45 degrees, mounted on a flat base plate. A study on the influence of speed on five Froude numbers was also performed, from 0.16 to 0.48 for the right vertical profile. And to study the influence of water depth, the free surface was moved vertically in various positions relative to the junction between the plate and the profile and the results were presented.
- It was observed that both qualitatively and quantitatively the grids used led to realistic results with a high degree of confidence.

Following the analysis of the numerical results of the systematic studies with and without free surface, it is recommended that from a hydrodynamic point of view the mounting of the

profile on the hull should be done at an angle of less than 15 in relation to the no
direction on the hull. downstream so that the horseshoe of vortices is diminished in intensity
and the value of the resistance to advancement of the profile as well as that induced by the
coating in the general economy is minimal.

Chapter 7. Personal contributions and perspectives

The research is anchored in the current global context, starting from the need for shipowners and naval designers to reduce greenhouse gas emissions in response to the measure imposed by the International Maritime Organization. As a result, the originality of the research and studies carried out, together with the assumed scientific objectives of the doctoral thesis, is materialized through a series of novelty elements, which increase the scientific value of doctoral studies.

The original contributions of the author of the doctoral thesis can be summarized as follows:

- A complete methodology was proposed and used to validate a numerical simulation by determining numerical and experimental errors;
- A systematic study on a natural scale of a hydrodynamic profile, NACA 0012 was carried out in the hull basin of the Faculty of Naval Architecture, the study being part of a research grant IDEI 790.
- A methodology was developed and validated for a complex study on the flow without free surface around the junctions, by tilting with 3 angle steps, lateral, upstream and downstream, as well as curving the plate with 4 radii of curvature, at 3 Reynolds numbers;
- A study methodology was developed and validated on the free surface flow around the junctions by tilting with 3 angle steps, lateral, upstream and downstream, with a general purpose CFD program, Ansys Fluent;
- Studies have led to the recommendation that the hydrodynamic appendix be mounted on curved surfaces, assimilated to the ship's hull, with a maximum of 15 from the n direction on the curved surface and upstream-downstream in order to reduce their own forward resistance but also reduce evolution turbulent structures.

Regarding the perspectives that reside from the studies presented in the doctoral thesis, the following are listed:

- Study of the flow around the junction between a plate and a profile with the same geometric conFiguretions but if the support plate penetrates the free surface and the submerged profile is parallel to it;
- Study of the flow around the junctions with angle of attack to study the influence of the load-bearing force on the flow with / without free surface around the junctions;
- Studies on the flow around a profile mounted on the hull of a ship, upstream and downstream of the engine.

References:

[1].United Nations Framework Convention on Climate Change, *"Kyoto Protocol Reference Manual"*, 2008.

[2].International Maritime Organization, *"Second IMO GHG Study", Phase1*, MEPC 59/INF.10, 2008/2009.

[3].International Maritime Organization, *"Second IMO GHG Study", Phase2*, MEPC 59/INF.10, 2009.

[4].International Maritime Organization, *"Study of Greenhouse Gas emissions from Ships"*, 2000.

[5].International Maritime Organization, MEPC, Circ. 471, 2005.

[6].International Maritime Organization, MEPC 62nd session, 11-15 July, 2011.

[7].Ungureanu, C., Marcu, O., Ionas, O., *"Energy efficiency in ship design"*, Annals of "Dunarea de Jos" University Galati. Fascicle XI, Shipbuilding, 2013; pp. 61-68.

[8].AEA Energy & Environment, *"Green-house gas emissions from shipping: trends, projections and abatement potential*", Report, 2008.

[9].Det Norske Veritas, *"Assessment of measures to reduce future CO2 emissions from shipping"*, 2010.

[10].MAN, *Diesel-electric Propulsion Plants*, 2012.

[11].Peter Naaijen & Vincent Koster, *Performance of auxiliary wind propulsion for merchant ships using kite***,** International Conference on Marine Research and Transportation, 2007.

[12].Wubbo J. Ockels, Richard Ruiterkamp, Bas Lansdorp, *Ship propulsion by Kites combining energy production by Laddermill principle and direct kite propulsion,* Kite Sailing Symposium, 2006.

[13].Michael Erhard and Hans Strauch, *Control of Towing Kites for Seagoing Vessels*, IEEE Transactions on Control Systems Technology, Volume: 21, 2013, Issue: 5.

[14].Jorg Sommer, *Ship propulsion by renewable energies available at sea,* MARIN, 2013.

[15].G. Wursig, B. Scholz, *"MSC.285(86) and Code for gas-fuelled ships (IGF-Code)-technical challenges and perspective*", Germanisher Lloyd, 2011.

[16].Jan Øivind Svardal & Friedrich Mewis, *Three Years of Experience with the Mewis Duct–A Contribution to Ship Efficiency*, International Conference on Ship Efficiency, 2011.

[17].Johan H. de Jong*, A Framework for Energy Saving Device (ESD) Decision Making, MARIN,* International Conference on Ship Efficiency, 2011.

[18].John Carlton, *Marine Propellers and Propulsion*, Elsevier, 2nd edition, 2007.

[19].Manen, J.D. van, Oossanen, P. van, *Propulsion. In Principles of Naval Architecture*, (ed. E.V. Lewis), 1988, Society of Naval Architects and Marine Engineers, New Jersey.

[20].Prantl L., *In Verhanlugen des dritten internationalen Mathematiker-Kongresses in Heidelberg,* 1904, traducere de J.A.K. Ackroyd, B.P. Axcell, A.I. Ruban, Butterwoth-Heinemann, Oxford, UK, 2001.

[21].Baker, C.J., *The Laminar Horseshoe Vortex*, Journal of Fluid Mechanics, 1979, vol.95.

[22].Baker, C.J., *The Turbulent Horseshoe Vortex*, Journal of Wind Engineering and Industrial Aerodynamics, 1980, vol.18.

[23].Dickinson, S.C., *Time dependent flow visualization in the separated region of an appendage-flat plate junction*, Experiments in Fluids 6,1987,141.

[24].Mehta RD.. *Effect on a wing nose shape on the flow in a wing/body junction* Aerosp.J.1984, 88:456–60.

[25].Rood EP.,*The governing influence of the nose radius on the unsteady effects of large scale flow structure in the turbulent wing and plate junction flow*. In ASME Forum on

Unsteady Flow, FGD, ed. PH Rothe, 1984 c, 15:7–9. New York: Am. Soc. Mech. Eng., Fluids Eng. Div.
[26].Fleming J, Simpson RL, Devenport WJ., *An Experimental Study of a Turbulent Wing-Body Junction and Wake Flow*. VPI&SU Report VPI-AOE-179, Va. Polytech. Inst. State Univ., Blacksburg, Va, 1991.
[27].Fleming J, Simpson RL, Devenport WJ., *An experimental study of a turbulent wing- body junction flow*. Exp. Fluids, 1993, 14:366–78.
[28].Roach PE, Turner JT.,*Secondary loss generation by gas turbine support struts*. Int. J. Heat Fluid Flow, 1985, 6:79–88.
[29].Ungureanu, C., Lungu, A., *Numerical Simulation of the Turbulent Flow around a Strut Mounted on a Plate*, Numerical Analysis and Applied Mathematics, AIP Proceedings, Melville New York, Vol. 1168, 2009, pp. 689-692.
[30].Ungureanu, C., Lungu, A., *Numerical Investigation of the Wing-Body Junction Flows,* Annals of "Dunarea de Jos" University Galati. Fascicle XI, Shipbuilding, 2009, pp. 17-23.
[31].Ungureanu, C., Lungu, A., *Numerical Studies on Free Surface Flow around a Hydrofoil Mounted on a Plate*, Numerical Analysis and Applied Mathematics, AIP Proceedings, Melville New York, Vol. 1281, 2010, pp. 115-118.
[32].Shizawa T, Honami S, Yamamoto M. *Experimental study of horseshoe vortex at wing/body junction with attack angle by triple hot-wire*. 1996, AIAA-96-0323. Presented at Am. Inst. Aeronaut. Astronaut. Aerosp. Sci. Meet., 34th, Reno.
[33].Ahmed A, Khan MJ. *Effect of sweep on wing-body juncture flows*, 1995, AIAA-95-0868. Presented at Am. Inst. Aeronaut. Astronaut. Aerosp. Sci. Meet., 33rd, Reno.
[34].Bernstein L, Hamid S.,*On the effect of a strake-like junction fillet on the lift and drag of a wing*, Aerosp. J., 1996,100:39–52.
[35].Metcalf B., Longo J., Ghosh S., Stern F., *Unsteady free-surface wave-induced boundary-layer separation for a surface-piercing NACA 0024 foil: Towing tank experiments*, Journal of Fluids and Structures 22, 2006, 77–98.
[36].Ungureanu, C., *Towing Tank Experiments for a Surface Piercing NACA 0012 Hydrofoil,* Annals of "Dunarea de Jos" University Galati. Fascicle XI, Shipbuilding, 2011, pp. 5-10.
[37].Ovidiu Ionas, *Nave tehnice*, Note de curs, Galati 2012.
[38].Gui L., Longo J., Metcalf B., Shao J., Stern F*., Forces, moment and wave pattern for surface combatant in regular head waves*, 2001.
[39].Dan Obreja si Leonard Domnisoru, *Theoretical and experimental investigation on the total resistance of an underwater ROV remotely operating vehicle*, International Congress of International Maritime Association of the Mediterranean, 2011.
[40].Longo J., Huang H.P., Stern F., *Solid/free-surface juncture boundary layer and wake*, Experiments in Fluids 25 ,1998, 283—297.
[41].Kang D.H., Longo J., Marquardt M., Stern F., *Solid/free-surface juncture boundary layer and wake with waves*, 27th Symposium on Naval Hydrodynamics Seoul, Korea 5-10 October 2008.
[42].Thwaites, B., ``*Incompressible Aerodynamics*," Oxford University Press, 1960.
[43].Kwak D., Rogers S.E., Kaul U.K.,Chang J.L.C., *A Numerical Study of Incompressible Juncture Flows*, NASA Technical memorandum, 1986.
[44].Visbal, M. R., "*Structure of Laminar Juncture Flows*", AIAA Journal, Vol. 29, 1991, No. 8, pp. 1273-1282.
[45].Hung C., Sung C., and Chen C., "*Computations of Saddle Point of Attachment*", AIAA Journal, Vol. 30, No. 6, 1992, pp. 1561-1569.
[46].Coon M.D., Tobak M., "*Experimental Study of Saddle Point of Attachment in Laminar Juncture Flow*", AIAA Journal, 1995, 33(12):2288-2292.

[47].Sumer B.M., Cristiansen N., Fredsoe J., *The horseshoe vortex and vortex shedding around a vertical wall-mounted cylinder exposed to waves*, J. Fluid Mech., vol. 332, 1997, pp. 41–70.
[48].Hara Y., Higuchi H., Kawamura T., Hayashi T., *A Computational Study on the Flow Structure around a Yawed Circular Cylinder- A Consideration on the Structure near the Upstream Juncture*, J of Wind Engineering, 2003.
[49].Muzzammil M. si Gangadhariah T., *The mean characteristics of horseshoe vortex at a cylindrical pier*, Journal of Hydraulic Research Vol. 41, No. 3, 2003, pp. 285–297.
[50].Besir S., Adil Ozturk N., H¨useyin A., *Horseshoe vortex system in the vicinity of the vertical cylinder mounted on a flat plate*, Flow Measurement and Instrumentation 18, 2007, 57–68.
[51].Alin N., Fureby C., *Large Eddy Simulation of Junction Vortex Flows*, 46th AIAA Aerospace Sciences Meeting and Exhibit, AIAA 2008-668, 2008, Reno, Nevada.
[52].Frederich O., Wassen E., Thiele F., *Prediction of the Flow Around a Short Wall-Mounted Finite Cylinder using LES and DES*, Journal of Numerical Analysis, Industrial and Applied Mathematics, (JNAIAM), vol. 3, no. 3-4, 2008, pp. 231-247.
[53].Lungu A., Ungureanu C., *„Numerical Study of a 3-D Juncture Flow"*, Proceedings of the Conference on Numerical Analysis and Applied Mathematics, AIP Proceedings, Melville New York, Vol. 1048, 2008, pp. 839-842.
[54].Guillermo P.S., Thorsten S., Jochen F., Michael K., Wolfgang R., *Large Eddy Simulations and Experiments of Flow Around Finite-Height Cylinders*, Flow Turbulence Combust, 2010, 84:239–275.
[55].Wang J.M., Bi W.T., Wei Q.D., *Effects of an upstream inclined rod on the circular cylinder–flat plate junction flow*, Exp Fluids, 2009, 46:1093–1104.
[56].Ming Z., Liang C., Tongming Z., *Direct numerical simulation of three-dimensional flow past a yawed circular cylinder of infinite length*, Journal of Fluids and Structures 25, 2009, 831–847.
[57].Besir S., Adil Ozturk N., *Behaviour of flow at the junction of cylinder and base plate in deep water*, Measurement 42, 2009, 225–240.
[58].AEA Energy & Environment, *"Green-house gas emissions from shipping: trends, projections and abatement potential*", Report, 2008.
[59].Det Norske Veritas, *"Assessment of measures to reduce future CO_2 emissions from shipping"*, 2010.
[60].MAN, *Diesel-electric Propulsion Plants*, 2012.
[61].Peter N., Vincent K., *Performance of auxiliary wind propulsion for merchant ships using kite*, International Conference on Marine Research and Transportation, 2007.
[62].Wubbo J., Ockels RFlemingichard R., Bas Lansdorp, *Ship propulsion by Kites combining energy production by Laddermill principle and direct kite propulsion,* Kite Sailing Symposium, 2006.
[63].Michael E., Hans S., *Control of Towing Kites for Seagoing Vessels*, IEEE Transactions on Control Systems Technology, Volume: 21, 2013, Issue: 5.
[64].Jorg S., *Ship propulsion by renewable energies available at sea,* MARIN, 2013.
[65].Wursig G., Scholz B., *"MSC.285(86) and Code for gas-fuelled ships (IGF-Code)-technical challenges and perspective*", Germanisher Lloyd, 2011.
[66].Jan Øivind Svardal & Friedrich Mewis, *Three Years of Experience with the Mewis Duct–A Contribution to Ship Efficiency*, International Conference on Ship Efficiency, 2011;
[67].Johan H. de Jong*, A Framework for Energy Saving Device (ESD) Decision Making, MARIN,* International Conference on Ship Efficiency, 2011.
[68].John C., *Marine Propellers and Propulsion*, Elsevier, 2nd edition, 2007.

[69].Manen, J.D. van, Oossanen, P. van, *Propulsion. In Principles of Naval Architecture*, (ed. E.V. Lewis), 1988, Society of Naval Architects and Marine Engineers, New Jersey.
[70].Prantl L., *In Verhanlugen des dritten internationalen Mathematiker-Kongresses in Heidelberg,* 1904, traducere de J.A.K. Ackroyd, B.P. Axcell, A.I. Ruban, Butterwoth-Heinemann, Oxford, UK, 2001.
[71].Baker C.J., *The Laminar Horseshoe Vortex*, Journal of Fluid Mechanics, vol.95, 1979.
[72].Baker C.J., *The Turbulent Horseshoe Vortex*, Journal of Wind Engineering and Industrial Aerodynamics, vol.18, 1980.
[73].Dickinson S.C., *Time dependent flow visualization in the separated region of an appendage-flat plate junction*, Experiments in Fluids 6, 1987,141.
[74].Mehta R.D., *Effect on a wing nose shape on the flow in a wing/body junction* Aerosp.J. 1984, 88:456–60.
[75].Rood E.P.,*The governing influence of the nose radius on the unsteady effects of large scale flow structure in the turbulent wing and plate junction flow*. In ASME Forum on Unsteady Flow, FGD, ed. PH Rothe, 1984c, 15:7–9. New York: Am. Soc. Mech. Eng., Fluids Eng. Div.
[76].Fleming J., Simpson R.L., Devenport WJ. 1991. *An Experimental Study of a Turbulent Wing-Body Junction and Wake Flow*. VPI&SU Report VPI-AOE-179, Va. Polytech. Inst. State Univ., Blacksburg, Va.;
[77].Fleming J, Simpson RL, Devenport WJ. 1993. *An experimental study of a turbulent wing-body junction flow*. Exp. Fluids 14:366–78;
[78].Roach PE, Turner JT. 1985. *Secondary loss generation by gas turbine support struts*. Int. J. Heat Fluid Flow. 6:79–88
[79].Ungureanu, C., Lungu, A., *Numerical Simulation of the Turbulent Flow around a Strut Mounted on a Plate*, Numerical Analysis and Applied Mathematics, AIP Proceedings, Melville New York, Vol. 1168, pp. 689-692, 2009;
[80].Ungureanu, C., Lungu, A., *Numerical Investigation of the Wing-Body Junction Flows,* Annals of "Dunarea de Jos" University Galati. Fascicle XI, Shipbuilding, pp. 17-23, 2009
[81].Ungureanu, C., Lungu, A., *Numerical Studies on Free Surface Flow around a Hydrofoil Mounted on a Plate*, Numerical Analysis and Applied Mathematics, AIP Proceedings, Melville New York, Vol. 1281, pp. 115-118, 2010;
[82].Shizawa T, Honami S, Yamamoto M. 1996. *Experimental study of horseshoe vortex at wing/body junction with attack angle by triple hot-wire*. AIAA-96-0323. Presented at Am. Inst. Aeronaut. Astronaut. Aerosp. Sci. Meet., 34th, Reno;
[83].Ahmed A, Khan MJ. 1995. *Effect of sweep on wing-body juncture flows*. AIAA-95-0868. Presented at Am. Inst. Aeronaut. Astronaut. Aerosp. Sci. Meet., 33rd, Reno
[84].Bernstein L, Hamid S. 1996, *On the effect of a strake-like junction fillet on the lift and drag of a wing*, Aerosp. J. 100:39–52;
[85].B. Metcalf, J. Longo, S. Ghosh, F. Stern, *Unsteady free-surface wave-induced boundary-layer separation for a surface-piercing NACA 0024 foil: Towing tank experiments*, Journal of Fluids and Structures 22 (2006) 77–98
[86].Ungureanu, C., *Towing Tank Experiments for a Surface Piercing NACA 0012 Hydrofoil,* Annals of "Dunarea de Jos" University Galati. Fascicle XI, Shipbuilding, pp. 5-10, 2011;
[87].Ovidiu Ionas, *Nave tehnice*, Note de curs, Galati 2012;
[88].L.Gui, J. Longo, B. Metcalf, J Shao, F Stern*, Forces, moment and wave pattern for surface combatant in regular head waves*, 2001;
[89].Dan Obreja si Leonard Domnisoru, *Theoretical and experimental investigation on the total resistance of an underwater ROV remotely operating vehicle*, International Congress of International Maritime Association of the Mediterranean, 2011;

[90].J. Longo, H. P. Huang, F. Stern, *Solid/free-surface juncture boundary layer and wake*, Experiments in Fluids 25 (1998) 283—297;
[91].D.H. Kang , J. Longo, M. Marquardt , F. Stern, *Solid/free-surface juncture boundary layer and wake with waves*, 27th Symposium on Naval Hydrodynamics Seoul, Korea 5-10 October 2008;
[92].Thwaites, B., ``*Incompressible Aerodynamics*," Oxford University Press, 1960;
[93].D. Kwak, S E Rogers, Uk Kaul, J LC Chang, *A Numerical Study of Incompressible Juncture Flows*, NASA Technical memorandum, 1986;
[94].Visbal, M. R., "*Structure of Laminar Juncture Flows*", AIAA Journal, Vol. 29, No. 8, 1991, pp. 1273-1282;
[95].Hung, C, Sung, C. and Chen, C., "*Computations of Saddle Point of Attachment*", AIAA Journal, Vol. 30, No. 6, June 1992, pp. 1561-1569;
[96].Coon, M.D., Tobak, M., "*Experimental Study of Saddle Point of Attachment in Laminar Juncture Flow*", AIAA Journal, 33(12):2288-2292, 1995;
[97].Sumer BM, Cristiansen N., Fredsoe J, *The horseshoe vortex and vortex shedding around a vertical wall-mounted cylinder exposed to waves*, J. Fluid Mech. (1997), Š vol. 332, pp. 41–70;
[98].Y Hara, H Higuchi, T Kawamura, T Hayashi, *A Computational Study on the Flow Structure around a Yawed Circular Cylinder- A Consideration on the Structure near the Upstream Juncture*, J of Wind Engineering, 2003;
[99].Muzzammil M. si Gangadhariah T., *The mean characteristics of horseshoe vortex at a cylindrical pier*, Journal of Hydraulic Research Vol. 41, No. 3 (2003), pp. 285–297
[100].Besir Sahin, N. Adil Ozturk, H¨useyin Akilli, *Horseshoe vortex system in the vicinity of the vertical cylinder mounted on a flat plate*, Flow Measurement and Instrumentation 18 (2007) 57–68;
[101].N.Alin, C. Fureby, *Large Eddy Simulation of Junction Vortex Flows*, 46th AIAA Aerospace Sciences Meeting and Exhibit, AIAA 2008-668, 2008, Reno, Nevada;
[102].O. Frederich , E. Wassen & F. Thiele, *Prediction of the Flow Around a Short Wall-Mounted Finite Cylinder using LES and DES*, Journal of Numerical Analysis, Industrial and Applied Mathematics, (JNAIAM), vol. 3, no. 3-4, , pp. 231-247, 2008;
[103].Lungu, A., Ungureanu, C., *„Numerical Study of a 3-D Juncture Flow"*, Proceedings of the Conference on Numerical Analysis and Applied Mathematics, AIP Proceedings, Melville New York, Vol. 1048, pp. 839-842, 2008;
[104].Guillermo Palau-Salvador, Thorsten Stoesser, Jochen Fröhlich, Michael Kappler, Wolfgang Rodi, *Large Eddy Simulations and Experiments of Flow Around Finite-Height Cylinders*, Flow Turbulence Combust (2010) 84:239–275;
[105].J. M. Wang, W. T. Bi, Q. D. Wei, *Effects of an upstream inclined rod on the circular cylinder–flat plate junction flow*, Exp Fluids (2009) 46:1093–1104;
[106].Ming Zhao, Liang Cheng, Tongming Zhou, *Direct numerical simulation of three-dimensional flow past a yawed circular cylinder of infinite length*, Journal of Fluids and Structures 25 (2009) 831–847;
[107].Besir Sahin, N. Adil Ozturk, *Behaviour of flow at the junction of cylinder and base plate in deep water*, Measurement 42 (2009) 225–240;
[108].Tuan, V.M., Lungu, A., Ungureanu, C., *„Numerical Simulation of the 3D Flow Around an Inclined Circular Cylinder Mounted on a Curved Plate",* Annals of "Dunarea de Jos" University Galati. Fascicle XI, Shipbuilding, pp. 5-12, 2012;
[109].A Stanbrook, *Experimental Observation of Vortices in Wing-Body Junctions*, R.A.E. Report Aero. 2589, 1957;

[110].MCMAHON H., HUBBARTJ,. & KUBENDRALN, *Mean velocities and Reynolds stresses in a juncture flow*. NASA Contractor Rep. 3605, 1982;
[111].Fleming J, Simpson RL, Devenport WJ. 1991. *An Experimental Study of a Turbulent Wing-Body Junction and Wake Flow*. VPI&SU Report VPI-AOE-179, Va. Polytech. Inst. State Univ., Blacksburg, Va.;
[112].Devenport WJ, Simpson RL. 1990a. *Time-dependent and time-averaged turbulence structure near the nose of a wing-body junction*. J. Fluid Mech. 210:23–55
[113].Devenport WJ, Simpson RL. 1990b. *An Experimental Investigation of the Flow Past an Idealized Wing-Body Junction*. VPI&SU Rep. VPI-AOE-172, Va. Polytech. Inst. State Univ., Blacksburg, Va;
[114].Devenport WJ, Simpson RL. 1992. *Flow past a wing-body junction: experimental evaluation of turbulence models*. AIAA J.30:873–81;
[115].Fleming J, Simpson RL, Devenport WJ. 1993. *An experimental study of a turbulent wing-body junction flow*. Exp. Fluids 14:366–78;
[116].Olcmen MS, Simpson RL. 1994. *Influence of wing shapes on surface pressure fluctuations at wing-body junctions*. AIAA J. 32:6–15;
[117].Olcmen MS, Simpson RL. 1995. *An experimental study of three-dimensional pressure-driven turbulent boundary layer*. J. Fluid Mech. 290:225–62;
[118].Olcmen MS, Simpson RL. 1996a. *Experimental transport-rate budgets in complex three- dimensional turbulent flows at a wing/body junction*. AIAA-96-2035. Presented at Am. Inst. Aeronaut. Astronaut. Fluid Dyn. Conf., 27th, New Orleans;
[119].Olcmen MS, Simpson RL. 1996b. *Theoretical and experimental pressure-strain comparison in a pressure-driven three-dimensional turbulent boundary layer*. AIAA-96-2141. Presented at Am. Inst. Aeronaut. Astronaut. Theor. Fluid Mech. Meet., 1st, New Orleans;
[120].Olcmen MS, Simpson RL. 1997a. *Experimental evaluation of turbulence diffusion models in complex 3-D flow near a wing/body junction*. AIAA-97-0650. Presented at Am. Inst. Aeronaut. Astronaut. Aerosp. Sci. Meet., 35th, Ren;
[121].Olcmen MS, Simpson RL. *Some features of a turbulent wing-body junction vortical flow*, International Journal of Heat and Fluid Flow 27 (2006) 980–993;
[122].Parneix S, Durbin PA, Behnia M. *Computation of 3d turbulent boundary layers using the v2-f model*. Flow, Turbulence and Combustion 60: 19–46, 1998;
[123].Olcmen MS, Simpson RL. *Experimental transport-rate budgets in complex 3-D turbulent flow near a wing/body junction*, International Journal of Heat and Fluid Flow 29 (2008) 874–890
[124].S.C. Dickinson, *Time dependent flow visualization in the separated region of an appendage-flat plate junction*, Experiments in Fluids, 1988;
[125].D.A. Jones si D.B. Clarke, *Simulation of a Wing-Body Junction Experiment using the Fluent Code*, DSTO –TR-1731, 2005;
[126].Khalil A. Kairouz, Hamid R. Rahai, Yen si Hsu (2007), *Turbulent junction flow with an upstream ribbed surface*, International Journal of Heat and Fluid Flow 26 (2005) 771–779;
[127].Song Fu, Zhixiang Xiao, Haixin Chen, Yufei Zhang, Jingbo Huang, *Simulation of wing-body junction flows with hybrid RANS/LES methods*, International Journal of Heat and Fluid Flow 28 (2007) 1379–1390;
[128].Joongcheol Paik, Cristian Escauriaza, and Fotis Sotiropoulos, *On the bimodal dynamics of the turbulent horseshoe vortex systemin a wing-body junction*, PHYSICS OF FLUIDS 19, 045107, 2007;
[129].M. M. Ambrogi, R. Broglia, A. Di Mascio, *Numerical Simulation of a flow around an America's Cup class Keel*, Proceedings of the Eighteenth (2008) International Offshore and Polar Engineering Conference, Vancouver, BC, Canada, July 6-11, 2008;

[130].Liu Zhihua, Xiong Ying, Tu Chengxu, *Numerical simulation and control of horseshoe vortex around an appendage–body junction*, Journal of Fluids and Structures, Volume 27, Issue 1, January 2011, Pages 23-42;
[131].A.M. Levchenya, E.M. Smirnov, V.D. Goryachev, *RANS-based numerical simulation and visualization of the horseshoe vortex system in the leading edge end wall region of a symmetric body*, International Journal of Heat and Fluid Flow 31 (2010) 1107–1112;
[132].Renato Paciorri, Aldo Bonfiglioli, Andrea di Mascio and Bernardo Favini, *RANS simulations of a junction flow*, International Journal of Computational Fluid Dynamics, Vol. 19, No. 2, February 2005, 179–189;
[133].Fabien Gand, *Dynamique des ´ecoulements de jonction en r´egime turbulent*, These de doctorat de l'Universit´e Pierre et Marie Curie, 2011;
[134].Gand F., Brunet V., Deck S., *Experimental and Numerical Investigation of a Wing-Body Junction Flow*, AIAA Journal, vol 50, no 12, pp. 2711-2719., 2012;
[135].Hussein H.J. si Martinuzzi R.J., *Energy balance for turbulent flow around a surface mounted cube placed in a channel*, Physics of Fluids 8, 764, (1996);
[136].Giancarlo Alfonsi, Carlo Restano, Leonardo Primavera, *Coherent structures of the flow around a surface-mounted cubic obstacle in turbulent channel flow*, Journal of Wind Engineering and Industrial Aerodynamics 91 (2003) 495–511;